Instituto Universitario de Investigación
en Ingeniería de Aragón
Universidad Zaragoza

PhD Thesis

Non-invasive techniques for respiratory information extraction based on pulse photoplethysmogram and electrocardiogram

**Técnicas no invasivas para la
extracción de información respiratoria basadas en
el fotopletismograma de pulso y el electrocardiograma**

Jesús Lázaro Plaza

Supervisors:
Eduardo Gil Herrando
Pablo Laguna Lasaosa
Raquel Bailón Luesma

July 2015

Acknowledgments

It has been a long time since I decided to work towards this Ph.D. thesis. Now I can see that it is almost finished and I would like to thank many people who, in a more or less directly way, have been involved in the process making it easier or even possible. Thank you all. It is fantastic to be surrounded by good people.

A mis directores de tesis: Pablo, Eduardo y Raquel, por hacer posible esta tesis con sus ideas infinitas, sus aportaciones y su ayuda de principio a fin. Vuestra pasión por la investigación es contagiosa, y esta es una de las razones que me han traído a este punto.

A los miembros del grupo BSICoS, compañeros de lujo, por su feedback y colaboración, y por construir un ambiente de trabajo excelente. A mis compañeros de laboratorio: Sanjuan, Alba, Michele, Violeta, Ana, Mariola y Arantxa.

To Ki. My visit to his lab in Worcester would not have been so positive without his help and attention in both professional and personal aspects. I would like to extend this acknowledgment to Yunyoung and to my lab colleagues who always treated me as one of them: to Hugo, Bersain, Natasha, Chris, and Jeff. I would like to thank also to Karim and Terry for making me feel that I was not alone since the first minute.

To Yunyoung and Ainara, for accepting to read and prepare a report about this Ph.D. thesis within a not so long period of time.

A mis amigos, por hacer más llevaderos los malos momentos, y mucho mejores los buenos. A Fernando, Sanjuan, Susana, David, Jules, Mou, Aitor, VM, Pelos y un largo etcétera.

A mi familia, particularmente a mis padres, por apoyarme y animarme siempre a seguir adelante. A Silvia, por TODO. Por último, a la pequeña Ainara, por ser el último empujoncito para presentar esta tesis.

Abstract

The main objective of this thesis is to develop non-invasive methods for respiration information extraction from two biomedical signals which are widely adopted in clinical routine: the electrocardiogram (ECG) and the pulse photoplethysmographic (PPG) signal. This study is motivated by the desirability of monitoring respiratory information from non-invasive devices allowing to substitute the current respiration-monitoring techniques which may interfere with natural breathing and which are unmanageable in some applications such as stress test or sleep studies. Furthermore, if these non-invasive devices are those already used in the clinical routine, the respiratory information obtained from them represents an added value which allows a more complete overview of the patient status.

This thesis is divided into 6 chapters. Chapter 1 of this thesis introduces the problematic, motivations and objectives of this study. It also introduces the physiological origin of studied ECG and PPG signals, and why and how they carry autonomic- and respiration-related information which can be extracted from them.

Chapter 2 of this thesis addresses the derivation of respiratory information from ECG signal. Several ECG derived respiration (EDR) methods have been presented in literature. Their performance usually decrease considerably in highly non-stationary and noisy environments such as stress test. However, some alternatives aimed to this kind of environments have been presented, such as one based on electrical axis rotation angles (obtained from the ECG), which to the best of our knowledge was the best suited for stress test. This method requires three orthogonal leads, and it is very dependent on each one of those leads, i.e., the performance of the method is significantly decreased if there is any problem at any one of the required leads. A novel EDR method based on QRS slopes and R-wave angle is presented in this thesis. The proposed method demonstrated to be robust in highly non-stationary and noisy environments and so to be applicable to exercise conditions including sports training. Furthermore, it

is independent on a specific lead set, and so, a problem at any lead do not imply a significantly reduction of the performance.

Chapter 3 addresses the derivation of respiratory information from PPG signals. A novel method for deriving respiratory rate from PPG signal is presented. It exploits respiration-related modulations in pulse width variability (PWV) which is related to pulse wave velocity and dispersion. The proposed method is much less affected by the sympathetic tone than other methods in literature which are usually based on pulses amplitude and/or rate. This leads to highest accuracy than other PPG-based method. Furthermore, a method for combining information from several respiratory signals was developed and used to obtain a respiratory rate estimation from the proposed PWV-based in combination with other known PPG-based methods, improving the accuracy of the estimation and outperforming other methods in literature which involve ECG or BP recording.

Chapter 4 addresses the derivation of respiratory information from smart-phone-camera-acquired-PPG (SCPPG) signals by adapting the methods for deriving respiratory rate from PPG signal presented in Chapter 3. The proposed method accurately estimates respiratory rate from SCPPG signals at its normal spontaneous ranges (0.2-0.4 Hz) and even at higher rates (up to 0.5 Hz or 0.6 Hz, depending on the used device). The only requirement is that these smartphones and tablets contain a flashlight and a video camera to image a fingertip pressed to it. As smartphones and tablets have become common, they meet the criteria of ready access and acceptance. Hence, a mobile phone/tablet approach has the potential to be widely-accepted by the general population and can facilitate the capability to measure some of the vital signs using only fingertip of the subject.

Chapter 5 of this thesis proposes a methodology for obstructive sleep apnea syndrome (OSAS) screening in children just based on PPG signal. OSAS is a sleep-respiration-related dysfunction for which polysomnography (PSG) is the gold standard for diagnosis. PSG consists of overnight recording of many signals during sleep, therefore, it is quite involved and difficult to use in ambulatory scenario. The method presented in this thesis is aimed to diagnose the OSAS in children based just on PPG signal which would allow us to consider an ambulatory diagnosis with both its social and economic advantages.

Finally, Chapter 6 summarizes the original contributions and main conclusions of the thesis, and proposes possible extensions of the work.

Resumen y conclusiones

El objetivo principal de esta tesis es el desarrollo de métodos no invasivos para la extracción de información respiratoria a partir de dos señales biomédicas ampliamente utilizadas en la rutina clínica: el electrocardiograma (ECG) y la señal fotopletismográfica de pulso (PPG). La motivación de este estudio es la conveniencia de monitorizar información respiratoria a partir de dispositivos no invasivos que permita sustituir las técnicas actuales que podrían interferir con la respiración natural y que presentan inconvenientes en algunas aplicaciones como la prueba de esfuerzo y los estudios del sueño. Además, si estos dispositivos no invasivos son los ya utilizados en la rutina clínica, la información respiratoria extraída de ellos representa un valor añadido que permite tener una visión más completa del paciente.

Esta tesis se divide en 6 capítulos. El Capítulo 1 introduce la problemática, motivaciones y objetivos del estudio. También introduce el origen fisiológico de las señales estudiadas ECG y PPG, y cómo y por qué tienen información autonómica y respiratoria que se puede extraer de ellas.

El Capítulo 2 aborda la obtención de información respiratoria a partir del ECG. Se han propuesto varios métodos para la obtención de la respiración a partir del ECG (EDR, del inglés "ECG derived respiration"). Su rendimiento se suele ver muy afectado en entornos altamente no estacionarios y ruidosos como la prueba de esfuerzo. No obstante, se han propuesto algunas alternativas, como una basada en el ángulo de rotación del eje eléctrico (obtenido del ECG), que es el que mejor funciona en prueba de esfuerzo según nuestros conocimientos. Este método requiere de tres derivaciones ortogonales y es muy dependiente de cada una de ellas, i.e., el método no es aplicable o su rendimiento se reduce significativamente si hay algún problema en alguna de las derivaciones requeridas. En el Capítulo 2 se propone un método EDR nuevo basado en las pendientes del QRS y el ángulo de la onda R. El método presentado demostró ser robusto en entornos altamente no estacionarios y ruidosos y por tanto ser aplicable durante ejercicio incluyendo entrenamiento deportivo. Además, es independiente de un

conjunto específico de derivaciones y, por tanto, un problema en alguna de ellas no implica una reducción considerable del rendimiento.

El Capítulo 3 aborda a obtención de información respiratoria a partir de la señal PPG. Se propone un método nuevo para obtener la tasa respiratoria a partir de la señal PPG. Explota una modulación respiratoria en la variabilidad de anchura de pulso (PWV) relacionada con la velocidad y dispersión de la onda de pulso. La PWV está mucho menos afectada por el tono simpático que otros métodos presentados en la literatura que suelen basarse en la amplitud y/o la tasa de pulso. Esto permite una mayor precisión que otros métodos basados en PPG. Además, se propone un método para combinar información de diferentes señales respiratorias, y se utiliza para estimar la tasa respiratoria a partir de la PWV en combinación con otros métodos basados en la señal PPG, mejorando la precisión de la estimación incluso en comparación con otros métodos en la literatura que requieren el ECG o la presión sanguínea.

El Capítulo 4 aborda la extracción de información respiratoria a partir de señales PPG registradas con smarthpones (SCPPG), mediante la adaptación de los métodos basados en la señal PPG presentados en el Capítulo 3. Los métodos propuestos estimaron de forma precisa la tasa respiratoria para a partir de señales SCPPG en sus rangos espontáneos habituales (0.2-0.4 Hz) e incluso a tasas más altas (hasta 0.5 Hz o 0.6 Hz, dependiendo del dispositivo utilizado). El único requerimiento es que el smartphone tenga un luz tipo flash y una cámara para grabar una yema del dedo sobre ella. La popularidad de los smartphones los convierte en dispositivos de acceso y aceptación rápidos. Así, para la población general es potencialmente aceptable un método que funciona en smartphones, pudiendo facilitar la medida de algunas constantes vitales utilizando solo la yema del dedo.

El Capítulo 5 se propone un método para el diagnóstico del síndrome de apnea obstructiva del sueño (OSAS) en niños basado únicamente en la señal PPG. El OSAS es una disfunción relacionada con la respiración y el sueño que se diagnostica mediante polisomnografía (PSG). La PSG es el registro nocturno de muchas señales durante el sueño, siendo muy difícil de aplicar en entornos ambulatorios. El método que presenta esta tesis está enfocado a diagnosticar el OSAS en niños utilizando únicamente la señal PPG que permitiría considerar un diagnóstico ambulatorio con sus ventajas económicas y sociales.

Finalmente, el Capítulo 6 resume las contribuciones originales y las conclusiones principales de esta tesis, y propone posibles extensiones del trabajo.

Contents

List of Figures

List of Tables

If you want to conquer the anxiety of life,
live in the moment, live in the breath.
Amit Ray.

Chapter 1

Introduction

1.1 Motivations

Monitoring respiratory information is useful in several situations, e.g., respiratory rate is a sensitive clinical parameter in a multitude of pulmonary diseases [1], such as acute respiratory dysfunction, for which respiratory rate remains the first and often the most sensitive marker [2, 3]. Another example is detection of periodic breathing, which shares pathophysiological aspects with the central sleep apnea syndrome and with CheyneStokes respiration in patients with heart failure [4], and results in elevated mortality in this last kind of patients [5]. Respiratory rate is very useful also in sports training, because it is a reliable marker for the anaerobic threshold, which is defined as the theoretical highest exercise level that can be maintained for prolonged periods [6–9].

Respiration is usually recorded by spirometry, pneumography, or plethysmography. These techniques require cumbersome devices which may interfere with natural breathing and which are unmanageable in some situations such as ambulatory monitoring, stress tests, or sleep studies [10], where the patient comfort is critically relevant for affecting physiological sleep as minimally as possible.

Therefore, obtaining respiratory information from non-invasive devices is a very relevant task. It is even more desirable that these non-invasive devices are those already used in the clinical routine and thus, respiratory information obtained from them allows to have a more complete overview of the patient status. One of the most used signals in the clinical monitoring is the electrocardiogram (ECG) on which many markers of several cardiac diseases are based. ECG has also other uses such as heart rate monitoring

and autonomic nervous system (ANS) assessment, which result interesting in several applications such as stress monitoring and sport performance.

Another signal from which obtaining respiratory information results particularly interesting is the PPG signal. PPG signal is usually provided by a simple, economical and comfortable device called pulse oximeter. The form factor of the pulse oximeter is commonly a fingertip, and it is widely adopted in the clinical routine as SpO_2 monitor. SpO_2 is a very important parameter in studies concerning respiration and essential in many applications such as sleep apnea diagnosis. Obtaining accurate respiratory signal from a pulse oximeter would allow us to consider an ambulatory diagnosis with its both social and economic advantages. Because of these properties, PPG signal receives especial attention in this thesis.

In this thesis, novel methods for obtaining respiratory information from ECG signals, and also from PPG signals are presented. Some algorithms for combining information of different methods aimed to increase the robustness are also developed. Finally, an obstructive sleep apnea syndrome (OSAS)-in-children screening method based only in PPG signal is proposed.

1.2 Autonomic nervous system

The brain and the spinal cord compose the *central nervous system*. A large segment of the nervous system operates at a subconscious level and it is called the ANS. It controls many functions of the internal organs, movements of the gastrointestinal tract, secretion by many of the glands of the body, and including the level of pumping activity by the heart [11]. ANS controls the heart rate by exciting the sinus node. In absence of ANS influence, the intrinsic heart rate is about 100 to 120 beats per minute [12].

ANS is composed of two branches. On one hand, the *sympathetic nervous system*. It "activates" the body when necessary, e.g., in an alarm situation. An animal in this state decides almost instantly whether to stand and fight or to run, and because of this, this reaction is so-called the *fight or flight reaction*. In either event, the sympathetic alarm reaction makes the subsequent activities of the animal vigorous [11]. Some of the effects of a sympathetic activation are, among others, heart rate increase and vasoconstriction.

On the other hand, the *parasympathetic nervous system* "relaxes" the body and it is the responsible of the so called *rest and digest* status. A parasympathetic activation induces, among other processes, heart rate decrease. The parasympathetic branch acts in a much more specific way than

the sympathetic branch, which commonly generates a mass response. For instance, parasympathetic branch cardiovascular control usually acts only on the heart rate [11].

Some processes are known to be controlled by only one of the branches, e.g., arteries constriction is controlled by only the sympathetic branch, and respiration is controlled by only the parasympathetic branch. However, the two branches acts in a reciprocal manner, with increases in the activity of one of them associated with decreases in the activity of the other one, at least in part [13]. In this way, the overall status of the organism depends on which ANS branch is predominating and how big this predominance is at each moment. This sympathetic-parasympathetic balance is commonly referred to *sympathovagal balance.*

1.3 Biomedical signals

1.3.1 Electrocardiogram

The ECG is the measurement of the electrical activity of the heart recorded superficially over the skin by two electrodes. The voltage variations between the electrodes are originated by the action potentials of the cardiac cells that make them to contract. The resulting beat can be seen in the ECG as a set of waves. The morphology and temporal variations of those waves represent information which is used for diagnosis of diseases that affect the electrical activity of the heart. The time between successive beats represents also useful information [14].

The morphology of each heartbeat in a normal ECG signal is composed of several waves. ANS rhythmically excites the sinus node (S-A node) which generates an electrical impulse. This electrical impulse is transmitted to along the atria through the internodal pathways, leading to an atrial depolarization and so an atrial contraction. This atrial depolarization is reflected in the ECG by the P wave. Subsequently, the impulse is delayed in the atrioventricular node (A-V node) allowing the blood to get into ventricles before their contraction. The A-V node transmit the electrical impulse to the bundle of His (A-V bundle), which in conjunction with the Purkinje fibers rapidly gets the electrical impulse to all parts of the ventricles, leading to their depolarization associated to their contraction and so the blood pumping [11]. Ventricular depolarization is reflected in the ECG by the QRS complex which is the result of superposition of 3 waves: Q, R, and S waves. QRS complex reflects also, in a very minor part, the atrial repolarization
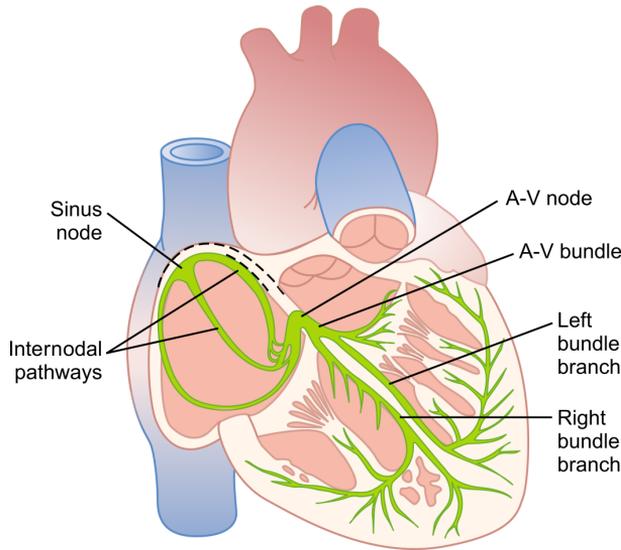
Figure 1.1: Sinus node, and the Purkinje system of the heart, showing also the A-V node, atrial internodal pathways, and ventricular bundle branches (From [11]).

associated to the atrial relaxation. However, this effect cannot usually be observed in the ECG because it is overlapped in time with the ventricular depolarization which generates the great major part of QRS complex. The following wave to QRS complex which is usually the last wave of the heartbeat is known as T wave, and it reflects the ventricular repolarization which occur during the ventricular relaxation. The heart anatomy parts named in this paragraph are illustrated in Fig. 1.1, and a normal ECG can be seen in Fig. 1.2.

Electrocardiogram recording techniques

The electrodes are placed over the skin in positions where the spatio-temporal variations of the cardiac electrical field are reflected enough. A specific position of a pair of electrodes is called *lead*. The recording of that pair of electrodes is denoted with the name of that lead. The ECG is usually recorded by using a multi-lead set-up which uses unipolar and bipolar leads. An ECG lead is a unipolar lead if it records the voltage variation in one electrode, taking the reference in another virtual electrode where the voltage remains almost constant during the whole cardiac cycle. On the other hand, bipolar leads are those leads which record the voltage between two electrodes [14]. The clinical routine has established a 12 lead set-up which is known as
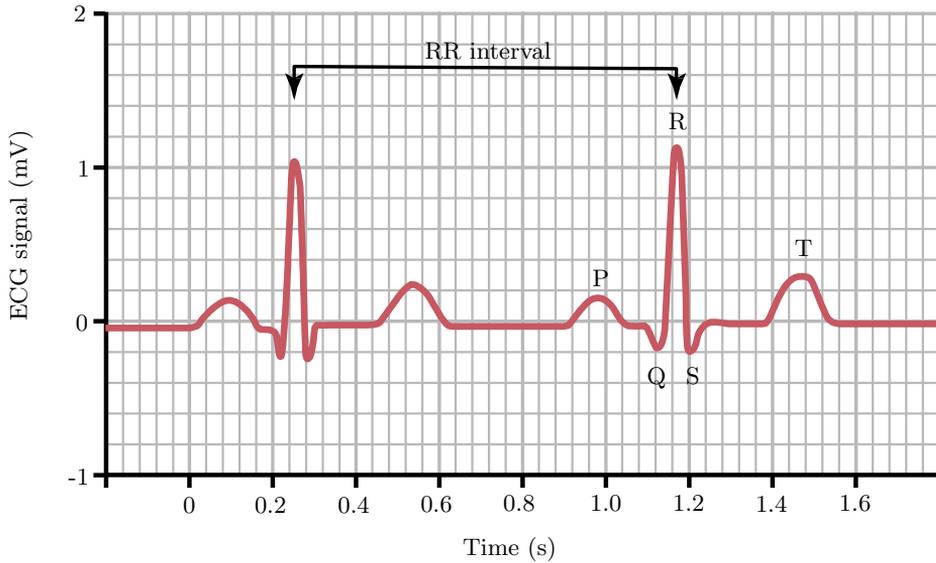
Figure 1.2: Normal electrocardiogram signal (From [11]).

12-standard-leads ECG which is composed of 3 bipolar leads and 9 unipolar leads.

The 3 bipolar leads of the 12-standard-leads ECG are known as the *bipolar limb leads* and they were introduced by Einthoven in the early 20th century:

$$I = V_{\text{LA}} - V_{\text{RA}} \tag{1.1}$$

$$II = V_{\text{LL}} - V_{\text{RA}} \tag{1.2}$$

$$III = V_{\text{LL}} - V_{\text{LA}}, \tag{1.3}$$

where V_{LA}, V_{RA} and V_{LL} denote the voltage recorded by electrodes placed at the left arm, right arm and left leg, respectively. The bipolar limb leads describe a triangle known as "Einthoven's triangle" which has the heart at its center.

The 9 unipolar leads of the 12-standard leads ECG can be divided into 2 groups. On one hand, the *augmented unipolar limb leads* which were introduced by Golderberg [15, 16] by modifying a previous procedure proposed by Wilson et al. [17]. The procedure proposed by Wilson measures 3 leads known as *V leads* (VR, VL, VF) which represent the voltage variations at a single location of the three locations of the Einthoven's triangle, based on a relatively neutral reference electrode obtained by pooling the 3 limb electrodes in a common terminal. Golderberg proposed to disconnect the

central terminal from the limb to which the exploring electrode was placed, getting bigger the voltage variations in the V leads and defining the augmented leads [18]:

$$aVR \quad = \quad V_{\mathrm{RA}} - \frac{V_{\mathrm{LA}} + V_{\mathrm{LL}}}{2} \tag{1.4}$$

$$aVL \quad = \quad V_{\mathrm{LL}} - \frac{V_{\mathrm{RA}} + V_{\mathrm{LL}}}{2} \tag{1.5}$$

$$aVF \quad = \quad V_{\mathrm{LL}} - \frac{V_{\mathrm{LA}} + V_{\mathrm{RA}}}{2}. \tag{1.6}$$

On the other hand, the *precordial leads* whose electrodes are placed directly over the chest, nearer to the heart than the limb leads as shows Fig. 1.3. The directions of the 12-standard-leads ECG are shown in Fig. 1.4.
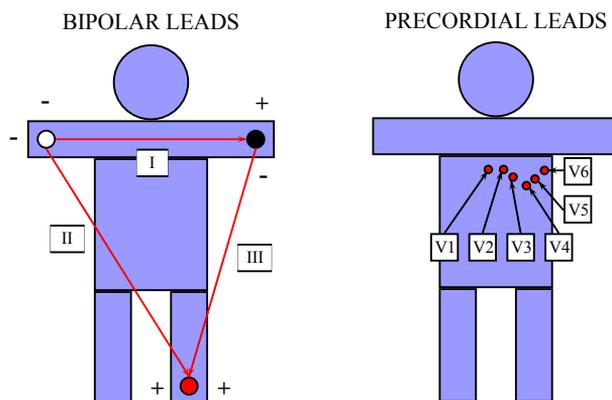
Figure 1.3: Electrode locations for the 12-standard-leads ECG.

Vectorcardiogram

The vectorcardiogram (VCG) is obtained from an ECG set-up composed of 3 orthogonal leads. A VCG set-up is attractive because it reflects the heart electrical activity in 3 perpendicular directions X, Y and Z. The interpretation of the VCG is not limited to separate leads, but additional information is obtained from the three-dimensional beat "loops" traced by the end point of the vector which defines the dominant direction of the electrical wavefront [14] (see Fig. 1.5).
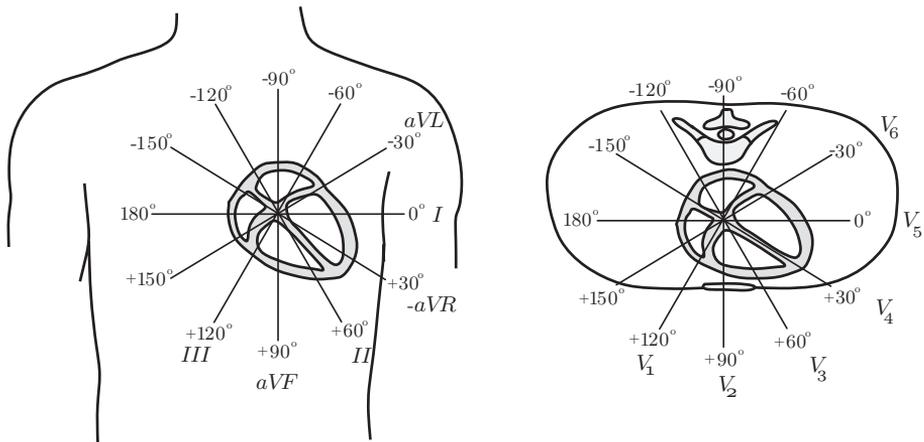
Figure 1.4: Directions of the 12-standard-leads ECG: (a) Bipolar and augmented limb leads, and (b) precordial leads (From [14]).
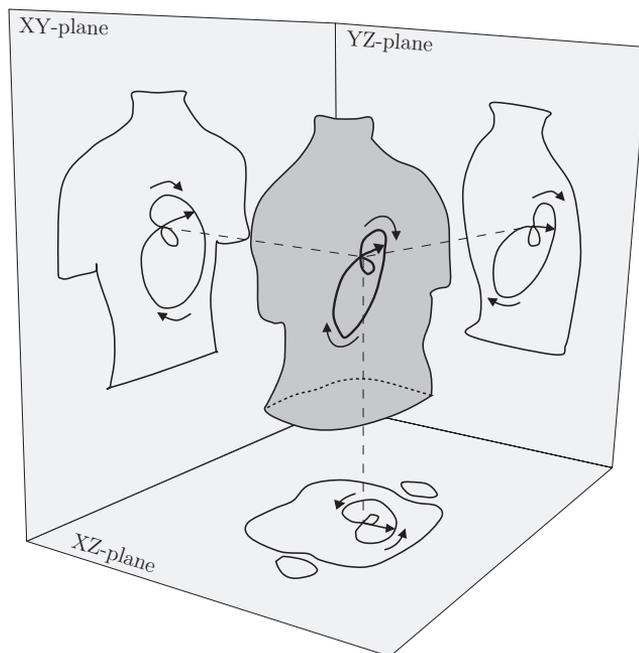
Figure 1.5: A VCG loop and its projection onto the three orthogonal planes. The two arrows outside each loop indicate the direction in which the loop evolves (From [14]).

Autonomic information in the electrocardiogram

The autonomic control of the heart rate have been exploited for ANS assessment in many studies. There is ANS information in beat occurrence

since the ANS controls the heart rate by exciting the sinus node. Heart rate varies along the time, e.g., it is lower in rest conditions than during exercise but, even during periods with the same heart rate mean, there are still variations in heart rate. These short-term variations in heart rate are known as heart rate variability (HRV), and they remain the most extended tool for ECG-based ANS assessment. The methods of HRV measurement were standardized and its physiological and pathophysiolocal correlates were defined by a Task Force constituted by the European Society of Cardiology and the North American Society of Pacing and Electrophysiology [19].

In this way, HRV analysis is subjected to sinus beat occurrence time. The most appropriate fiducial point to determine such beat occurrence is the P wave onset. However, P wave has a very low energy so using this wave to accurately determine the fiducial points is an extremely difficult task. For this reason, the fiducial point is usually based on QRS complex which has a much larger energy and so its detection is much more reliable. The use of RR intervals (led by successive R points) is generally accepted, considering that PR interval is relatively fixed and so, that the RR intervals reflect the activity of the sinus node [14]. It is necessary to remark that sometimes a mass of heart cells not located in the sinus node may generate an electrical impulse before the sinus node, generating a phenomenon known as *ectopic beat*. These ectopic beats does not reflect the activity of the sinus node, so they must be excluded in HRV analysis leading to a new interval series commonly denoted normal-to-normal intervals, or NN intervals.

Several NN interval series representations have been used. The simplest one is the so-called *interval tachogram* which is a signal composed of successive NN intervals:

$$d_{\mathrm{IT}}(k) = t_k - t_{k-1},\tag{1.7}$$

where t_k denotes the time occurrence of the kth sinus beat.

Another NN interval series representation is the *inverse interval tachogram*, which is similar to the interval tachogram but reflecting the heart rate:

$$d_{\mathrm{IIT}}(k) = \frac{1}{t_k - t_{k-1}}.\tag{1.8}$$

Note that both interval tachogram and its inverse are discrete signals that represent different amplitudes related to the NN interval series at each heartbeat, but heartbeats occur non-uniformly in time. For this reason, it is more common to use functions which represent the same information on a

continuous-time basis taking in account the time instant when each heart-beat occurs. These functions are known as *interval function* and *inverse interval function* and they are defined as:

$$d_{\mathrm{IF}}^{u}(t) = \sum_{k} [t_k - t_{k-1}] \, \delta \, (t - t_k) \tag{1.9}$$

$$d_{\mathrm{IIF}}^{u}(t) = \sum_{k} \left[\frac{1}{t_k - t_{k-1}} \right] \delta \, (t - t_k), \tag{1.10}$$

where the superscript "u" denotes that the signal is unevenly sampled.

Methods of HRV measurement can be divided into 2 groups. On one hand the *time domain methods*, which are based on statistical or geometric measurements of the NN interval series, such as the standard deviation (SD) of the NN intervals (so-called SDNN), the root mean square (RMS) of differences of successive NN intervals (so-called rMSSD), or the number of differences of successive NN intervals greater than 50 ms (so-called NN50), among others.

On the other hand, the *frequency domain methods* are subjected to a power spectrum density (PSD) estimation from a fragment of an NN interval series representation, usually of 2-5 minutes of length. Two main spectral bands are studied in an HRV PSD: the low frequency (LF) (tipically [0.04, 0.15] Hz), and the high frequency (HF) (typically [0.15, 0.4] Hz) bands.

The physiological interpretation of these frequency components of HRV has been studied by inferring sympathetic and/or parasympathetic block-ades. Sympathetic blockade leads to a power decrease in LF band, while parasympathetic blockade leads to a power decrease in both LF and HF band [20]. In this way, HF band is accepted to be majorly contributed by parasympathetic system, and LF is thought to reflect both sympathetic and parasympathetic systems. Consequently, the LF/HF ratio is considered by some investigators to mirror sympathovagal balance or to reflect the sym-pathetic modulations [19]. In fact, normal range of human respiration in rest conditions is [0.08, 0.5] Hz, so it is not a surprising situation that res-piration, which is parasympathetic related, is in the LF band. Respiration may also exceed the classical range of HF, as it usually does in exercise conditions [21]. In these situations when the respiratory rate is out of the classical HF band, the analysis of HRV within the standard frequency bands would yield inaccurate estimates of the ANS activity [22]. Because of this, in some studies the HF band is centered at the respiratory rate using either a constant or a time-dependent bandwidth [23, 24].

Autonomic information in the ECG is not limited to the HRV. There are other methods to extract ANS-related information from the ECG such as heart rate turbulence (HRT), which describes short-term fluctuations in heart rate that follow ventricular ectopic beats [25]. Systolic blood pressure (BP) produced by a ventricular ectopic beat is considerably lower than that of a normal sinus beat [26]. This phenomenon acts as trigger of a pattern in the heart rate, which in normal subjects shows a briefly acceleration and subsequently a deceleration before returning to baseline [25]. The control system that provokes this pattern is the baroreflex sytem, which is part of ANS and one of the mechanisms of the body to maintain BP at the homeostatic levels. Different patterns may be observed in subjects with some ANS-related pathology, and the clinical use of these difference has been studied in several applications such as prediction of mortality after acute myocardial infarction [27].

Respiratory information in the electrocardiogram

It is well known that respiration affects ECG signals in several ways. On one hand, respiration modulates the heart rate, which is higher during inspiration than during expiration [28–30]. This phenomenon is known as respiratory sinus arrhythmia (RSA). It has been reported that the amplitude of these heart rate oscillations decreases as the respiratory rate increases [31].

On the other hand, ECG morphology is also affected by respiration through relative movements of the electrodes with respect to the heart, and changes of impedance distribution in thorax due to the filling and emptying of the lungs [10].

Several methods for deriving respiratory information from ECG signals have been proposed. A new ECG-morphology-based method for deriving respiratory rate from ECG signals which exploits the respiration-induced variations in QRS slopes and R-wave angle is proposed in Chapter 2 of this thesis, with the purpose to serve as EDR even at highly non-stationary and noisy scenarios.

1.3.2   Pulse photoplethysmographic signal

Photoplethysmography is a technique introduced by Hertzman [32] which allows to measure blood volume variations in the microvascular bed of tissue. The signals acquired by using this technique are known as PPG signals. Photoplethysmography consists of illuminating the tissue and simultaneously measuring the transmitted (*transmission mode* PPG signal) or the

reflected light (*reflection mode* PPG light) using a specific wavelength. An example of PPG signal can be observed in Fig. 1.6.
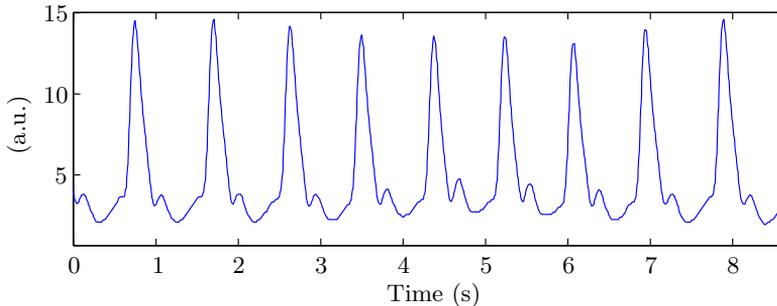
Figure 1.6: Example of PPG signal.

The PPG signal has two components: one component reflecting the arterial pulse produced by the heartbeats (AC component), and another component due to the non-pulsating blood volume and the surrounding tissue, producing a signal with slow changes (DC component). The morphology of the PPG pulses can be divided into two phases. On one hand, the rise of the pulse which corresponds to the systole, and the descent of the pulse which corresponds to the diastole and the wave reflections. PPG pulses from subjects with no arterial compliance problems usually present a *dichrotic notch*. Figure 1.7 shows morphology of PPG pulses from 2 subjects in ears, fingers, and toes [33].

Photoplethysmography-based techniques have been proposed for many clinical settings such as physiological monitoring, vascular assessment, and ANS study [35]. Probably, the most clinically adopted PPG-signals-based device is the pulse oximeter, which is mainly used to monitor the peripheral oxygen saturation (SpO_2) and it usually offers more physiological information such as pulse rate. It is important to remark that oxygenated haemoglobin and non-oxygenated haemoglobin have different light-absorption properties, and that these properties depend on the light wavelength. Exploiting these facts, SpO2 can be measured by using two PPG signals acquired at the same location by using two different wavelengths, typically in the red and infrared bands. The method is based on the ratio between AC and DC components of the two PPG signals:

$$R = \frac{AC_{R}/DC_{R}}{AC_{IR}/DC_{IR}}, \tag{1.11}$$
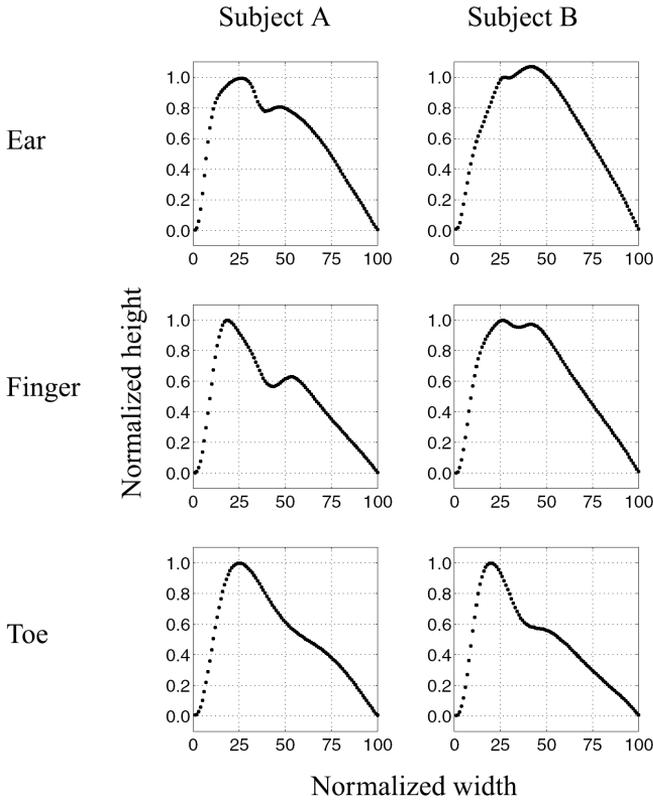
Figure 1.7: Morphology of PPG pulse from two subjects (From [34]).

where AC_R, DC_R, AC_{IR}, and DC_{IR} denote the AC and DC components of the red ("R" subindex) and the infrared ("IR" subindex) PPG signals. The manufacturers calibrate pulse oximeters empirically by using PPG signals obtained from a large group of healthy volunteers and a reference blood oxygen saturation from a standard in vitro CO-oximeter [36].

Smartphone-camera-acquired pulse photoplethysmographic signal

Smartphone devices can record PPG signals based on light emitted by flash and received by a camera [37, 38]. The smartphone-camera-acquired PPG (SCPPG) signals are usually extracted from an average of a pixel region of the green video signal at each frame. The reason for using only the green band is that there is high absorption by hemoglobin in the green range, and it has been demonstrated to give a stronger cardiac pulse signal than the red or blue bands during remote PPG imaging [39–42]. Then the signal is

inverted by multiplying it by -1 in order to obtain the traditional waveform. An example of a SCPPG signal can be observed in Fig. 1.8.

Smartphones are interesting devices in ambulatory scenarios due to significant advancements in the computational power which enables complex signal processing algorithms to be performed in real time. Certainly, built-in wireless communications feature of the smartphones facilitates ease of data transfer. These features make smartphones very valuable as take-anywhere and easy-to-use physiological monitors [41].
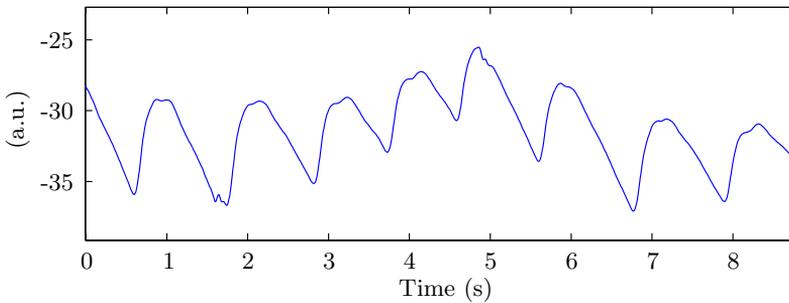
Figure 1.8: Example of SCPPG signal.

It should be noted that, however, SCPPG signals are more vulnerable to ambient-light interferences and variations in finger pressure over the sensor, making them, in general, noisier than conventional PPG signals obtained by pulse oximeter sensors. Furthermore, their sampling rate is lower. Thus, deriving physiological information from SCPPG signals remains a more challenging situation than deriving it from conventional PPG signals, and the performance of known methods which have been tested with conventional PPG signals must be tested also with SCPPG signals.

Photoplethysmography for blood pressure monitoring

BP is the pressure exerted by the blood flux over the arteries walls. When the heart beats, a blood volume is pumped out from it to the arteries increasing BP which reaches its maximum in that cardiac cycle, known as *systolic pressure*. When the heart relaxes between successive beats, BP decreases and it falls to its minimum value in that cardiac cycle, which is known as *diastolic pressure*. BP is usually quantified in the clinical routine with a pair of numbers which correspond to the systolic and the diastolic pressures, e.g., 120/80 mmHg.

Several techniques for measuring BP have been proposed, such as *auscultatory*, *oscillometric*, *ultrasound*, and *tonometry* methods. The auscultatory methods have been the most used methods in clinical settings, but they are gradually being replaced by other techniques that are more adequate for automatic measures [43], such as the oscillometric methods [44].

Photoplethysmography is also applied by some BP monitoring methods also known as *finger cuff* methods. These methods consist in arranging a finger cuff around a finger of a patient, which exerts pressure to that finger in order to maintain the artery diameter (blood volume) measured by an infrared PPG signal. This PPG signal is considered to be inversely proportional to the artery diameter and it is used for controlling the amount of exerted pressure, trying to keep constant the diameter of the finger artery. Then, the exerted pressure is directly linked to the BP [45,46]. This method has been validated using intra-arterial pressures invasively measured [47]. However, it is unmanageable in clinical settings because of its cost, inconvenience, and relative inaccuracy for measuring absolute levels of BP. Nevertheless, it is very interesting in research studies assessing short-term changes of BP and its variability [43], because it offers a continuous monitoring (not limited to the systolic/diastolic BP) in a non-invasive way. An example of BP signal measured by a cuff-finger based BP monitor (Finometer [46]) can be observed in Fig. 1.9.
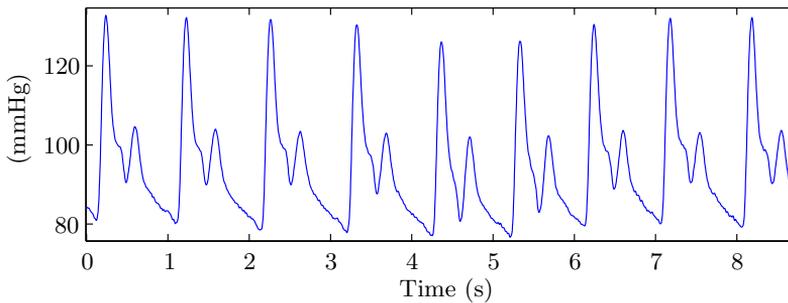
Figure 1.9: Example of BP signal recorded by Finometer system [46].

Autonomic information in the PPG signal

The useful information for clinical/physiological monitoring in PPG signals is not limited to the SpO_2, but also for other parameters such as its pulse rate and its variability (PRV), which is not an exact surrogate of HRV [48]

but they are highly correlated even during non-stationary conditions [49,50]. Similarly, PRT have been studied as a surrogate of HRT [51].

PPG signals reflect not only cardiac information but also vascular information, allowing us to asses ANS information through its effects on blood vessels, such as vasoconstriction which is reflected in the PPG signal by decreases in the signal amplitude fluctuation [52,53]. Vasoconstrictions events detected with PPG-based techniques have been proposed for OSAS screening either by themselves [54] and in combination with other ANS-related information such as HRV [55]. The use of HRV requires ECG as an additional recording. This is a disadvantage that takes more relevance in sleep studies context where a high number of sensors over the patient can affect the physiological sleep. In Chapter 5 of this thesis, a similar method to that presented in [55] is described, this time evaluating the possibility of using the PRV obtained from the PPG signal instead of the HRV. Although the high correlation between HRV and PRV decreases during obstructive apnea episodes [56], PRV still carries ANS-related information which can be exploited.

Respiratory information in the pulse photoplethysmographic signal

Deriving respiratory information from PPG signal is especially interesting. PPG signal can be provided by a pulse oximeter, which is economical, comfortable, and widely used in clinical routine for SpO_2 measurement. It allows to know if a low oxygen saturation is due to low respiratory rates or is the result of a low degree of gas exchange in the lungs, which can represent a dangerous physiological condition [57]. SpO_2 is a very important parameter in studies concerning respiration and essential in many situations such as sleep apnea diagnosis. Obtaining accurate respiratory signal from a pulse oximeter would allow us to consider an ambulatory diagnosis with its both social and economic advantages. In the health/sports tracking applications, the use of PPG signal has the advantage of the ability to acquire the signal at different parts of the body (i.e. fingers, ears, forehead) depending on the specific activity.

Known methods for deriving respiratory information from the PPG signal exploit variations on pulse morphology and/or occurrence. PRV has a respiratory component as HRV does because they are highly correlated and so, PRV can be used as respiratory information source similarly to HRV. Respiration also modulates the morphology of the PPG signal. Inspiration

can lead to a reduction in tissue blood volume, and this lowers the amplitude of the PPG signal. This reduction in tissue blood volume is generated by two different mechanisms: a reduction of cardiac output, and a reduction of intra-thoracic pressure [58]. A new PPG-morphology-based method for deriving respiratory rate from PPG signals which exploits the respiration-induced variations in pulse width is proposed in Chapter 3 of this thesis. This method was adapted and evaluated over SCPPG signals as described in Chapter 4 of this thesis.

1.3.3   Obstructive sleep apnea syndrome

OSAS is characterized by an interruption of the airflow to the lungs produced by an upper airways occlusion during sleep. Then SpO_2 goes down across time and mechanical respiratory efforts are intensified in order to reopen upper airways. If these efforts are not enough and hypercapnia level evolves dangerous, an arousal is generated to reactive all the peripheral systems and the respiration is restored. These episodes could occur hundreds of times in a single night and may produce serious health implications [59].

The open-close cycle in the upper airways produces a regular oscillatory state of peripheral systems such as cardiac and vascular. For instance, heart rate decrements during apnea and increases during restore breathing, while vascular system presents vasoconstriction during apnea and vasodilatation after apnea [55]. Complications of OSAS in adults may include increasing risk of hypertension [60] and stroke [61], and other important implications such as motor vehicle accidents [62, 63]. Complications of OSAS in children are quite different since they are in their growth process. These complications may include growth abnormalities [64–66], neurologic disorders [67–69], and cor pulmonale [70–72], especially in severe cases [73].

Polysomnography (PSG) is the gold standard procedure for OSAS diagnosis. It consists of an overnight recording which require a sleep laboratory and includes a high number of biomedical signals [63], being quite involved and difficult to use in ambulatory scenario. In Chapter 5 of this thesis, a technique for ambulatory diagnosis of OSAS in children based on PPG signal is presented.

1.4   Objective and outline of the thesis

The main objective of this thesis is to develop non-invasive methods for respiration information extraction from biomedical signals which are widely

adopted in clinical routine. Novel methods for deriving respiratory rate from ECG and from PPG signal are developed.

The content of the thesis is organized as follows:

- **Chapter 2:** A novel beat-morphology based method for estimating respiratory rate from ECG signals is presented in this chapter. It is based on QRS slopes and R-wave angle, which reflect respiration-induced beat morphology variations. Evaluation is performed over two databases containing ECG and respiratory signals simultaneously recorded during two clinical tests with different characteristics: tilt test, representing abrupt cardiovascular changes, and stress test representing more gradual cardiovascular changes but a highly noisy environment. The research described in this chapter generated the following publications:

  - J. Lázaro, A. Alcaine, D. Romero, E. Gil, P. Laguna, E. Pueyo, and R. Bailón. Electrocardiogram derived respiratory rate from QRS slopes and R-wave angle, *Annals of Biomedical Engineering*, 40(10):2072-2083, 2014.
  - J. Lázaro, A. Alcaine, D. Romero, E. Gil, P. Laguna, L. Sörnmo, and R. Bailón. Electrocardiogram derived respiration from QRS slopes: Evaluation with stress testing recordings, *XL International Conference on Computing in Cardiology*, 655-658, 2013.
  - J. Lázaro, A. Alcaine, E. Gil, P. Laguna and R. Bailón. Electrocardiogram derived respiration from QRS slopes. *35nd Annual International Conference of the IEEE EMBS*, 3913-3916, 2013.

- **Chapter 3:** A novel method for deriving respiration from PPG signal is presented. This method is based on the pulse width variability (PWV), and it exploits the respiratory information present in the pulse wave velocity and dispersion. PWV information is also combined with other PPG-based methods such as pulse amplitude variability (PAV) and PRV. Evaluation is performed over one of the databases used in Chapter 2: the database that contains signals recorded during a tilt table test, which in addition to ECG and respiratory signals, it also contains PPG and BP signals simultaneously recorded. The research described in this chapter generated the following publications:

  - J. Lázaro, E. Gil, R. Bailón, A. Mincholé, and P. Laguna. Deriving respiration from photoplethysmographic pulse width, *Medical & Biological Engineering & Computing*, 51:233-242, 2013.

– M. Pelaez, M. Orini, J. Lázaro, R. Bailon, and E. Gil. Cross time-frequency analysis for combining information of several sources. Application to estimation of spontaneous respiratory rate from photoplestimography, *Computational and Mathematical Methods in Medicine*, Volume 2013, Article ID 631978, 8 pages, 2013

– J. Lázaro, E. Gil, R. Bailón, and P. Laguna. Deriving Respiration from the Pulse Photoplethysmographic Signal, *XXXVIII International Conference on Computing in Cardiology*, 713-716, 2011.

- **Chapter 4:** The method for deriving respiratory rate from PPG signal described in Chapter 3 is adapted to derive respiratory rate from SCPPG signal in this chapter. Evaluation is performed on a database containing SCPPG signals recorded from 30 subjects during controlled respiration experiments at rates from 0.2 to 0.6 Hz with an increment of 0.1 Hz, using three different devices: iPhone 4S, iPod 5, and HTC. The research described in this chapter generated the following publications:

  – J. Lázaro, Y. Nam, E. Gil, P. Laguna, and K. H. Chon. Respiratory rate derived from smartphone-camera-acquired pulse photoplethysmographic signals, *Physiological Measurement*, under review (major revision).

  – J. Lázaro, R. Bailón, P. Laguna, Y. Nam, K. H. Chon, and E. Gil. Respiratory rate influence in the resulting magnitude of pulse photoplethysmogram derived respiration signals. *XLI International Conference on Computing in Cardiology*, 289-192, 2014.

  – J. Lázaro, Y. Nam, E. Gil, P. Laguna, and K. H. Chon. Smartphone-camera-acquired pulse photoplethysmographic signal for deriving respiratory rate. *8th Conference of the European Study Group on Cardiovascular Oscillations*, 121-122, 2014

- **Chapter 5:** A technique for ambulatory diagnosis of the OSAS in children based on PPG signal is presented in this chapter. Decreases in amplitude fluctuations of the PPG signal (DAP) events have been proposed as OSAS discriminator in the literature, since they are related to vasoconstriction associated to apnea. HRV analysis during these DAP events has been proposed to discriminate between DAP

events related or unrelated to an apneic event. The use of HRV requires ECG as an additional recording, meaning a disadvantage that takes more relevance in sleep studies context where the number of sensors is tried to be minimized in order not to affect the physiological sleep. This study proposes the use of PRV extracted from the PPG signal instead of HRV. Results suggest that PRV can be used in apnea detectors based on DAP events, to discriminate apneic from nonapneic events avoiding the need for ECG recordings. The research described in this chapter generated the following publications:

- J. Lázaro, E. Gil, J. M. Vergara, and P. Laguna. Pulse rate variability analysis for discrimination of sleep-apnea-related decreases in the amplitude fluctuations of PPG signal in children, *IEEE Journal of Biomedical and Health Informatics*, 18(1):240-246, 2014.

- R. Jané, J. Lázaro, P. Ruiz, E. Gil, D. Navajas, R. Farré, and P. Laguna, Obstructive sleep apnea in a rat model: Effects of anesthesia on autonomic evaluation from heart rate variability measures, *XL International Conference on Computing in Cardiology*, 1011-1014, 2013.

- J. Lázaro, E. Gil, J. M. Vergara, and P. Laguna, OSAS detection in children by using PPG amplitude fluctuation decreases and pulse rate variability. *XXXIX International Conference on Computing in Cardiology*, 185-188, 2012.

• **Chapter 6:** The final chapter contains the conclusions and the possible extensions of this thesis.

Fill your paper with the
breathings of your heart.
William Wordsworth.

Chapter 2

ECG derived respiration from QRS slopes and R-wave angle

2.1   Introduction

Respiration affects ECG signals in several ways. On one hand, it is well known that respiration modulates the heart rate, which is higher during inspiration than during expiration [28–30]. It has been reported that the amplitude of this oscillation decreases when the respiratory rate increases [31]. On the other hand, ECG morphology is also affected by respiration through movements of the electrodes with respect to the heart, and changes of impedance distribution in thorax due to the filling and emptying of the lungs [10].

Several algorithms for deriving respiratory rate from the ECG have been developed. Some of them are collected in [10]. Probably, the simplest morphology-based methods are those based on the R-wave amplitude, either with respect to the baseline or with respect to the S-wave amplitude [74]. Other more complex morphological features of the ECG signal have been exploited to obtain respiratory rate, such as variations of QRS area [75] or electrical axis rotation [76]. In [21], respiratory rate is derived from beat-to-beat variations of the heart electrical axis between VCG loops. There also have been proposed methods that exploit both beat occurrence and morphology such as [77] or [78].

In this thesis, a novel beat-morphology-based technique have been developed. It exploits morphological variations in the ECG, in particular those

variations of QRS slopes and R-wave. Both QRS slopes and R-wave angles have been previously proposed as a marker of ischemia [79–81].

Evaluation of proposed methods was performed over two databases which contains ECG and respiration signals simultaneously recorded during two tests which represent different conditions. One of them contains signals recorded during a tilt table test, which is characterized by abrupt cardiovascular changes. The other one contains signals recorded during a stress test, representing a highly non-stationary and noisy environment.

2.2 Materials

2.2.1 Tilt test data

The tilt test dataset is composed by 17 (11 men) recordings from volunteers, aged 28.5 ± 2.5 years, during a tilt table test. Tilt test is clinically used for testing the sympathetic nervous system response to blood pressure variations induced by postural changes [82]. In particular, the tilt table test was performed according to the following protocol: 4 min in early supine position, 5 min tilted head-up to an angle of 70°, and 4 min to later supine position. The transitions between these 3 stages lasted 18 s.

Following signals were simultaneously recorded:

1. The respiration signal, by using a pneumogram transducer (TSD201, Biopac) and an amplifier (RSP100C, Biopac), with a sampling rate of 125 Hz.

2. The 12 standard lead ECG signal, by using removable Ag-AgCl electrodes and an amplifier (ECG100C, Biopac), with a sampling rate of $f_s^{\mathrm{E}} = 1000$ Hz.

3. The BP signal, by using a non-invasive device (Finometer, Finapress Medical Systems), which provides a continuous signal placed in the right index finger, with a sampling rate of 250 Hz.

4. The PPG signal, by using a transducer (TSD200, Biopac) and an amplifier (OXY100C, Biopac), with a sampling rate of 250 Hz.

Further details of this data can be found in [83].

2.2.2 Stress test data

This database contains recordings from 14 volunteers (10 males) aged 28 ± 4 years and 20 patients (16 males) aged 58 ± 14 years, referred to the Depart-

ment of Clinical Physiology at the University Hospital of Lund, Sweden, for stress testing. The stress test was performed on a bicycle ergometer Siemens-Elema Ergoline 900C. The initial workload (50 W for males and 30 W for females) was increased at a rate of 15 W/ min for males and 10 W/min for females, until a rate of perceived exertion (according to Borg scale [84]) of 15 for volunteers and of 17 for patients was reached, unless other clinical stopping criteria (e.g., chest pain or tachycardia) occurred first.

Following signals were simultaneously recorded:

1. The respiration signal, by an airflow thermistor (Sleepmate), an amplifier (DA100C, Biopac) and a digitalizer (MP100, Biopac), with a sampling rate of 50 Hz.

2. The 12 standard lead ECG signal, by using the Siemens-Elema Megacart front-end, with a sampling rate of 1000 Hz.

Further details of this data can be found in [21].

2.3 Methods

2.3.1 Preprocessing

VCG was obtained by using the inverse Dower matrix [85], whose degree of accuracy is generally accepted to be high enough to be considered as a satisfactory method of derivation of the QRS complex [86]. QRS complexes in all ECG leads were automatically detected by using a wavelet-based detector [87] and ectopic/misdetected beats were identified and removed using an algorithm described in [88]. Normal sinus beat locations are denoted $n_{N_{l,i}}$, where l represents ECG lead and i normal sinus beat order. Baseline was removed by a cubic-spline interpolation technique, which results in a linear filtering with a time-variable cut-off frequency, better tracking rapid baseline wander when compared to a fixed cut-off frequency approach while maintaining beat-to-beat variations. Then, for each lead l and normal sinus beat i, wave delineation was performed by using a wavelet-based technique [87] determining Q ($n_{Q_{l,i}}$), R ($n_{R_{l,i}}$), and S ($n_{S_{l,i}}$) peaks (or QRS end when no S wave is present), and QRS onset ($n_{ON_{l,i}}$).

2.3.2 Non-standard leads

Two non-standard leads were derived: the loop derived lead (LDL) and the N-loops derived lead (NLDL). Both of them are based on VCG-QRS loops.

LDL was presented in [80]. It tries to enhance the QRS magnitude by projecting VCG-QRS loop onto its dominant direction $\boldsymbol{u}_i$, obtained as:

$$\boldsymbol{u}_i = [u_{X_i}, u_{Y_i}, u_{Z_i}]^T = [l_X(n_{0_i}), l_Y(n_{0_i}), l_Z(n_{0_i})]^T, \qquad (2.1)$$

being $l_X(n)$, $l_Y(n)$, and $l_Z(n)$ the 3 VCG leads, and:

$$n_{0_i} = \underset{n \in \Omega_{\mathrm{QRS}_i}}{\arg\max} \left[l_X^2(n) + l_Y^2(n) + l_Z^2(n) \right], \qquad (2.2)$$

where Ω_{QRS_i} is a 140 ms interval starting 10 ms before the earliest QRS onset in the 3 VCG leads, n_{ON_i}:

$$n_{\mathrm{ON}_i} = \min \left\{ n_{\mathrm{ON}X,i}, n_{\mathrm{ON}Y,i}, n_{\mathrm{ON}Z,i} \right\} \qquad (2.3)$$

$$\Omega_{\mathrm{QRS}_i} = [n_{\mathrm{ON}_i} - 0.01 f_s^{\mathrm{E}}, \quad n_{\mathrm{ON}_i} + 0.13 f_s^{\mathrm{E}}]. \qquad (2.4)$$

Then, the LDL $l_{\mathrm{LDL}}(n)$ is computed at each beat as:

$$l_{\mathrm{LDL}}(n) = \frac{[l_X(n), l_Y(n), l_Z(n)] \, \boldsymbol{u}_i}{||\boldsymbol{u}_i||}, \quad \forall n \in \Omega_{\mathrm{QRS}_i}. \qquad (2.5)$$

In this way, the beat-to-beat variations of the dominant direction of VCG-QRS loop are followed by $l_{\mathrm{LDL}}(n)$. Following these variations may be counter-productive in this application, since they are in part due to respiration [10, 75, 76]. For this reason, NLDL is proposed as a slight modification of LDL. The NLDL is similar to the LDL, but the dominant direction of VCG-QRS loops is estimated with the first N beats and it is not updated. In mathematical terms, the NLDL is defined as:

$$\bar{\boldsymbol{u}} = \sum_{i=1}^{N} \left\{ \frac{\boldsymbol{u}_i}{||\boldsymbol{u}_i||} \right\} \qquad (2.6)$$

$$l_{\mathrm{NLDL}}(n) = \frac{[l_X(n), l_Y(n), l_Z(n)] \, \bar{\boldsymbol{u}}}{||\bar{\boldsymbol{u}}||}, \qquad (2.7)$$

being N set to 5 beats in this work.

2.3.3 QRS slopes measurement

QRS slopes were measured by using the algorithm presented in [79]. For each beat, two slopes are measured: upward slope of the R wave ($\mathcal{I}_{\mathrm{US}_{l,i}}$) and downward slope of the R wave ($\mathcal{I}_{\mathrm{DS}_{l,i}}$).

First, time instants associated with the maximum variation points of the ECG signal between $n_{Q_{l,i}}$ and $n_{R_{l,i}}$, and between $n_{R_{l,i}}$ and $n_{S_{l,i}}$ are computed as:

$$n_{U_{l,i}} = \arg\max_n \left\{ \left| l'_l(n) \right| \right\}, \qquad n \in \left[n_{Q_{l,i}}, n_{R_{l,i}} \right] \tag{2.8}$$

$$n_{D_{l,i}} = \arg\max_n \left\{ \left| l'_l(n) \right| \right\}, \qquad n \in \left[n_{R_{l,i}}, n_{S_{l,i}} \right], \tag{2.9}$$

where $l'_l(n)$ is the first derivative of lead l computed as:

$$l'_l(n) = l_l(n) - l_l(n-1). \tag{2.10}$$

Finally, a straight line is fitted to the ECG signal by least squares in two 8 ms-length intervals, one of them centred at $n_{U_{l,i}}$ and the other one at $n_{D_{l,i}}$. The slopes of these lines are denoted $\mathcal{I}_{US_{l,i}}$ and $\mathcal{I}_{DS_{l,i}}$, respectively. Fig. 2.1 illustrates relevant points taking part in this measurement algorithm.

2.3.4 R-wave angle measurement

The R-wave angle is also used to derive respiratory rate in this work. This angle was defined as in [81], i.e., it corresponds to the smallest angle formed by the straight lines that define $\mathcal{I}_{US_{l,i}}$ and $\mathcal{I}_{DS_{l,i}}$. Assuming a two-dimensional euclidean space coordinate system, the general equation that defines this angle is:

$$\phi = \arctan\left(\left| \frac{\mathcal{I}_1 - \mathcal{I}_2}{1 + \mathcal{I}_1\mathcal{I}_2} \right| \right), \tag{2.11}$$

where $\mathcal{I}_1$ and $\mathcal{I}_2$ denote the slopes of the straight lines forming the angle.

The units of the horizontal axis (time) and vertical axis (voltage) were rescaled to match the particular case of conventional ECG tracings in clinical printouts, where a speed of 25 mm/s and a gain of 10 mm/mV are used as in [81], so the angle expression assuming a sampling rate of 1000 Hz and amplitude expressed in mV results in:

$$\phi_{R_{l,i}} = \arctan\left(\left| \frac{\mathcal{I}_{US_{l,i}} - \mathcal{I}_{DS_{l,i}}}{0.4 \left(6.25 + \mathcal{I}_{US_{l,i}}\mathcal{I}_{DS_{l,i}} \right)} \right| \right). \tag{2.12}$$

2.3.5 Electrocardiogram derived respiration signals

Based on QRS slopes or R-wave angle

An ECG derived respiration (EDR) signal was generated for each one of the QRS slopes series by assigning to each beat occurrence $n_{N_{l,i}}$, the value of
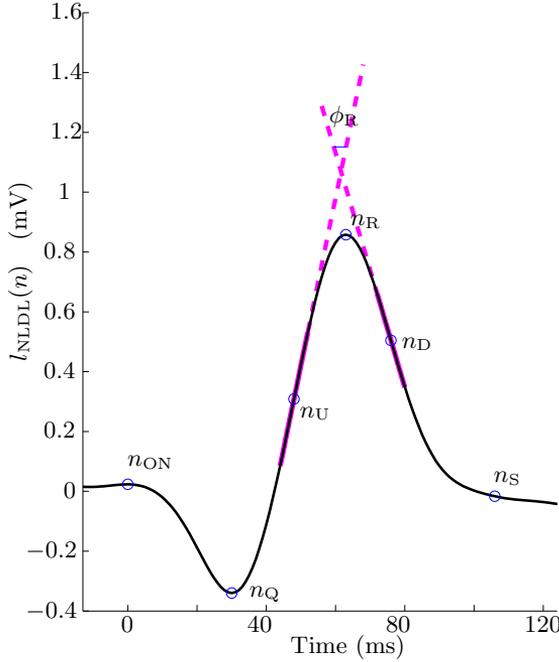
Figure 2.1: Relevant points over an example of QRS from $l_{\mathrm{NLDL}}(n)$. Thick magenta lines represent the two straight lines best suited to the QRS slopes by least square, and from which the slope series are obtained. R-wave angle series are obtained from the smallest angle formed by these two lines.

its associated QRS slope:

$$d^u_{\{\mathrm{US,\ DS}\}_l}(n) = \sum_i \mathcal{I}_{\{\mathrm{US,\ DS}\}_{l,i}} \delta\left(n - n_{\mathrm{N}_{l,i}}\right), \qquad (2.13)$$

where the superindex "u" denotes the signal is unevenly sampled. An EDR signal was generated for each one of the R-wave angle series in a similar way:

$$d^u_{\mathrm{R}_l}(n) = \sum_i \phi_{\mathrm{R}_{l,i}} \delta\left(n - n_{\mathrm{N}_{l,i}}\right). \qquad (2.14)$$

Then, a median absolute deviation (MAD)-based outlier rejection rule was applied as in [10], and subsequently, a 4 Hz evenly sampled version of each EDR signal was obtained by cubic-splines interpolation. Finally, a band-pass filter (0.075–1) Hz was applied. These filtered signals are denoted with the same nomenclature than the unevenly sampled versions, but without the superindex "u", e.g., $d_{\mathrm{US_{NLDL}}}(n)$ is the 4-Hz, outlier-rejected, evenly sampled, band-pass filtered version of $d^u_{\mathrm{US_{NLDL}}}(n)$.

Fig. 2.2 shows an example of some EDR signals and the reference respiratory signal $r(n)$ from stress test dataset during resting, stress peak and recovery phases. It can be observed that EDR signals and $r(n)$ are oscillating at very similar rates, which notably differ at each phase of the protocol.

A total of 51 EDR signals were studied corresponding to the 2 QRS slopes and 1 angle series ($\mathcal{I}_{\mathrm{US}_{l,i}}$, $\mathcal{I}_{\mathrm{DS}_{l,i}}$ and $\phi_{\mathrm{R}_{l,i}}$) in the 17 studied leads.
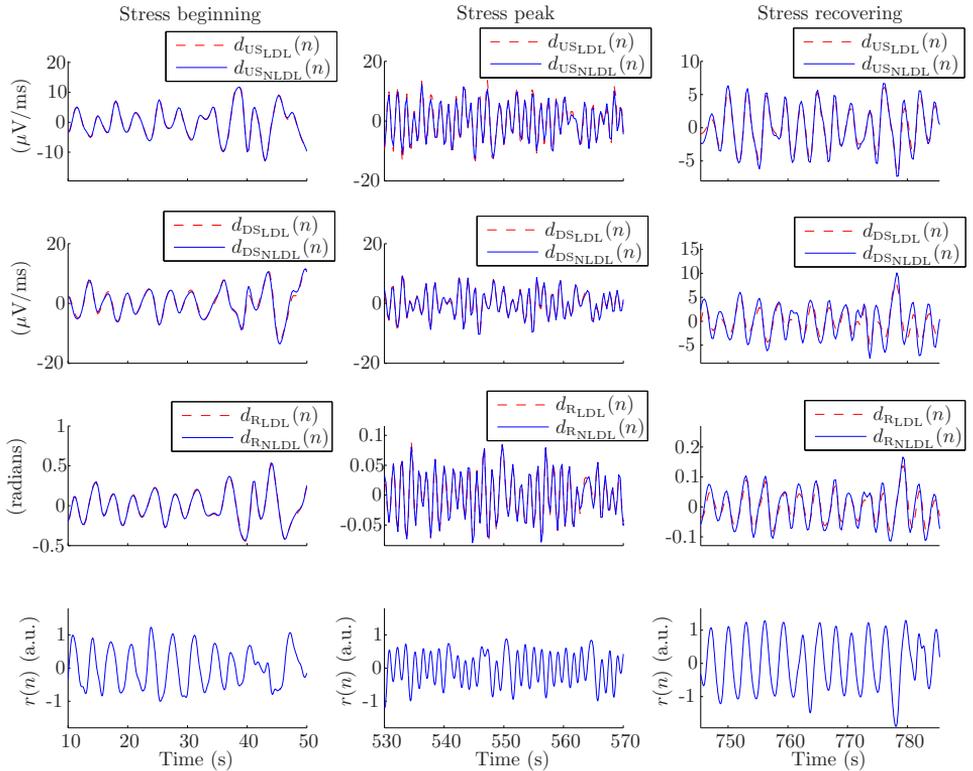
Figure 2.2: Example of some EDR signals and the reference respiratory signal $r(n)$ from stress test dataset during different phases of the protocol: stress beginning (≈ 0.3 Hz), peak (≈ 0.7 Hz) and recovery (≈ 0.35 Hz). It can be observed that EDR signals and $r(n)$ are oscillating at very similar rates, which notably differ at each phase of the protocol.

Based on electrical axis rotation angles

Three additional EDR signals were also studied for comparison purposes. These EDR signals were presented in [21] and they are based on heart-electrical-axis-rotation angle variations induced by respiration. The EDR signals are defined by the series of least-squares-estimated rotation angles between successive QRS-VCG loops and a reference loop.

The basis of the method is the minimization of a normalized distance ϵ between a reference loop ($\boldsymbol{Y}_{\mathrm{R}}$) and each observed loop ($\boldsymbol{Y}$) with respect to rotation, amplitude scaling, and time synchronization [89, 90]. In mathematical terms, the normalized distance ϵ for each QRS-VCG loop is defined as:

$$\epsilon = \frac{||\boldsymbol{Y}_{\mathrm{R}} - \gamma \boldsymbol{J}_{\boldsymbol{\tau}} \boldsymbol{Y} \boldsymbol{Q}||_F^2}{||\gamma \boldsymbol{J}_{\boldsymbol{\tau}} \boldsymbol{Y} \boldsymbol{Q}||_F^2}, \tag{2.15}$$

where $|| \cdot ||_F^2$ denotes the Frobenius norm, and

- $\boldsymbol{Y}_{\mathrm{R}}$ is an $N_s \times 3$ matrix (being N_s the number of samples of the QRS analysis window) containing the reference loop. Each column contains the QRS corresponding to each one of the 3 VCG leads.

- γ is a scalar that controls the amplitude scaling.

- $\boldsymbol{J}_{\boldsymbol{\tau}}$ is an $N_s \times (N + 2\Delta)$ matrix which controls the time synchronization:

$$\boldsymbol{J}_{\boldsymbol{\tau}} = [\boldsymbol{0}_{\Delta-\tau} \ \boldsymbol{I} \ \boldsymbol{0}_{\Delta-\tau}], \tag{2.16}$$

  where Δ is the number of symmetrically augmented samples which allow for time synchronization with $\tau = -\Delta, \ldots, \Delta$.

- $\boldsymbol{Y}$ is an $(N + 2\Delta) \times 3$ matrix containing the observed loop.

- $\boldsymbol{Q}$ is the rotation matrix and can be viewed as three successive rotations around each axis (VCG leads) defined by the rotation angles Φ_X, Φ_Y, and Φ_Z:

$$
\begin{aligned}
\boldsymbol{Q} &= \begin{bmatrix} 1 & 0 & 0 \\ 0 & \cos(\Phi_X) & \sin(\Phi_X) \\ 0 & -\sin(\Phi_X) & \cos(\Phi_X) \end{bmatrix} \times \begin{bmatrix} \cos(\Phi_Y) & 0 & \sin(\Phi_Y) \\ 0 & 1 & 0 \\ -\sin(\Phi_Y) & 0 & \cos(\Phi_Y) \end{bmatrix} \times \\
&\quad \times \begin{bmatrix} \cos(\Phi_Z) & \sin(\Phi_Z) & 0 \\ -\sin(\Phi_Z) & \cos(\Phi_Z) & 0 \\ 0 & 0 & 1 \end{bmatrix} = \\
&= \begin{bmatrix} * & \sin(\Phi_Z)\cos(\Phi_Y) & \sin(\Phi_Y) \\ * & * & \sin(\Phi_X)\cos(\Phi_Y) \\ * & * & * \end{bmatrix},
\end{aligned} \tag{2.17}
$$

  where $*$ denotes an omitted matrix entry.

The ϵ minimization process consists of estimating γ and $\boldsymbol{Q}$ for every τ and subsequently selecting that τ for which ϵ is minimum. The maximum-likelihood estimator of $\boldsymbol{Q}$ is computed by left ($\boldsymbol{U}_\tau$) and right ($\boldsymbol{V}_\tau$) singular

vectors from the SVD of $\boldsymbol{Y}_{\mathrm{R}}^T \boldsymbol{J}_\tau \boldsymbol{Y}$, and subsequently, γ_τ is obtained by [89, 90]:

$$\hat{\boldsymbol{Q}}_\tau = \boldsymbol{V}_\tau \boldsymbol{U}_\tau^T \qquad (2.18)$$

$$\hat{\gamma}_\tau = \frac{\mathrm{tr}\left(\boldsymbol{Y}_{\mathrm{R}}^T \boldsymbol{Y}_{\mathrm{R}}\right)}{\mathrm{tr}\left(\boldsymbol{Y}_{\mathrm{R}}^T \boldsymbol{J}_\tau^T \boldsymbol{Y} \hat{\boldsymbol{Q}}_\tau\right)}. \qquad (2.19)$$

Rotation angle series Φ_{X_i}, Φ_{Y_i}, and Φ_{Z_i} can be derived from that $\hat{\boldsymbol{Q}}_\tau$ which yields the minimal normalized distance ϵ by using the structure in (2.17). Subsequently, these three series were processed in the same way than QRS slopes and R-wave angle EDR signals (MAD-outlier-rejection rule, 4-Hz-spline interpolation, and (0.075-1 Hz) band-pass filtering) obtaining three EDR signals denoted $d_{\Phi_X}(n)$, $d_{\Phi_Y}(n)$ and $d_{\Phi_Z}(n)$ in this study.

2.3.6 Respiratory rate estimation algorithm

Respiratory rate estimation is based on the algorithm presented in [21]. It allows to combine information from several EDR signals increasing the robustness of the estimation. Let M be the number of EDR signals used for estimating respiratory rate. The algorithm can be divided into 3 phases: the power spectrum (PS) estimation, the peak-conditioned average, and the respiratory rate estimation.

The PS estimation is performed by using the Welch periodogram. For the jth EDR signal and k^{th} running interval of T_s-s length, the PS $S_{j,k}(f)$ is generated by an average of PS obtained from subintervals of T_m-s length $(T_m < T_s)$ using an overlap of $T_m/2$ s, after a power normalization in $[0, 1]$ Hz band (i.e., the power in this band is forzed to value 1). A spectrum is generated every t_s s.

The second phase is a peak-conditioned average. First, for each $S_{j,k}(f)$, the location of largest peak $f_{\mathrm{P}}^{\mathrm{I}}(j, k)$ is detected. Subsequently, a reference interval $\Omega_{\mathrm{R}}(k)$ where respiratory rate is estimated to be, is defined as:

$$\Omega_{\mathrm{R}}(k) = [f_{\mathrm{R}}(k-1) - \delta, \quad f_{\mathrm{R}}(k-1) + \delta], \qquad (2.20)$$

where $f_{\mathrm{R}}(k-1)$ is a respiratory frequency reference obtained from previous $(k-1)$ steps.

Then, $f_p^{\mathrm{II}}(j, k)$ is chosen as the nearest peak to $f_{\mathrm{R}}(k-1)$, among all peaks larger than 85% of $f_p^{\mathrm{I}}(j, k)$ inside $\Omega_{\mathrm{R}}(k)$. Note that $f_p^{\mathrm{II}}(j, k)$ can be the same $f_p^{\mathrm{I}}(j, k)$ if the largest peak is inside $\Omega_{\mathrm{R}}(k)$ and it is also the nearest to $f_{\mathrm{R}}(k-1)$. An example of selection of $f_p^{\mathrm{I}}(j, k)$ and $f_p^{\mathrm{II}}(j, k)$ is shown in Fig. 2.3.
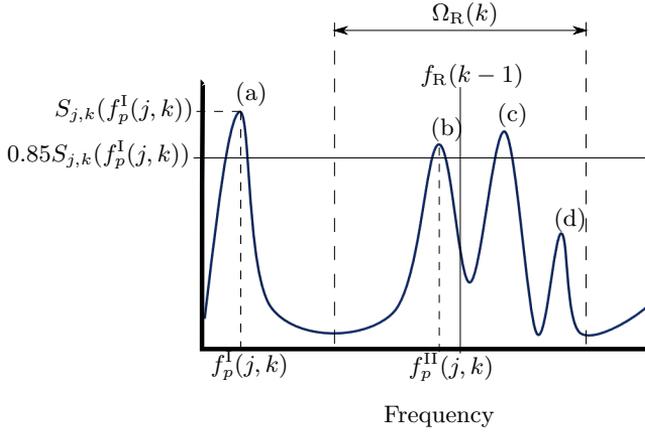
Figure 2.3: Example of selection of $f_p^{\mathrm{I}}(j,k)$ and $f_p^{\mathrm{II}}(j,k)$ for an hypothetical $S_{j,k}(f)$ and for a given $f_{\mathrm{R}}(k-1)$. Peak (a) is selected as $f_p^{\mathrm{I}}(j,k)$ because it is the highest peak. Then, peaks higher than 85% of the amplitude of peak (a) within $\Omega_{\mathrm{R}}(k)$ are detected, finding peaks (b) and (c), and discarding peak (d). Peak (b) is selected as $f_p^{\mathrm{II}}(j,k)$ because it is the nearest to $f_{\mathrm{R}}(k-1)$.

Afterwards, L_s spectra $S_{j,k}(f)$ are "peak-conditioned" averaged; only those $S_{j,k}(f)$ which are sufficiently peaked take part in the averaging. In this thesis, "peaked" denotes that $f_p^{\mathrm{II}}(j,k)$ exists and a certain percentage ξ of the spectral power must be contained in an interval centred around it. In mathematical terms, this averaging is defined as:

$$\bar{S}_k(f) = \sum_{l=0}^{L_s-1} \sum_{j} \chi_{j,k-l}^{\mathrm{A}} \chi_{j,k-l}^{\mathrm{B}} S_{j,k-l}(f), \qquad (2.21)$$

where $\chi_{j,k-l}^{\mathrm{A}}$ and $\chi_{j,k-l}^{\mathrm{B}}$ represent two criteria aimed at deciding whether power spectrum $S_{j,k-l}(f)$ is peaked enough or not, preventing those not peaked enough spectra from taking part in the average. On one hand, χ^{A} lets those spectra whose peakness is greater than a fixed value take part in the average, as shown in (4.28), and on the other hand, χ^{B} compares the spectra of different EDR signals, letting those spectra more peaked in each time instant take part in the average, although all them had passed the χ^{A} criterion, as shown in (4.29). Note that χ^{B} has no effect if the estimation is being accomplished from only one EDR signal ($M = 1$).

$$\chi_{j,k}^{\mathrm{A}} = \begin{cases} 1, & P_{j,k} \geq \xi \\ 0, & otherwise \end{cases} \qquad (2.22)$$

$$\chi_{j,k}^{\text{B}} = \begin{cases} 1, & P_{j,k} \geq \max_{j} \{P_{j,k}\} - \lambda \\ 0, & otherwise \end{cases} , \qquad (2.23)$$

where $P_{j,k}$ is defined by the percentage of power around $f_p^{\text{II}}(j,k)$ with respect to the total power in $\Omega_{\text{R}}(k)$:

$$P_{j,k} = \frac{\displaystyle\int_{\max\left\{f_p^{\text{II}}(j,k)-0.4\delta,\ f_{\text{R}}(k-1)-\delta\right\}}^{\min\left\{f_p^{\text{II}}(j,k)+0.4\delta,\ f_{\text{R}}(k-1)+\delta\right\}} S_{j,k}(f)df}{\displaystyle\int_{f_{\text{R}}(k-1)-\delta}^{f_{\text{R}}(k-1)+\delta} S_{j,k}(f)df}. \qquad (2.24)$$

Then, the algorithm searches the largest peak $f_p^{\text{I}a}(k)$ in $\bar{S}_k(f)$, and subsequently $f_p^{\text{II}a}(k)$ defined as the nearest to $f_{\text{R}}(k-1)$ inside $\Omega_{\text{R}}(k)$ which is at least larger than 85% of $f_p^{\text{I}a}(k)$. At this time the reference frequency $f_{\text{R}}(k)$ is updated as:

$$f_{\text{R}}(k) = \beta f_{\text{R}}(k-1) + (1-\beta) f_p(k), \qquad (2.25)$$

where β denotes the forgetting factor and $f_p(k)$ is defined by

$$f_p(k) = \begin{cases} f_p^{\text{II}a}(k), & \exists f_p^{\text{II}a}(k) \\ f_p^{\text{I}a}(k), & otherwise \end{cases} . \qquad (2.26)$$

Figure 2.4 shows an example of Welch periodogram spectra from $d_{\text{US}}(n)$, $d_{\text{DS}}(n)$, and $d_{\text{R}}(n)$, with limits of the integral that define $P_{j,k}$.

Finally, estimated respiratory rate $\hat{f}(k)$ is defined as:

$$\hat{f}(k) = \alpha \hat{f}(k-1) + (1-\alpha) f_p(k) \qquad (2.27)$$

$$\alpha = \begin{cases} \alpha_2, & \exists f_p^{\text{II}a}(k) \\ \alpha_1, & otherwise \end{cases} , \qquad (2.28)$$

where $\alpha_2 \leq \alpha_1$, providing more memory when $f_p^{\text{II}a}(k)$ could not be set.

Note that $\bar{S}_k(f)$ is the result of an average from zero up to $M \times L_s$ power spectra. If no spectrum takes part in the average, the algorithm increases the reference interval by doubling the δ value and repeats the process from the search of $f_p^{\text{II}}(j,k)$ in individual power spectra. In the case that no spectrum is peaked enough after this second iteration, respiratory rate is not estimated at that time instant.

At initialization time, in order to reduce the risk of spurious frequency selection, δ is set to 0.125 Hz and $f_{\text{R}}(0)$ is set to 0.275 Hz, allowing the algorithm to pick peaks inside the normal range of spontaneous respiratory rate ($[0.15, 0.4]$ Hz). Occasionally, respiratory rate can be outside this band
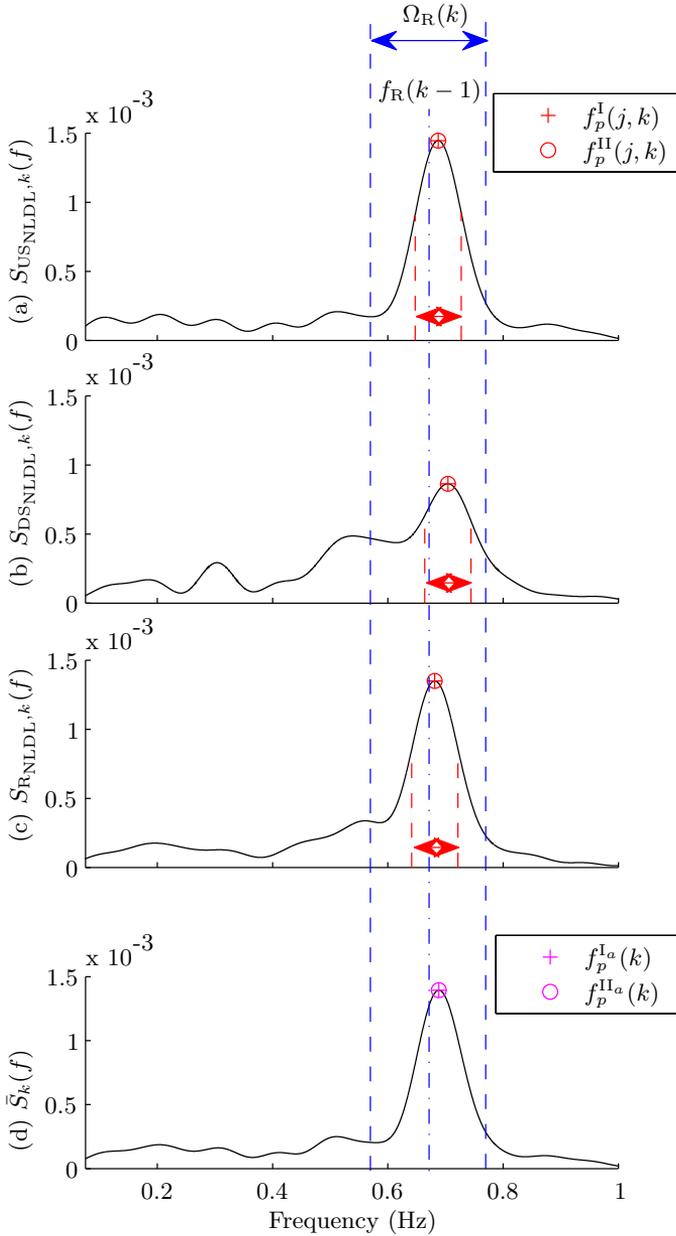
Figure 2.4: Example of Welch periodogram spectra from $d_{\mathrm{US_{NLDL}}}(n)$ (a), $d_{\mathrm{DS_{NLDL}}}(n)$ (b), and $d_{\mathrm{R_{NLDL}}}(n)$ (c). Limits of the integral that define $P_{j,k}$ (see eq. 2.24) are shown with red slashed lines (numerator), and with blue slashed lines ($\Omega_{\mathrm{R}}(k)$, denominator). The resulting peakness-conditioned average $\bar{S}_k(f)$ for NLDL combination is also shown (d). Note that $\bar{S}_k(f)$ is obtained not only from the 3 Welch periodograms at instant k, but also from those Welch periodograms obtained at the last $L_s - 1$ instants (see 2.21).

so algorithm could not be initialized as proposed. To deal with that issue, if $f_{\mathrm{R}}(k)$ is not set after 5 averages $\bar{S}_k(f)$, then δ is increased allowing algorithm to pick peaks in the full $[0, 1]$ Hz studied band.

Concatenation of all $\bar{S}_k(f)$ results in a time-frequency map $\bar{S}(k, f)$ as shown in Fig. 2.6. The parameter values for the Welch periodograms used in [21] are also used here: $L_s = 5$, $T_s = 42s$, $T_m = 12s$ and $t_s = 5s$. Parameter β, which controls the change of location of $\Omega_{\mathrm{R}}(k)$, was set to 0.7 as in [21]; δ was set to 0.1 setting the maximum length of $\Omega_{\mathrm{R}}(k)$ to 0.4 Hz; α_1 and α_2 were set to 0.7 and 0.3, fixing the maximum allowed changes in respiratory frequency inside (α_2) and outside (α_1) $\Omega_{\mathrm{R}}(k)$. λ was set to 0.05 because that value was observed to achieve a good compromise for peak spectrum acceptance/rejection. The minimum peakness to fulfill the χ^{A} criterion, ξ, was set to 0.65 based on a study with a different dataset containing 3-leads ECG recordings during stress testing [91], thus avoiding overfitting.

Four different combinations were studied: the QRS slopes and R-wave angle from the standard 12 leads (12ECG), from VCG, from LDL, and from NLDL. In order to study whether respiratory information in QRS slopes and R-wave angle is complementary or redundant, respiratory rate was also estimated from combinations of only QRS slopes (12ECG$_{\mathrm{S}}$, VCG$_{\mathrm{S}}$, LDL$_{\mathrm{S}}$, NLDL$_{\mathrm{S}}$) and only R-wave angles (12ECG$_{\mathrm{R}}$, VCG$_{\mathrm{R}}$, LDL$_{\mathrm{R}}$, NLDL$_{\mathrm{R}}$). For comparison purposes, a combination composed of the three rotation angle series [10] (Φ) was also studied.

Fig. 2.5 illustrates a block diagram of this algorithm.
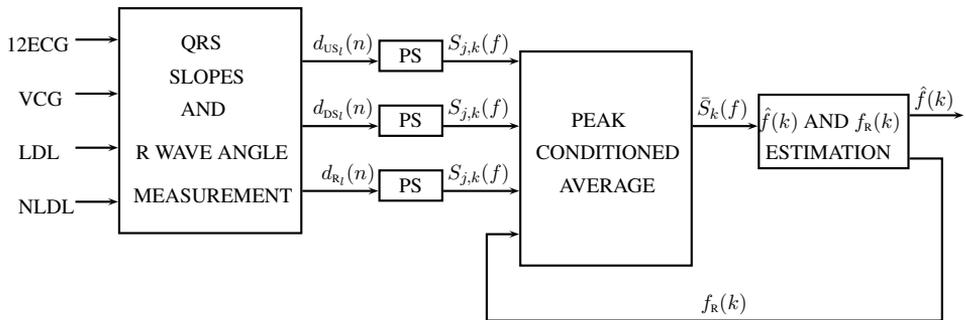
Figure 2.5: Block diagram of respiratory rate estimation algorithm.
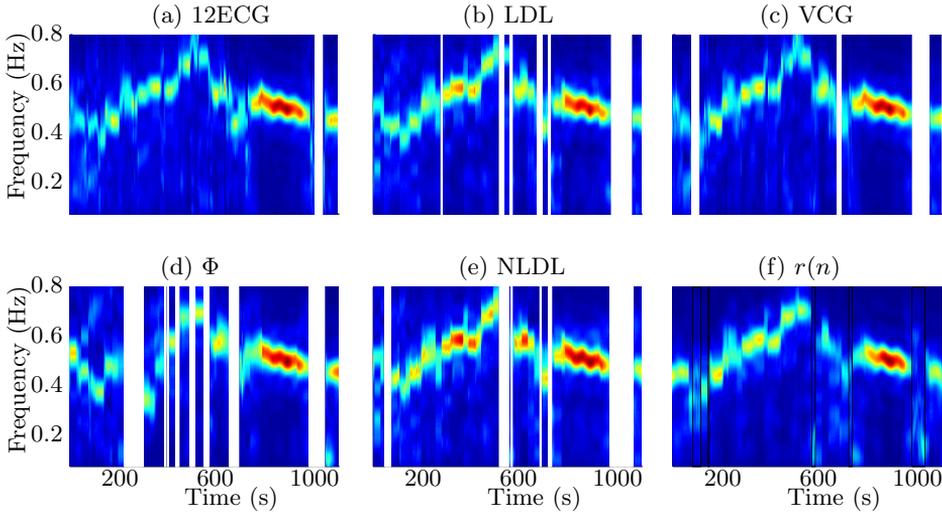
Figure 2.6: Example of peak-conditioned averaged running spectra obtained from the studied combinations: a) 12ECG, b) LDL, c) VCG, d) Φ, e) NLDL, and f) reference respiratory signal. Note that a time instant at which spectrum is not drown (white) means that no spectrum was peaked enough at that time instant. In case of reference respiratory signal, the time instants where no spectrum was peaked enough are represented by black rectangles at where a concatenation of Welch periodograms $(S_{r,k}(f))$ is shown for visual purposes.

2.3.7 Performance measurements

In order to evaluate the proposed methods, two performance measures were used: the relative and absolute error of the respiratory rate estimations defined as:

$$e_{\mathrm{A}}(k) = \hat{f}(k) - f_{\mathrm{RES}}(k) \tag{2.29}$$

$$e_{\mathrm{R}}(k) = \frac{e_{\mathrm{A}}(k)}{f_{\mathrm{RES}}(k)}, \tag{2.30}$$

where $f_{\mathrm{RES}}(k)$ is the respiratory rate estimated from the reference respiratory signal by using the same method. Note that the same absolute differences can correspond to very different relative error due to the $f_{\mathrm{RES}}(k)$ normalization.

2.4 Results

The mean and standard deviation (STD) of absolute and relative error signals were computed for each subject. Then, the intersubject mean of those

Table 2.1: Inter–subject mean of means and SDs of $e_A(k)$ and $e_R(k)$ obtained for the tilt test dataset.

		$e_R(k)$ [%]		$e_A(k)$ [mHz]		Time measuring [%]
		Mean	STD	Mean	STD	Mean
12ECG	Combination	0.46	5.69	−0.05	10.50	100
	Best ($d_{R_{V6}}(n)$)	−1.68	5.63	−5.18	13.94	89.42
	Worst ($d_{US_{aVR}}(n)$)	16.23	23.80	18.16	44.06	38.81
VCG	Combination	0.50	4.11	0.20	7.56	99.84
	Best ($d_{R_X}(n)$)	−0.49	7.27	−2.83	14.68	92.30
	Worst ($d_{DS_Y}(n)$)	0.35	12.03	−5.72	24.48	77.68
LDL	Combination	0.66	4.80	0.48	8.54	96.36
	Best ($d_{US_{LDL}}(n)$)	0.02	5.47	−0.72	10.30	94.19
	Worst ($d_{DS_{LDL}}(n)$)	1.10	7.36	0.43	13.89	85.21
NLDL	Combination	0.71	4.61	0.52	8.58	95.37
	Best ($d_{US_{NLDL}}(n)$)	−0.20	6.34	−3.14	13.26	73.62
	Worst ($d_{R_{NLDL}}(n)$)	3.05	8.24	5.04	14.64	87.33
Φ	Combination	0.48	6.19	−0.81	12.18	96.26
	Best ($d_{\Phi_X}(n)$)	1.29	6.84	0.49	12.26	91.32
	Worst ($d_{\Phi_Y}(n)$)	16.04	22.02	17.11	30.81	63.59

Table 2.2: Inter–subject mean of means and SDs of $e_A(k)$ and $e_R(k)$ obtained for the stress test dataset.

		$e_R(k)$ [%]		$e_A(k)$ [mHz]		Time measuring [%]
		Mean	STD	Mean	STD	Mean
12ECG	Combination	1.95	9.26	4.76	28.63	99.81
	Best ($d_{R_{V4}}(n)$)	−0.63	7.38	−3.46	26.18	62.55
	Worst ($d_{R_I}(n)$)	1.32	14.36	−19.66	53.65	38.96
VCG	Combination	0.52	8.99	0.46	30.36	96.09
	Best ($d_{US_Z}(n)$)	−1.14	8.03	−11.05	29.75	73.05
	Worst ($d_{R_Y}(n)$)	−5.32	13.17	−34.51	47.98	49.32
LDL	Combination	0.04	8.30	−2.10	28.15	85.17
	Best ($d_{DS_{LDL}}(n)$)	−0.65	8.48	−4.34	28.90	67.39
	Worst ($d_{R_{LDL}}(n)$)	−2.40	10.95	−12.61	38.53	66.66
NLDL	Combination	0.76	7.30	1.43	22.53	85.07
	Best ($d_{R_{NLDL}}(n)$)	−0.03	7.76	3.27	27.30	68.21
	Worst ($d_{US_{NLDL}}(n)$)	−1.47	9.80	−14.66	30.76	67.18
Φ	Combination	−1.62	9.65	−14.80	39.72	91.07
	Best ($d_{\Phi_Z}(n)$)	−1.99	10.74	−17.45	38.50	70.38
	Worst ($d_{\Phi_Y}(n)$)	3.38	16.39	4.64	52.45	72.93

Table 2.3: Inter–subject mean of means and SDs of $e_A(k)$ and $e_R(k)$, obtained for combinations of only QRS slopes and only R-wave angles.

		$e_R(k)$ [%]		$e_A(k)$ [mHz]		Time measuring [%]
		Mean	STD	Mean	STD	Mean
Tilt test dataset	12ECG$_S$	0.55	6.89	-0.84	14.40	100.00
	12ECG$_R$	-0.07	6.44	-1.90	12.82	100.00
	VCG$_S$	0.80	5.06	0.46	8.93	99.42
	VCG$_R$	0.31	4.61	-0.41	9.29	96.87
	LDL$_S$	1.20	6.24	1.06	10.76	93.75
	LDL$_R$	0.53	6.33	-0.52	13.42	85.70
	NLDL$_S$	0.51	6.43	-0.52	11.75	88.39
	NLDL$_R$	3.05	8.28	5.04	14.64	87.33
Stress test dataset	12ECG$_S$	2.11	9.50	5.74	29.02	98.65
	12ECG$_R$	-0.23	10.11	-2.82	36.74	96.44
	VCG$_S$	1.95	9.11	4.89	26.63	93.85
	VCG$_R$	0.56	9.51	-0.35	26.18	87.17
	LDL$_S$	-0.60	7.53	-5.07	26.09	77.32
	LDL$_R$	-2.40	10.95	-12.61	38.53	66.66
	NLDL$_S$	0.47	7.19	-0.11	21.85	78.94
	NLDL$_R$	-0.03	7.76	-3.27	27.30	68.21

means and STDs were also computed. Obtained results from the studied combinations of EDR signals are shown in Table 2.1 for the tilt test dataset, and in Table 2.2 for the stress test dataset. For each studied combination, the EDR signals that obtained the best and worst results in terms of root mean square of $e_R(k)$ (less is better) are also shown.

Results obtained for combinations of only slopes and only R-wave angles are shown in Table 2.3.

In order to study the performance of the methods at different respiratory rates, they were evaluated separately as a function of the rate of reference respiratory signal. Furthermore, recordings from patients of stress test dataset were observed to have more irregular breathing patterns when compared with healthy volunteers (see Fig. 2.7). This makes the task of deriving respiratory rate more challenging with patients than with volunteers. Table 2.4 shows results for different ranges of respiratory rate, and for patients and volunteers separately.

Table 2.4: Inter–subject mean of means and STDs of $e_{\mathrm{A}}(k)$ and $e_{\mathrm{R}}(k)$ obtained for the stress test dataset for different respiratory rate ranges for the stress test dataset, and from patients and volunteers separately.

		$e_{\mathrm{R}}(k)$ [%]		$e_{\mathrm{A}}(k)$ [mHz]		Time measuring [%]
		Mean	STD	Mean	STD	Mean
12ECG	$f_{\mathrm{RES}} < 0.3$	1.61	8.68	4.34	23.11	98.05
	$f_{\mathrm{RES}} \in [0.3, 0.5)$	0.28	8.63	−3.23	33.14	94.01
	$f_{\mathrm{RES}} \in [0.5, 0.7)$	−1.92	5.73	−10.78	32.07	96.58
	$f_{\mathrm{RES}} \geq 0.7$	−5.00	1.76	−35.92	12.99	100
	Patients	1.86	8.88	5.90	32.45	99.63
	Volunteers	2.04	9,68	3.55	24.95	100
VCG	$f_{\mathrm{RES}} < 0.3$	1.74	8.46	4.80	21.62	90.13
	$f_{\mathrm{RES}} \in [0.3, 0.5)$	0.55	5.53	2.18	21.25	90.80
	$f_{\mathrm{RES}} \in [0.5, 0.7)$	0.39	3.48	2.60	19.16	96.05
	$f_{\mathrm{RES}} \geq 0.7$	1.01	1.86	7.29	13.42	81.43
	Patients	0.98	7.23	4.29	29.41	95.66
	Volunteers	0.03	10.87	−3.65	31.38	96.55
LDL	$f_{\mathrm{RES}} < 0.3$	3.19	7.06	8.64	18.23	76.50
	$f_{\mathrm{RES}} \in [0.3, 0.5)$	−0.30	5.40	−1.05	21.30	76.66
	$f_{\mathrm{RES}} \in [0.5, 0.7)$	−2.87	4.61	−16.26	26.90	73.56
	$f_{\mathrm{RES}} \geq 0.7$	−5.57	4.19	−44.92	32.29	48.18
	Patients	−0.56	7.82	−4.56	34.11	81.54
	Volunteers	0.68	8.81	0.53	21.76	89.03
NLDL	$f_{\mathrm{RES}} < 0.3$	1.74	8.46	4.80	21.62	72.96
	$f_{\mathrm{RES}} \in [0.3, 0.5)$	−0.45	4.37	−2.61	16.70	79.78
	$f_{\mathrm{RES}} \in [0.5, 0.7)$	−2.66	3.16	−14.43	18.04	77.78
	$f_{\mathrm{RES}} \geq 0.7$	−1.25	2.01	−9.04	14.39	42.11
	Patients	1.34	6.75	3.46	24.19	80.35
	Volunteers	0.15	7.90	−0.74	20.75	90.14
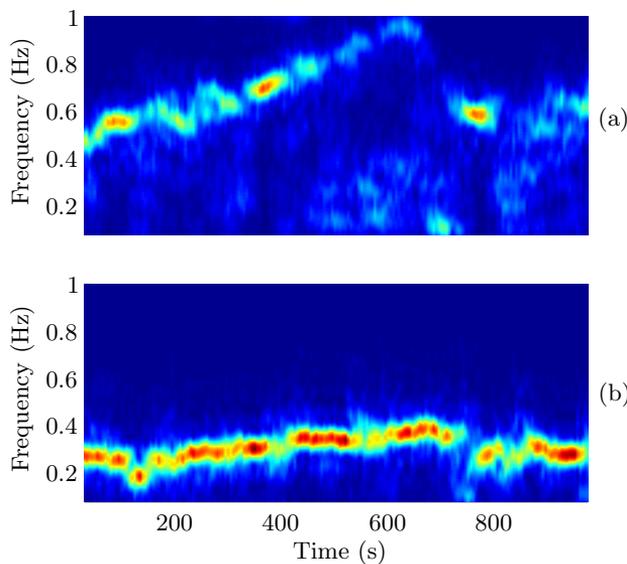
Figure 2.7: Example of Welch periodograms obtained from reference respiratory signal of a patient (a), and a volunteer (b). Volunteer is breathing more regularly, so respiratory rate is more marked in the associated spectrum.

2.5 Discussion

In this chapter a new beat-morphology-based method for deriving respiratory rate from the ECG is presented. First, EDR signals are estimated based on the beat-to-beat variations of QRS slopes and R-wave angle, which have been obtained from different leads. Then, respiratory rate is estimated using an algorithm which includes peak-conditioned averaging to selectively combine information from different EDR signals, and restricted interval peak search. The method has been evaluated in two different challenging scenarios: tilt table test and stress test.

The performance of the methods is assessed in terms of the respiration rate estimation error, as well as of the percentage of the record duration where an estimate is given (measuring time). In the tilt table test scenario, combining information from different EDR signals results in a reduction of estimation error and an increase of the measuring time for all sets of analyzed leads. In the stress test scenario, characterized by noisier and more non stationary signals, combining information from different EDR signals

always results in an increase of the measuring time but, sometimes, at the expense of a slight increase of the estimation error. However, even in those cases (12ECG), the combination is advantageous since the slight increase in estimation error ($1.95 \pm 9.26\%$ [4.76 ± 28.63 mHz] vs. $-0.63 \pm 7.38\%$ [-3.46 ± 26.18 mHz]) is more affordable than the decrease in measuring time (37.26%).

Best performance as a compromise between estimation error and measuring time is achieved by VCG combination in both scenarios (estimation error of $0.50 \pm 4.11\%$, measuring time of 99.84% in tilt table test, estimation error of $0.52 \pm 8.99\%$, measuring time of 96.09% in stress test). VCG combination outperforms 12ECG combination in estimation error terms ($0.50 \pm 4.11\%$ vs. $0.46 \pm 5.69\%$ in tilt test, and $0.52 \pm 8.99\%$ vs. $1.95 \pm 9.26\%$ in stress test), suggesting that inverse Dower transformation enhances beat morphological variations induced by respiration. Although there is a clear advantage in combining information from different EDR signals, it is preferable to use less EDR signals with higher signal to noise ratio (SNR) than more EDR signals with lower SNR. Leads LDL and NLDL also combine information from VCG leads. However, in tilt table test EDR signals derived from LDL and NLDL do not achieve better performance results than VCG combination. On the contrary, in the stress test scenario, NLDL combination obtains less estimation error, at the expense of reducing measuring time (from 96.09% to 85.07%). There is a reduction in estimation error from $0.52 \pm 8.99\%$ (0.46 ± 30.36 mHz) to $0.76 \pm 7.30\%$ (1.43 ± 22.53 mHz), which may be justified in applications where an accurate estimation of respiratory frequency is needed [24]. In applications where the interest is in the evolution of respiratory frequency during stress test, it may be more practical to have slightly less accurate estimates but during more time. In the stress test scenario, EDR signals derived from NLDL slightly outperforms those from LDL in estimation error terms. Moreover, NLDL does not require the update of the dominant direction beat-to-beat, representing a computational advantage.

For comparison purposes, a combination composed of the three electrical axis rotation angle series has been included, which yields an estimation error of $0.48 \pm 6.19\%$ with measuring time of 96.26% in tilt table test, and an estimation error of $-1.62 \pm 9.65\%$ with measuring time 91.07% in stress test. These results indicate that the proposed methodology outperforms electrical axis rotation angles in terms of estimation error and measuring time, which was the best suit for this purpose according to [21].

A possible explanation for the improvement of results for VCG combination with respect to Φ may be that, although both methods use the same

ECG signals ($l_X(n)$, $l_Y(n)$ and $l_Z(n)$), QRS slopes and R-wave angles are more robust in those situations when there is so much noise in one of the leads. Each one of the EDR signals combined in Φ (rotation angle series) uses the three VCG leads. Thus, if one lead is affected by noise or artifacts, the three EDR signals are affected. In opposite, each one of EDR signals used in VCG combination (QRS slopes and R-wave angle from each one of the VCG leads) are based on one single lead, so only those EDR signals based on that noisy lead are affected and their contribution to the respiratory rate estimate can be attenuated by the peaked-conditioned PS average.

In general, methods obtained similar results in absolute error terms for rates below 0.7 Hz. Worse performance is observed for respiratory rates above 0.7 Hz, either in absolute error terms or in percentage of time measuring. This may be due to the fact that respiratory rate is above 0.7 Hz only in 5 recordings belonging to patients, who present more irregular breathing patterns (see Fig. 2.7).

Regarding the separation of patients and healthy volunteers, a slight decrease in performance can be observed in patients with respect to volunteers in absolute error terms while relative error is slightly lower for patients, due to the fact that respiratory rate is higher for patients than for volunteers. The percentage of time offering estimates was also lower for patients than for volunteers.

All proposed combinations use in some way the 12-lead ECG, but having that number of leads is unmanageable in some situations, such as ambulatory scenarios based on Holter devices. All the 220 possible combinations of 3 leads from the 12-lead ECG were studied in the stress test dataset. The best results in relative error terms were obtained by the combination of V2, V5 and I leads ($-1.05 \pm 8.61\%$ during 95.52% of the time), and the worst results were obtained by the combination of V4, V5 and V6 ($10.05 \pm 15.85\%$ during 89.90% of the time). This suggests it is better to place electrodes in a spatially-dispersed way than placing them proximately to each other, and also that the area covered by the posterior leads is the one less suited for EDR since respiration induced changes at those ECG leads results in the lower EDR performance.

Furthermore, to assess the incremental value of QRS slopes and R-wave angle in estimating respiratory rate, they have been evaluated separately. Combination of QRS slopes and R-wave angles reduces estimation error and increases measuring time with respect to QRS slopes or R-wave angles alone. Although R-wave angles are computed from QRS slopes, their relation is

non-linear, which may exploit complementary respiratory information to that obtain by the linear combination of QRS slopes.

The two databases contains registers obtained during specific clinical tests involving different cardiovascular changes, so a measure of accuracy of the proposed methods in normal rest conditions has not been given. As a reference for this, respiratory rate estimation during only the first part of tilt test protocol (4 minutes in supine position) was evaluated for the four proposed combinations. The obtained results in $e_{R}(k)$ terms were $0.31 \pm 4.22\%$ (mean $\pm$ STD) during 100% of time for 12ECG, $0.88 \pm 3.03\%$ during 100% of time for VCG, $0.87 \pm 3.41\%$ during 99.39% of time for LDL, and $1.10 \pm 2.92\%$ during 100% of time for NLDL. For the four combinations, obtained results are better than those obtained when evaluating during the complete three parts of tilt test. This was expected since the first part of tilt test (rest) has no significant cardiovascular changes, nor usually significant respiratory rate changes.

2.6 Conclusions

This chapter addresses the derivation of respiratory information from ECG signals by exploiting the respiration-induced variations in QRS slopes and R-wave angle. The proposed methods are robust in highly non-stationary and noisy environments, and do not depend on a specific set of leads, and so, do not lead to a significantly lower performance in the case of there is any problem at any one of the leads. Results suggest that the proposed methods based on QRS slopes and R-wave angle series are the most suitable for respiratory rate estimation from ECG signals in tilt and stress test. In the stress test database, combination of EDR signals from NLDL lead achieved the lowest estimation error ($0.76 \pm 7.30\%$) while 12ECG combination obtained the largest measuring time (99.81%). Combination of EDR signals from VCG leads displayed the best trade-off between accuracy and measuring time (estimation error of $0.52 \pm 8.99\%$, measuring time of 96.09%), outperforming existing methods in literature.

Chapter 3

PPG derived respiration from pulse width variability

3.1 Introduction

There are several known methods for deriving respiration from the PPG signal such as PAV [92] and PRV. Both heart and respiratory rates were extracted by methods based on empirical mode decomposition in [93], and based on correntropy spectral density in [94]. In [95], both amplitude and frequency modulation of PPG signal due to respiration are used to compare two time–frequency methods for respiratory rate estimation. Both pulse amplitude and rate are affected not only by respiration but also are affected by other physiological modulations whose power is comparable or even larger than the respiration-related modulation, such as the Mayer waves [58, 96]. These non-respiration-related modulations usually lead to high errors. Another approaches to assess respiratory information using the PPG signal are those methods based on PTT [97, 98], which measures the time a pulse takes to get the periphery (measured by PPG signal) from the heart (measured by ECG signal). PTT is much less affected by non-respiration-related modulations, but requires the ECG as an additional recording. This is a disadvantage that takes even more relevance in some applications such as sleep studies context where a high number of sensors over the patient can affect the physiological sleep.

In this chapter, a new method for deriving respiratory rate from PPG based on PWV is presented. The hypothesis on which it is based is that res-

piration affects pulse wave width: during inspiration sympathetic activation stiffs arteries increasing pulse wave velocity in comparison with expiration, moreover there are intrathoracic pressure variations induced by respiration whose effect can add to the former constructively. The PWV method is also combined with PRV- and PAV-based methods which use also the PPG signal. Evaluation is performed over a database which contains simultaneous recordings of ECG, BP, PPG and respiration signals. For comparison, derived respiration (DR) signals obtained with other methods which involve the ECG, PPG, and BP signals were also evaluated.

3.2 Materials and methods

3.2.1 Data, signal preprocessing and significant points detection

The database used for evaluation is described in Section 2.2.1 at page 22, which contains ECG (sampling rate of $f_s^{\mathrm{E}} = 1000$ Hz), PPG (sampling rate of $f_s^{\mathrm{P}} = 250$ Hz), BP (sampling rate of 250 Hz) and respiration (sampling rate of 125 Hz) signals simultaneously recorded from 17 young healthy patients during a tilt table test.

The ECG baseline contamination was removed with a high-pass filter with a cutoff frequency of 0.03 Hz, and the 50 Hz powerline interference was attenuated with the non-linear technique described in [99]. Note that these prepossessing techniques are slightly different to those applied in Chapter 2, where baseline was estimated by cubic splines (and then subtracted) and no powerline filtering was applied. The fixed-cut-off-frequency based powerline attenuation technique was used instead of using the cubic-spline-based technique because no rapid baseline changes are expected in tilt test environments. Regarding the powerline attenuation, in Chapter 2 was not needed because the preprocessing included a 35-Hz-lowpass filtering which showed to be a good solution to the trade-off situation of maintain the respiration-related variations in QRS slopes and removing noise.

Then, as in Chapter 2, the locations of each R (n_{R_i}) and S (n_{S_i}) in lead V4 were obtained by the wavelet based QRS detector described in [87], and ectopic/misdetected beats were identified and removed using the algorithm described in [88]. Lead V4 was chosen because of its high SNR and also because it is one of those whose amplitude modulation is in phase with respiration. The preprocessing applied to the PPG and BP signals consists of a low-pass filtering with a cut-off frequency of 35 Hz. Subsequently, each

pulse apex point (n_{A_i}) in PPG and each systolic pressure point $(n_{A_i}^B)$ in BP were automatically determined using the algorithm described in [100] which uses the n_{R_i} previously obtained:

$$n_{A_i} = \arg\max_n x_{\text{PPG}}(n), \qquad n \in \left\{ \frac{f_s^P}{f_s^E} n_{R_i} + 0.15 f_s^P, \frac{f_s^P}{f_s^E} n_{R_{i+1}} \right\} \quad (3.1)$$

$$n_{A_i}^B = \arg\max_n x_{\text{BP}}(n), \qquad n \in \left\{ \frac{f_s^P}{f_s^E} n_{R_i} + 0.15 f_s^P, \frac{f_s^P}{f_s^E} n_{R_{i+1}} \right\}, \quad (3.2)$$

where f_s^E and f_s^P are the sampling rates of $x_{\text{ECG}}(n)$ and $x_{\text{PPG}}(n)$, respectively, which correspond to 1000 and 250 Hz.

Subsequently, baseline point of the ith PPG pulse was defined as the minimum previous to:

$$n_{B_i} = \arg\min_{n \in \left[n_{A_i} - 0.3 f_s^P, n_{A_i} \right]} \{ x_{\text{PPG}}(n) \} \quad (3.3)$$

Artifact detector

Artifactual PPG pulses were suppressed by using the artefact detector described in [54] which is based in Hjorth parameters 1 and 2. These parameters have been proposed in the electroencephalogram domain as an estimation of the central frequency, and half of the bandwidth, respectively. Thus, they can be used to estimate whether a signal is oscillatory or not. In mathematical terms, Hjorth parameters are defined as:

$$\mathcal{H}_1(n) = \sqrt{\frac{\bar{w}_2(n)}{\bar{w}_0(n)}} \quad (3.4)$$

$$\mathcal{H}_2(n) = \sqrt{\frac{\bar{w}_4(n)}{\bar{w}_2(n)} - \frac{\bar{w}_2(n)}{\bar{w}_0(n)}}, \quad (3.5)$$

where $\bar{w}_m$ denotes the mth-order spectral moment:

$$\bar{w}_m = \int_{-\pi}^{\pi} w^m S_{\text{PPG}}(e^{j\omega}) d\omega, \quad (3.6)$$

being $S_{\text{PPG}}(e^{j\omega})$ the power spectrum of PPG signal.

$\mathcal{H}_1(n)$ and $\mathcal{H}_2(n)$ can be estimated using the temporal expressions of the moments, and made as a function of time n by using a sliding window of P samples:

$$\hat{w}_i \approx \frac{2\pi}{P} \sum_{p=n-(P-1)}^{n} \left(x_{\text{PPG}}^{(m/2)}(p) \right), \qquad m = 0, 2, 4, \quad (3.7)$$

where $x_{\mathrm{PPG}}^{(m/2)}(n)$ is the $m/2$ derivative of $x_{\mathrm{PPG}}(n)$.

Two thresholds for $\mathcal{H}_1(n)$ (γ_1^l and γ_1^u) and one for $\mathcal{H}_2(n)$ (γ_2) were defined. The basis of the artifact detector is that a sample n is considered as artifact when one of the following criteria is fulfilled: a) the main frequency of the PPG signal is clearly different from the heart rate ($\mathcal{H}_1(n) \leq \gamma_1^l$ or $\mathcal{H}_1(n) \geq \gamma_1^u$); b) the PPG signal presents a very wide spectrum ($\mathcal{H}_2(n) \geq \gamma_2$).

The following values for parameters were used:

- $P = 5f_s^{\mathrm{P}}$

- $\gamma_1^u = \mathrm{median}\,(\mathcal{H}_1(n)) + 1.4\mathrm{Hz}$

- $\gamma_1^l = \mathrm{median}\,(\mathcal{H}_1(n)) - 1\mathrm{Hz}$

- $\gamma_2 = \mathrm{median}\,(\mathcal{H}_2(n)) + 3\mathrm{Hz}$

Further details are given in [54].

3.2.2   Pulse width variability

In order to measure the pulses width in PPG signal, it is necessary to locate the onset and end of each pulse wave. The detection is performed with a modification of the algorithm presented in [101] which was originally designed for detecting the wave boundaries in ECG signals. The algorithm uses a low-pass derivative:

$$x'_{\mathrm{PPG}}(n) = x_{\mathrm{PPG_{LP}}}(n) - x_{\mathrm{PPG_{LP}}}(n - 1), \qquad (3.8)$$

where $x_{\mathrm{PPG_{LP}}}(n)$ is the low-pass filtered version of PPG signal, using a cut–off frequency of f_{C} which was set to 5 Hz as shown in Section 3.3.1.

For the ith pulse wave, the algorithm uses the maximum upslope point:

$$n_{\mathrm{U}_i} = \arg\max_n \left\{ x'_{\mathrm{PPG}}(n) \right\}, \quad n \in [n_{\mathrm{A}_i} - 0.3f_s^{\mathrm{P}}, n_{\mathrm{A}_i}]. \qquad (3.9)$$

The pulse wave onset n_{O_i} search is limited to Ω_{O_i} interval:

$$\Omega_{\mathrm{O}_i} = [n_{\mathrm{A}_i} - 0.3f_s^{\mathrm{P}}, n_{\mathrm{U}_i}], \qquad (3.10)$$

and is determined as:

$$n_{\mathrm{O}_i} = \begin{cases} \arg\min\limits_{n \in \Omega_{\mathrm{O}_i}} \left\{ \left| x'_{\mathrm{PPG}}(n) - \eta x'_{\mathrm{PPG}}(n_{\mathrm{U}_i}) \right| \right\} & \text{if } C_1 \\ \text{last relative minimum of } x'_{\mathrm{PPG}}(n), & \text{if } C_2 \\ \arg\min\limits_{n \in \Omega_{\mathrm{O}_i}} \left\{ x'_{\mathrm{PPG}}(n) \right\}, & \text{otherwise} \end{cases} , \qquad (3.11)$$

where $\eta x'_{\text{PPG}}(n_{\text{U}_i})$ represents a beat varying threshold dependent on maximum upslope value of each pulse wave, and conditions C_1 and C_2 are defined by:

$$C_1 \quad : \quad \exists m \in \Omega_{\text{O}_i} \ni x'_{\text{PPG}}(m) \leq \eta x'_{\text{PPG}}(n_{\text{U}_i})$$
$$C_2 \quad : \quad \overline{C_1} \wedge \text{exists a relative minimum of } x'_{\text{PPG}}(n) \text{ in } \Omega_{\text{O}_i}.$$

Pulse wave ends n_{E_i} were detected in a similar way as n_{O_i} but using maximum downslope (n_{D_i}) instead of n_{U_i}, in the interval $[n_{\text{A}_i}, n_{\text{A}_i} + 0.3 f_s^{\text{P}}]$ and $\Omega_{\text{E}_i} = [n_{\text{D}_i}, n_{\text{A}_i} + 0.3 f_s^{\text{P}}]$. Fig. 3.1 illustrates the significant points determination rule of this algorithm.

Once n_{O_i} and n_{E_i} are detected, the pulse width is defined as the time difference between them, and the DR signal based on the PWV is defined as:

$$d_{\text{PWV}}^u(n) = \sum_i \frac{1}{f_s^{\text{P}}} \left(n_{\text{E}_i} - n_{\text{O}_i} \right) \delta \left(n - n_{\text{A}_i} \right), \tag{3.12}$$

where the superscript "u" denotes that the signal is unevenly sampled. Fig. 3.1 illustrates this definition and Fig. 3.2 shows an example of this DR signal where it becomes evident the close relation of temporal oscillations of this signal to those of respiration signal $r(n)$.
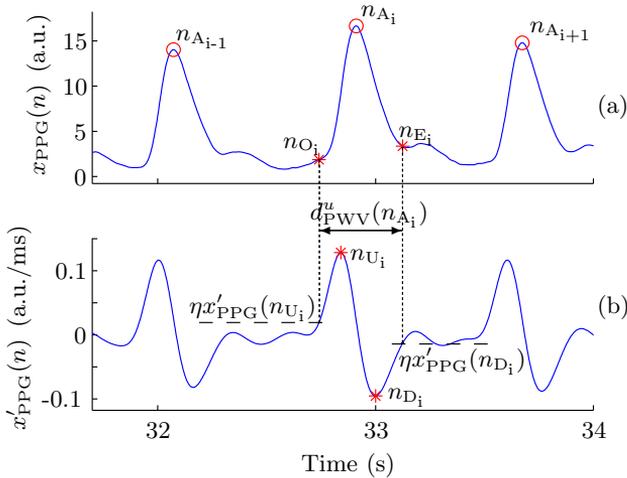
Figure 3.1: Example of $x_{\text{PPG}}(n)$ (a) and its low–pass derivative $x'_{\text{PPG}}(n)$ (b) with definitions of pulse onset (n_{O_i}) and end (n_{E_i}) points in PPG, and PWV based PPG DR signal.
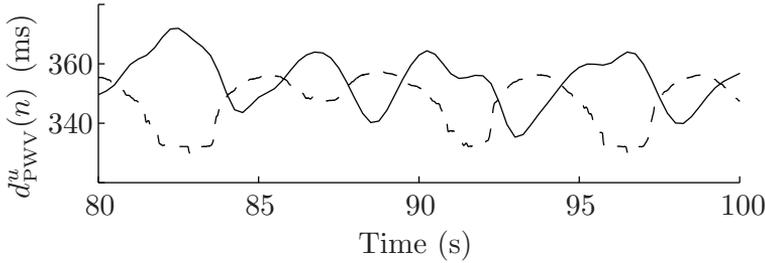
Figure 3.2: Example of $d_{\mathrm{PWV}}^u(n)$ (continuous line) and amplitude scaled reference $r(n)$ (dashed line) for comparison.

3.2.3　Other derived respiration signals

As mentioned previously, for comparison purposes, respiration has also been derived by other known methods which involve the ECG, BP, and PPG signals. Studied DR signals from PPG are three: PRV, PAV, and the PWV already presented.

The one based on PRV is defined as:

$$d_{\mathrm{PRV}}^u(n) = \sum_i f_s^{\mathrm{P}} \frac{1}{n_{\mathrm{A}_i} - n_{\mathrm{A}_{i-1}}} \delta\left(n - n_{\mathrm{A}_i}\right). \tag{3.13}$$

The PAV based DR signal takes its reference to derive amplitude at the basal point:

$$d_{\mathrm{PAV}}^u(n) = \sum_i \left[x_{\mathrm{PPG}}\left(n_{\mathrm{A}_i}\right) - x_{\mathrm{PPG}}\left(n_{\mathrm{B}_i}\right)\right] \delta\left(n - n_{\mathrm{A}_i}\right). \tag{3.14}$$

From the ECG, six DR signals were obtained: one based on HRV, two based on R amplitude variability, and three based on the electrical axis rotation angles called $d_{\Phi_X}^u(n)$, $d_{\Phi_Y}^u(n)$ and $d_{\Phi_Z}^u(n)$, which are computed by the same algorithm presented in [21] and also used in Chapter 2, based on spatio-temporal alignment of successive QRS–VCG loops with respect to a reference loop.

The HRV-based DR signal is computed similarly to the PRV based one:

$$d_{\mathrm{HRV}}^u(n) = \sum_i f_s^{\mathrm{E}} \frac{1}{n_{\mathrm{R}_i} - n_{\mathrm{R}_{i-1}}} \delta\left(n - n_{\mathrm{R}_i}\right). \tag{3.15}$$

The difference of two R wave amplitude based DR signals is the reference used to derive signal amplitude: one takes the reference as zero while the other one takes it as the amplitude of S point at the same beat:

$$d_{\mathrm{R}}^u(n) = \sum_i x_{\mathrm{ECG}}\left(n_{\mathrm{R}_i}\right) \delta\left(n - n_{\mathrm{R}_i}\right) \tag{3.16}$$

$$d_{\text{RS}}^u(n) = \sum_i \left[x_{\text{ECG}}\left(n_{\text{R}_i}\right) - x_{\text{ECG}}\left(n_{\text{S}_i}\right) \right] \delta\left(n - n_{\text{R}_i}\right), \qquad (3.17)$$

where $x_{\text{ECG}}(n)$ is the filtered ECG at lead V4.

Another method which involves the ECG derives respiration from PTT. The PTT signal was obtained and taken it as a DR signal as:

$$d_{\text{PTT}}^u(n) = \frac{1}{f_s^{\text{P}}} \left(n_{\text{M}_i} - \frac{f_s^{\text{P}}}{f_s^{\text{E}}} n_{\text{R}_i} \right) \delta\left(n - n_{\text{R}_i}\right), \qquad (3.18)$$

where the $f_s^{\text{P}}/f_s^{\text{E}}$ term is due to the different sampling rates of ECG and PPG signals, and n_{M_i} is the time instant when the PPG signal reaches 50% of amplitude between onset and apex points:

$$n_{\text{M}_i} = \underset{n \in [n_{\text{O}_i}, n_{\text{A}_i}]}{\arg\min} \left\{ \left| x_{\text{PPG}}(n) - \frac{x_{\text{PPG}}(n_{\text{O}_i}) + x_{\text{PPG}}(n_{\text{A}_i})}{2} \right| \right\}. \qquad (3.19)$$

A DR signal based on BP pulses width was obtained, hypothesizing that BP width variability (BWV) is modulated by respiration through the intrathoracic pressure variations described in Section on which also the PWV-based DR signal is based:

$$d_{\text{BWV}}^u(n) = \sum_i \frac{1}{f_s^{\text{P}}} \left(n_{\text{E}_i}^{\text{B}} - n_{\text{O}_i}^{\text{B}} \right) \delta\left(n - n_{\text{A}_i}^{\text{B}}\right), \qquad (3.20)$$

where $n_{\text{O}_i}^{\text{B}}$ and $n_{\text{E}_i}^{\text{B}}$ are the onset and end points of the ith pressure wave in BP (see Fig. 3.3) detected with the same algorithm used for the PPG signal.

Two other BP-based DR signals were also obtained: BP rate variability (BRV) $d_{\text{BRV}}^u(n)$ and BP amplitude variability (BAV) $d_{\text{BAV}}^u(n)$. The first one, defined in (3.21), is based on rate similarly to $d_{\text{PRV}}(n)$ and $d_{\text{HRV}}(n)$, and the second one is based on the beat-to-beat systolic pressure variability as defined in (3.22).

$$d_{\text{BRV}}^u(n) = \sum_i f_s^{\text{P}} \frac{1}{n_{\text{A}_i}^{\text{B}} - n_{\text{A}_{i-1}}^{\text{B}}} \delta\left(n - n_{\text{A}_i}^{\text{B}}\right) \qquad (3.21)$$

$$d_{\text{BAV}}^u(n) = \sum_i x_{\text{BP}}\left(n_{\text{A}_i}^{\text{B}}\right) \delta\left(n - n_{\text{A}_i}^{\text{B}}\right). \qquad (3.22)$$

Note that in $d_{\text{BAV}}^u(n)$ the absolute value of systolic pressure is considered, instead of referring it to the basal point as in $d_{\text{PAV}}^u(n)$, since, otherwise, respiratory modulation of systolic and diastolic pressures could compensate each other.

Fig. 3.3 illustrates definitions of all DR signals defined in this section, and Fig. 3.4 shows an example of the unevenly sampled version of each DR signal. Due to some outliers presence in the DR signals, a MAD based outlier rejection rules as described in [21] was applied. Finally, a 4 Hz evenly sampled version of each DR signal by cubic splines interpolation was obtained, and then filtered with a band-pass filter (0.075-1 Hz). The resulting signals are denoted without the superscript "u", e.g., $d_{\mathrm{PWV}}(n)$ is the 4 Hz outlier–rejected evenly sampled band–pass filtered version of $d_{\mathrm{PWV}}^{u}(n)$.
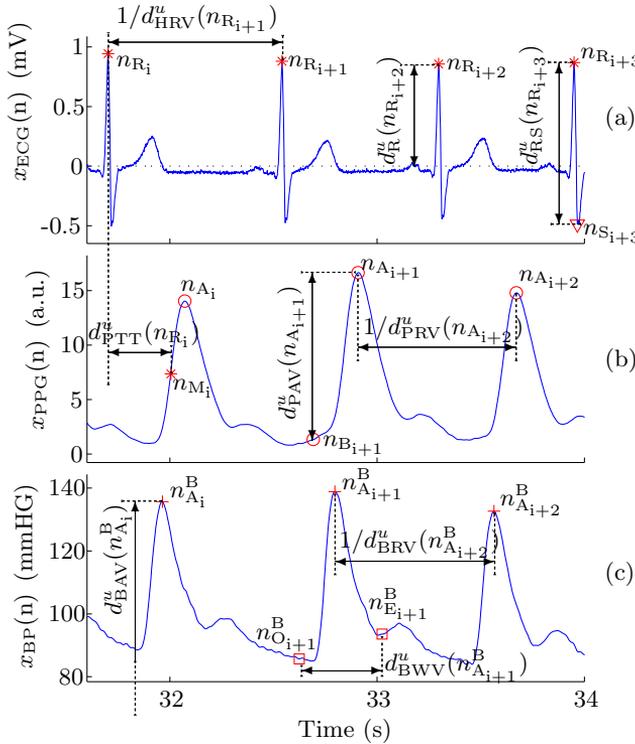
Figure 3.3: Examples of $x_{\mathrm{ECG}}(n)$ (a), $x_{\mathrm{PPG}}(n)$ (b), and $x_{\mathrm{BP}}(n)$ (c), with definitions of ECG DR and BP DR signals, and definitions of PRV and PAV based PPG DR signals.

3.2.4   Respiratory rate estimation

As the method presented in Section 2.3.6, the respiratory rate estimation algorithm is based on the method presented in [21]. There are some differences with respect to the method in Section 2.3.6, but it also allows to
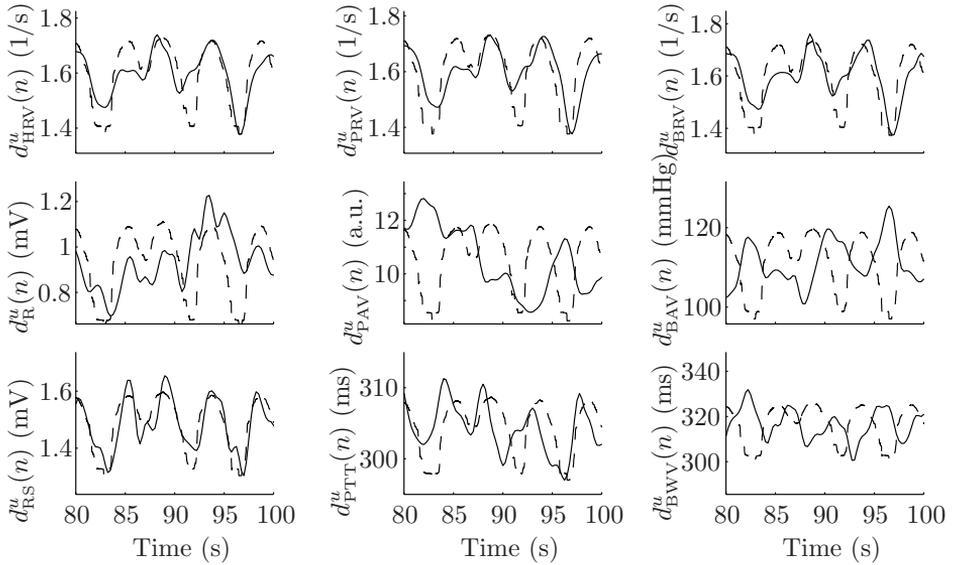
Figure 3.4: An example of some of the studied derived respiration signals (continuous line) and amplitude scaled reference $r(n)$ (dashed line) for comparison.

estimate the respiratory rate from up to M DR signals, combining them in order to increase robustness.

The first stage of the algorithm is the same as the first stage of the algorithm in Section 2.3.6: a power spectrum (PS) estimation based on the Welch periodogram. Following the same notation introduced in Section 2.3.6, $S_{j,k}(f)$ denotes the PS for the jth DR signal and k^{th} running interval of T_s-s length, generated by an average of PS obtained from subintervals of T_m-s length ($T_m < T_s$) using an overlap of $T_m/2$ s, after a power normalization in $[0, 1]$ Hz band. A spectrum is generated every t_s s.

Similarly to the method in Section 2.3.6, the location of largest peak of each $S_{j,k}(f)$ is detected and denoted $f_p^{\mathrm{I}}(j, k)$, and then, a reference interval $\Omega_{\mathrm{R}}(k)$ is established in order to search the respiratory peak $f_p^{\mathrm{II}}(j, k)$. One of the differences between this algorithm and the one presented in Section 2.3.6 is a redefinition of $\Omega_{\mathrm{R}}(k)$ which, although it is also located around a respiratory frequency reference obtained from previous $(k-1)$ steps (and denoted $f_{\mathrm{R}}(k-1)$), this time $\Omega_{\mathrm{R}}(k)$ is asymmetric with respect to $f_{\mathrm{R}}(k-1)$ as shows (3.23). The reason of this asymmetry is that the most important contamination present in PS is in the LF band due to the sympathetic system activity, reflected at some DR signals.

$$\Omega_{\mathrm{R}}(k) = [f_{\mathrm{R}}(k-1) - \delta, f_{\mathrm{R}}(k-1) + 2\delta]. \tag{3.23}$$

All peaks larger than 85% of $f_p^{\mathrm{I}}(j,k)$ inside $\Omega_{\mathrm{R}}(k)$ are detected, and $f_p^{\mathrm{II}}(j,k)$ is chosen as the nearest to $f_{\mathrm{R}}(k-1)$ (see Fig. 2.3). Note that, in a similar way to that in the method presented in Section 2.3.6, $f_p^{\mathrm{II}}(j,k)$ can be the same $f_p^{\mathrm{I}}(j,k)$ if the largest peak is also the nearest to $f_{\mathrm{R}}(k-1)$. Then, L_s spectra $S_{j,k}(f)$ are "peak-conditioned" averaged; only those $S_{j,k}(f)$ which are sufficiently peaked take part in the averaging. Similarly, "peaked" denotes that $f_p^{\mathrm{II}}(j,k)$ exists and a certain percentage (ξ) of the spectral power is contained in an interval centered around it. Peak-conditioned averaging is computed as in method in Section 2.3.6 (see eq. 2.21), using the same peakness-based criteria $\chi_{j,k-l}^{\mathrm{A}}$ and $\chi_{j,k-l}^{\mathrm{B}}$ defined in (4.28) and (4.29), respectively. Nevertheless, the peakness is redefined in order to take into account the new asymmetric $\Omega_{\mathrm{R}}(k)$:

$$P_{j,k} = \frac{\displaystyle\int_{\max\left\{f_p^{\mathrm{II}}(j,k)-0.6\delta,\ f_{\mathrm{R}}(k-1)-\delta\right\}}^{\min\left\{f_p^{\mathrm{II}}(j,k)+0.6\delta,\ f_{\mathrm{R}}(k-1)+2\delta\right\}} S_{j,k}(f)df}{\displaystyle\int_{f_{\mathrm{R}}(k-1)-\delta}^{f_{\mathrm{R}}(k-1)+2\delta} S_{j,k}(f)df}. \tag{3.24}$$

Then, similarly to the method presented in Section 2.3.6, the algorithm searches the largest peak $f_p^{\mathrm{I}a}(k)$ in $\bar{S}_k(f)$, and subsequently $f_p^{\mathrm{II}a}(k)$ defined as the nearest to $f_{\mathrm{R}}(k-1)$ inside $\Omega_{\mathrm{R}}(k)$ which is at least larger than 85% of $f_p^{\mathrm{I}a}(k)$, and uses them to set the respiratory peak $f_p(k)$ (see eq. 2.26) which at the same time used to set $f_{\mathrm{R}}(k)$ (see eq. 2.25) and the estimated respiratory rate $\hat{f}(k)$ (see eq. 2.27).

Similarly to the method presented in Section 2.3.6, $\bar{S}_k(f)$ is the result of an average from zero up to $M \times L_s$ PS, and if no spectrum takes part in the average the algorithm increases the reference interval by doubling the δ value and repeat the process from the search of $f_p^{\mathrm{I}}(j,k)$ and $f_p^{\mathrm{II}}(j,k)$ in individual PS. In the case that no spectrum is peaked enough after this second iteration, the method presented in Section 2.3.6 sets $f_{\mathrm{R}}(k)$ as the previous $f_{\mathrm{R}}(k-1)$ but it does not offer a respiratory rate estimation. In difference, this method offers an estimate by setting $\hat{f}(k)$ as the previous $\hat{f}(k-1)$. The reason of this difference is that noise level in a tilt test environment is considerably lower than that in a stress test environment and so, the signal to noise ratio is expected to be high enough in the entire recording and also respiratory rate variations are slower.

Figure 3.5 shows an example of Welch periodogram spectra from PRV, PAV, and PWV, with limits of the integral that define $P_{j,k}$.

Concatenation of all $\bar{S}_k(f)$ results in a time-frequency map $\bar{S}(k,f)$ as shown in Fig. 3.6. Values for L_s, T_s, and T_m were selected as in Chapter 2:
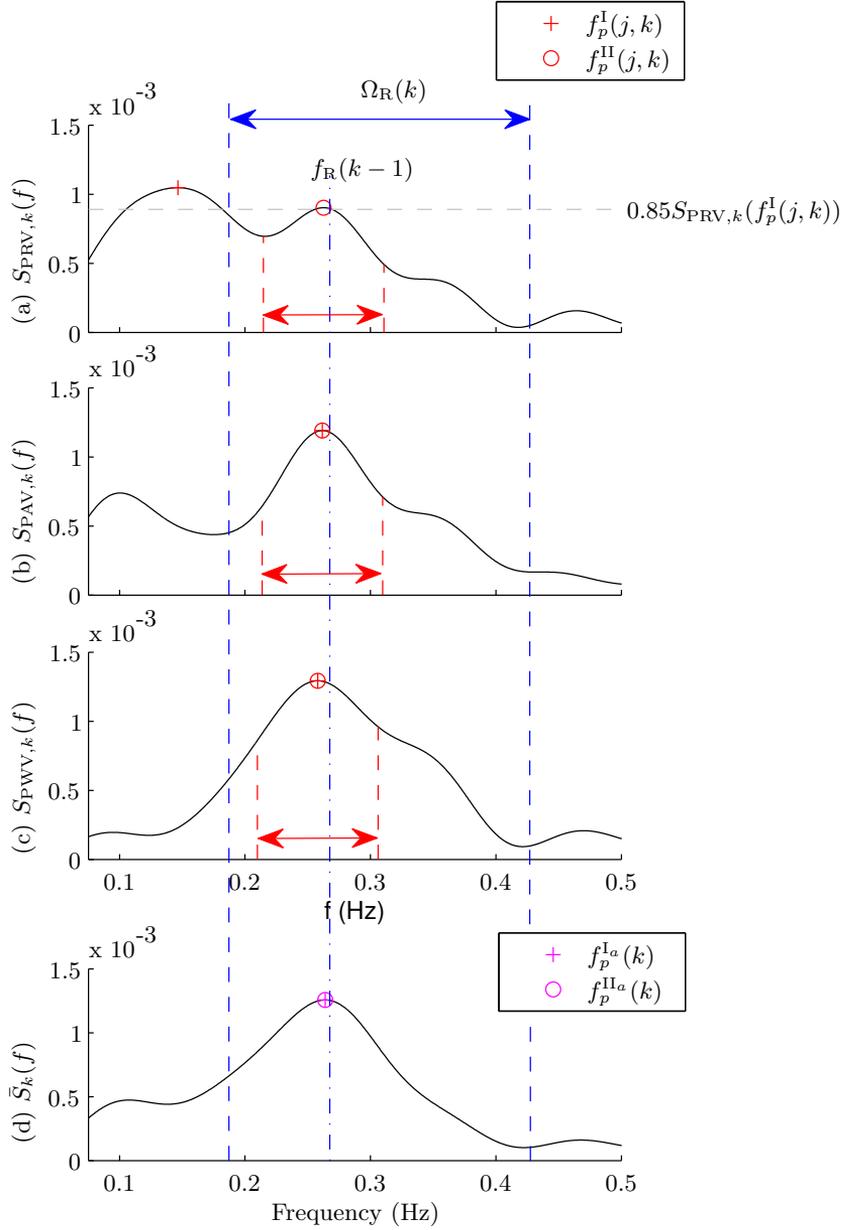
Figure 3.5: Example of Welch periodogram spectra from PRV (a), PAV (b), and PWV (c). Limits of the integral that define $P_{j,k}$ (see eq. 3.24) are shown with red slashed lines (numerator), and with blue slashed lines ($\Omega_R(k)$, denominator). The resulting peakness-conditioned average $\bar{S}_k(f)$ for combination of PRV, PAV, and PWV is also shown (d). Note that $\bar{S}_k(f)$ is obtained not only from the 3 Welch periodograms at instant k, but also from those Welch periodograms obtained at the last $L_s - 1$ instants (see 3.24).

42 s, 12 s and 5 s respectively. α_1 and α_2 which fix the maximum allowed changes in respiratory frequency inside (α_2) and outside (α_1) $\Omega_R(k)$, were set to 0.7 and 0.3 respectively as they were in the method presented in Section 2.3.6. The other parameters were empirically set for this work:

- $\xi = 0.4$ and $\lambda = 0.05$ are based on the observation of spectra to achieve a good compromise for peak spectrum acceptance/rejection.

- $\beta = 0.8$ is slightly higher than 0.7 used in Chapter 2, since in regular conditions respiratory frequency band is expected to change more gradually than in stress test. Thus, a higher filtering for f_R tracking has shown to be more adequate in this scenario.

- $\delta = 0.08$ Hz not allowing respiratory rate changes as fast as in Chapter 2, more adequate for tilt test recordings. Note that this value of δ sets the length of $\Omega_R(k)$ to 0.24 Hz which coincides with the typical HF bandwidth.

Figure 3.6 shows some examples of time-frequency maps.

3.2.5 Performance measurements

With the objective of evaluating the different methods for deriving respiration, a 4 Hz sampled, [0.075, 1] Hz band-pass filtered version of the respiratory signal $r(n)$ was obtained. Two error functions for each one of the 17 subjects in the database were computed: absolute error $e_A(k)$ and relative error $e_R(k)$:

$$e_A(k) = \hat{f}_d(k) - \hat{f}_{RES}(k) \tag{3.25}$$

$$e_R(k) = \frac{e_A(k)}{\hat{f}_{RES}(k)} \times 100, \tag{3.26}$$

where $\hat{f}_d(k)$ and $\hat{f}_{RES}(k)$ are the respiratory rates estimated from the evaluated DR signal and $r(n)$, respectively. Note that the same absolute differences can correspond to very different relative error due to the $\hat{f}_{RES}(k)$ normalization.

In order to study the optimal values for parameters η and f_C in the pulse width based DR signals, the performance measurement z was defined as the intersubject mean of intrasubject mean of the absolute value of relative error $|e_R(k)|$:

$$z = \frac{1}{M} \sum_{m=1}^{M} \overline{|e_R(k)|}_m, \tag{3.27}$$
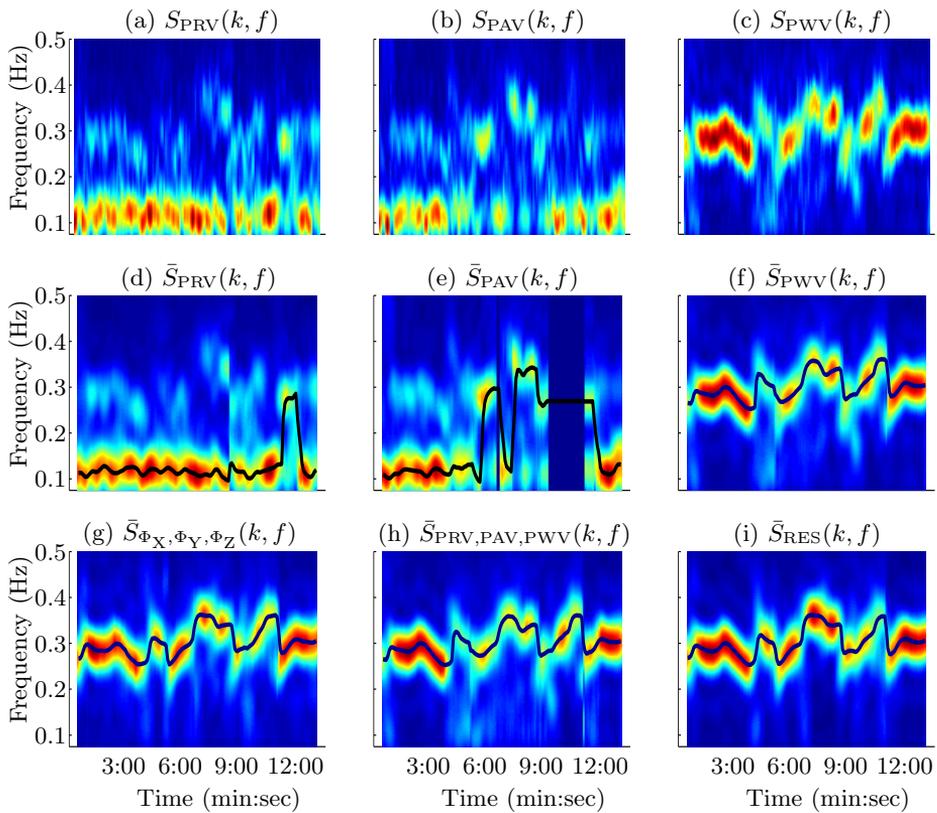
Figure 3.6: Examples of time-frequency maps: Welch periodograms for PRV (a), PAV (b), and PWV (c); peak-conditioned average with estimated rate in black line for PRV (d), PAV (e), PWV (f), combination of Φ_X, Φ_Y and Φ_Z (g), combination of PRV, PAV and PWV (h), and reference respiratory signal (i).

where M is the number of subjects in our database, and $\overline{|e_\mathrm{R}(k)|}_\mathrm{m}$ is the mean of $|e_\mathrm{R}(k)|$ obtained from m^{th} subject.

3.3   Results

3.3.1   Pulse width measurement parameters optimization

In reference to the parameters optimization of the pulse width measurement algorithm, they were computed all the 286 possible combinations corresponding to $\eta \in [0, 0.5]$ with a step of 0.05, and $f_\mathrm{C} \in [2.5, 15]$ Hz with a step of 0.5 Hz, for both PPG and BP signals. The values which minimized z were $\eta = 0.05$ and $f_\mathrm{C} = 5$ Hz for PPG signal (with $z = 5.26\%$), and $\eta = 0.3$ and $f_\mathrm{C} = 3$ Hz for BP signal (with $z = 5.66\%$).

These optimal values were used to obtain DR signals based on width ($d_\mathrm{PWV}^u(n)$ and $d_\mathrm{BWV}^u(n)$).

3.3.2   Evaluation of derived respiration signals

In order to evaluate the DR signals, the mean and standard deviation of both $e_\mathrm{R}(k)$ and $e_\mathrm{A}(k)$ signals were computed for each subject. Then, intersubject mean of both means and SD were computed for three groups of subjects: one group containing all the subjects, and other two groups which make a division of the subjects based on whether their mean respiratory rate $\bar{f}_\mathrm{RES}$ is greater than 0.15 Hz or not. In other words, whether their $\bar{f}_\mathrm{RES}$ overlaps in frequency with the sympathetic modulation or not. Respiratory rate was estimated from each DR and from 6 combinations: the four combinations of QRS slopes and R-wave angles studied in Chapter 2 (12ECG, VCG, LDL, and NLDL), one combining all three PPG-based DR signals $\mathrm{P_{COMB}}$, and other combining all three rotation angle series Φ_COMB. Results obtained for QRS slopes and R-wave angles are shown in Table 3.1 and, results obtained for each DR signals and combinations $\mathrm{P_{COMB}}$ and Φ_COMB are shown in Table 3.2. Moreover, the percentage of times in which each DR signal is used in $\mathrm{P_{COMB}}$ is shown in Table 3.3.

For comparison with [95], the median of $e_\mathrm{R}(k)$ for each subject was obtained for the two proposed methods: the PWV and the combination of PRV, PAV and PWV, $\mathrm{P_{COMB}}$. Table 3.4 shows inter–subject median and interquartile range (IQR) of these medians, for the same three groups of subjects over which the mean of means and SD were computed.

Table 3.1: Inter–subject mean of means and standard deviations of $e_A(k)$ in mHz and $e_R(k)$ in percentage obtained for the different combinations of QRS slopes and R-wave angles presented in Chapter 2.

	$e_R(k)$	[%]	$e_A(k)$	[mHz]
	Mean	SD	Mean	SD
12ECG	0.17	5.32	−0.51	10.57
VCG	−0.10	5.37	−1.33	9.94
LDL	0.69	4.75	0.44	8.54
NLDL	0.82	4.76	0.59	9.14

3.4 Discussion

As it was mentioned previously, deriving respiration from the PPG signal is especially interesting because it is recorded by a simple and cheap device which also results very comfortable for the patient and, in addition, is widely adopted as a SpO_2 monitor: the pulse oximeter. SpO_2 is a very important parameter in studies concerning respiration and essential in many applications such as sleep apnea diagnosis. Obtaining accurate respiratory signal from a pulse oximeter would allow us to consider an ambulatory diagnosis with its both social and economic advantages.

A method for deriving respiration from the PPG signal has been developed: the PWV, which has obtained very accurate results, comparable or even better than other known methods which involve ECG or BP.

In respiratory rate estimation from only one DR signal, this method based on PWV has obtained the best results ($1.27 \pm 7.81\%$; 0.14 ± 14.78 mHz), being much better than PRV ($-10.29 \pm 13.63\%$; -34.60 ± 33.73 mHz) or PAV ($-8.75 \pm 17.06\%$; -26.41 ± 41.84 mHz), which are more affected by the sympathetic modulation which results in a very high negative error in the $\bar{f}_{RES} \geq 0.15$ Hz group. The PWV based method results are also comparable to the pulse transit time (PTT) based one ($0.96 \pm 9.26\%$; -1.54 ± 18.57 mHz), which needs ECG in addition to PPG signal.

The BP width variability (BWV) based method also obtained very good results ($2.54 \pm 8.76\%$; 1.93 ± 15.08 mHz), but acquiring BP signal is more uncomfortable and expensive than acquiring PPG signal and the first one provides no information about SpO_2.

In P_{COMB}, the PWV based method have a fundamental role since PWV is much less affected by the sympathetic modulation (see Fig. 3.6). This fact explains why the PWV method is more often used in the $\bar{f}_{RES} \geq 0.15$ Hz group (67.63% of times) than in the $\bar{f}_{RES} < 0.15$ Hz group (42.41% of times),

Table 3.2: Inter–subject mean of means and standard deviations of $e_A(k)$ in mHz and $e_R(k)$ in percentage. Φ_{COMB} refers to the combination of the three rotation angle series, and P_{COMB} refers to the combination of PRV, PAV, and PWV.

			$e_R(k)$ [%]		$e_A(k)$ [mHz]	
			Mean	SD	Mean	SD
ECG methods	**HRV**	$\overline{f}_{RES} < 0.15$ Hz	4.19	11.91	4.08	13.75
		$\overline{f}_{RES} \geq 0.15$ Hz	-21.21	15.15	-62.78	46.31
		All	-12.25	14.00	-39.18	34.82
	R	$\overline{f}_{RES} < 0.15$ Hz	12.49	20.50	13.86	24.64
		$\overline{f}_{RES} \geq 0.15$ Hz	-7.55	15.48	-24.33	43.17
		All	-0.48	17.25	-10.85	36.63
	RS	$\overline{f}_{RES} < 0.15$ Hz	41.50	36.94	40.28	36.46
		$\overline{f}_{RES} \geq 0.15$ Hz	-7.55	15.48	-24.33	43.17
		All	14.84	21.13	18.28	35.05
	Φ_{COMB}	$\overline{f}_{RES} < 0.15$ Hz	13.30	11.20	4.71	4.31
		$\overline{f}_{RES} \geq 0.15$ Hz	0.81	4.58	1.50	10.52
		All	2.05	6.92	2.63	11.50
BP methods	**BRV**	$\overline{f}_{RES} < 0.15$ Hz	4.31	11.20	4.71	13.30
		$\overline{f}_{RES} \geq 0.15$ Hz	-19.21	14.49	-58.13	44.06
		All	-10.78	13.62	-35.95	33.33
	BAV	$\overline{f}_{RES} < 0.15$ Hz	1.28	10.66	0.93	13.14
		$\overline{f}_{RES} \geq 0.15$ Hz	-4.49	11.80	-14.68	34.63
		All	-2.78	11.40	-9.17	24.04
	BWV	$\overline{f}_{RES} < 0.15$ Hz	8.26	15.97	9.16	19.01
		$\overline{f}_{RES} \geq 0.15$ Hz	-0.58	4.82	-2.01	12.94
		All	2.54	8.76	1.93	15.08
PPG methods	**PRV**	$\overline{f}_{RES} < 0.15$ Hz	4.46	11.93	4.41	13.85
		$\overline{f}_{RES} \geq 0.15$ Hz	-18.34	14.56	-55.89	44.58
		All	-10.29	13.63	-34.60	33.73
	PAV	$\overline{f}_{RES} < 0.15$ Hz	0.35	12.27	-0.73	15.20
		$\overline{f}_{RES} \geq 0.15$ Hz	56.37	19.68	-40.43	-13.72
		All	-8.75	17.06	-26.41	4.84
	PWV	$\overline{f}_{RES} < 0.15$ Hz	5.32	13.27	5.85	16.06
		$\overline{f}_{RES} \geq 0.15$ Hz	-0.92	4.83	-2.97	14.08
		All	1.27	7.81	0.14	14.78
	P_{COMB}	$\overline{f}_{RES} < 0.15$ Hz	2.27	10.50	1.87	12.57
		$\overline{f}_{RES} \geq 0.15$ Hz	-1.50	4.58	-4.35	12.76
		All	-0.17	6.67	-2.16	12.69
Other	**PTT**	$\overline{f}_{RES} < 0.15$ Hz	5.88	13.62	6.20	15.58
		$\overline{f}_{RES} \geq 0.15$ Hz	-1.73	6.89	-5.76	20.21
		All	0.96	9.26	-1.54	18.57

Table 3.3: Percentage of utilization of each DR signal in combination of PRV, PAV and PWV.

	Percentage of use		
Group	**PRV**	**PAV**	**PWV**
$\bar{f}_{\mathrm{RES}} \geq 0.15$ Hz.	48.24%	37.80%	67.63%
$\bar{f}_{\mathrm{RES}} < 0.15$ Hz.	59.77%	61.27%	42.41%
All	52.31%	46.08%	58.73%

Table 3.4: Inter–subject median and IQR of medians of $e_{\mathrm{R}}(k)$ in percentage referent to PWV and combination of PRV, PAV and PWV.

	$e_{\mathrm{R}}(k)$ [%]			
	PWV		**P$_{\mathrm{COMB}}$**	
Group	**Median**	**IQR**	**Median**	**IQR**
$\bar{f}_{\mathrm{RES}} \geq 0.15$ Hz	-0.24	0.48	-0.67	0.41
$\bar{f}_{\mathrm{RES}} < 0.15$ Hz	1.72	1.60	0.31	0.69
All	0.02	1.48	-0.37	0.66

Table 3.3. Results referred to estimated rate from P$_{\mathrm{COMB}}$ ($-0.17 \pm 6.67\%$; -2.16 ± 12.69 mHz) are comparable with combination of three electrical axis rotation angle series ($2.05 \pm 6.92\%$; 2.63 ± 11.50 mHz) and have outperformed those obtained with only PWV. This means that it is reasonable to combine respiratory information of these three signals or, in other words, the respiratory information carried by these three signals can be complementary.

The obtained values of median and IQR of medians ($0.02 \pm 1.48\%$ for PWV and $-0.37 \pm 0.66\%$ for P$_{\mathrm{COMB}}$) are worst than those obtained in [95] ($\bar{f}_{\mathrm{RES}}$ between 0.2 and 0.3 Hz, $0.00 \pm 0.00\%$; $\bar{f}_{\mathrm{RES}}$ between 0.4 and 0.6 Hz, $0.00 \pm 1.18\%$ for supine position and $0.00 \pm 1.07\%$ for tilt position), but it must be kept in mind that the database used in [95] contains signals recorded during a controlled respiration experiment. Controlled respiration means the subjects are instructed to breathe according to a timed beeping sound. Thus, those generated rates were constant, so estimation methods were not required to follow rate variations which is not an easy task and, furthermore, all generated rates were higher than 0.2 Hz, not overlapping in frequency with the sympathetic modulation present below 0.15 Hz in LF band.

Note the same subjects used to evaluate performance of the methods were also used to optimize the parameters η and f_c, and this could bias the results. An additional test was performed: 8 randomly selected subjects

(training set) were used for parameters optimization and the remaining 9 subjects (test set) were used for the evaluation of PWV and P_{COMB} methods. Same values were obtained for optimal parameters ($\eta = 0.05$ and $f_c = 5$ Hz). Results were almost identical to the ones just commented above (see Table 1), obtaining a mean $\pm$ SD of frequency estimation error of $1.71 \pm 7.99\%$ (0.91 ± 13.74 mHz) for the PWV method, and $0.09 \pm 6.61\%$ (-1.75 ± 12.26 mHz) for the P_{COMB} method.

The algorithm for respiratory rate estimation is slightly different from that presented in Chapter 2 which was designed to work in the highly non-stationary and noisy environment of stress test. The main modifications include: (i) the reference interval $\Omega_R(k)$ (see eq. 3.23) for estimating respiratory frequency is asymmetric with respect to the reference frequency $f_R(k-1)$, since some of the DR signals in this study are contaminated with sympathetic-related LF components; (ii) respiratory rate estimated even when no spectrum is peaked enough according to χ^A and χ^B, because very noisy signal segments are not expected in the tilt test environment. As expected, obtained results (see Table 3.1) are similar to those obtained in Chapter 2 for tilt test (see Table 2.1). It is also remarkable that results obtained for combinations of QRS slopes and R-wave angles proposed in Chapter 2 (e.g., $0.82 \pm 4.76\%$; 0.59 ± 9.14 mHz for NLDL) outperformed those obtained with electrical axis rotation angles ($2.05 \pm 6.92\%$; 2.63 ± 11.50 mHz).

One limitation of this study is that methods have been evaluated only with recordings from healthy young people. The physiological source of the respiration-related modulations in PPG signal exploited by the presented methods is the autonomic control over the cardiovascular system. In addition, PPG pulses morphology is affected by age, due to arterial stiffness. So age, arterial or ANS diseases could affect results. Further studies must be elaborated to assess the performance of the presented methods over this kind of patients.

3.5 Conclusions

This chapter addresses the derivation of respiratory information from PPG signals by exploiting the respiration-induced variations in pulses width. The PWV method does not require the ECG as an additional recording as PTT-based methods does, and it is much more less affected by other physiological non-respiration-related modulations than PAV- and PRV-based methods are. It showed better performance than other single PPG-based DR signals

in respiratory rate error terms $(1.27 \pm 7.81\%)$. Additionally, when combining it with PRV and PAV methods which are also based on PPG, results improved to $(-0.17 \pm 6.67\%)$ even outperforming the ones obtained with other methods which involve ECG or BP registration. These results allow to derive respiration from PPG suitable for ambulatory analysis and for sleep apnea diagnosis due to the simplicity of PPG recordings.

*Anything can change, because the smartphone
revolution is still in the early stages.*
Tim Cook.

Chapter 4

Respiration derived from smartphone-camera-acquired PPG signals

4.1 Introduction

Smartphone devices can record PPG signals based on light emitted by flash and received by a camera [37, 38]. Smartphones are interesting devices in ambulatory scenarios due to significant advancements in the computational power which enables complex signal processing algorithms to be performed in real time. Certainly, built-in wireless communications feature of the smartphones facilitates ease of data transfer. These features make smartphones very valuable as take-anywhere and easy-to-use physiological monitors [41]. Obtaining respiratory rates from smartphone devices would represent a simple and automated way for assisting hospital clinical staff who are currently trained to measure it by counting the number of breaths in a 15 or 30-seconds window [102], making the process cumbersome and user-dependent. It has the potential for other applications, such as anxiety, fatigue or stress level monitoring at home, especially if respiratory rate information is combined with other physiological information accessible in the PPG signal, such as pulse rate and its variability [50] or BP [103].

It should be noted that, however, SCPPG signal is more vulnerable to ambient-light interferences and variations in finger pressure over the sensor, making them in general noisier than the standard pulse oximeter sensor. Furthermore, their sampling rate is lower. Thus, deriving physiological information from SCPPG signals remains a more challenging situation than

deriving it from conventional PPG signals, and the performance of known methods which have been tested with conventional PPG signals must be tested also with SCPPG signals.

In this chapter, the PPG-based methods for deriving respiratory rate presented in Chapter 3 (pulse-to-pulse methods) in combination with those presented in [104] (non-pulse-to-pulse methods), are applied and adapted to SCPPG signals. The methods in [104] were used with SCPPG signals in [105] and [41], but they were neither combined with each other, nor with the methods presented in Chapter 3.

Furthermore, the power of respiration-induced modulations on which these DR signals are based (rate, amplitude and width) may depend on the respiratory rate. In the case of PRV, it is known that respiratory sinus arrhythmia (which modulates the heart rate and therefore the pulse rate) is reduced at high respiratory rates [106]. The respiratory rate influence in the resulting magnitude of PPG-based DR signals is also studied in this chapter.

4.2 Materials

4.2.1 Smartphone-camera-acquired-PPG signals

SCPPG signals from 30 healthy subjects (22 men and 8 women, between 20 and 26 years old) were collected during controlled respiration experiments. Subjects were instructed to breathe at a constant rate according to a timed beeping sound, while placing the right index finger on the camera lens of the analyzed device. The data were collected for respiratory rates ranging from 0.2 to 0.6 Hz at an increment of 0.1 Hz, recording a total of 2 minutes of SCPPG signal for each subject, respiratory rate and device. The SCPPG signals were recorded with 3 different smartphone devices: iPhone 4S, iPod 5, and HTC One M8. The signals were extracted from average of 50x50 pixel region of the green video signal at each frame. The reason for using only the green band is that there is high absorption by hemoglobin in the green range, and it has been demonstrated to give a stronger cardiac pulse signal than the red or blue bands during remote PPG imaging [39–42].

4.2.2 Conventional PPG signals

The study of respiratory rate influence in the resulting magnitude of PPG-based DR signals included the analysis of PPG data recorded by a conventional photoplethysmograph. PPG and chest respiratory effort signals

were simultaneously recorded with Medicom MTD Poly10 and Poly4 using a sampling rate of 250 Hz, from 14 healthy volunteers during similar controlled respiration experiments. According to the chest respiratory effort signal, the subjects breathed at the requested respiratory rate with an error of 0.22 ± 1.05 mHz.

4.2.3 Polysomnographic recordings

This database includes PSG recordings from 21 children (11 boys and 10 girls) whose mean age was 4.47 ± 2.04 (mean $\pm$ standard deviation). Children were referred to hospital for suspected sleep-disordered breathing. Common PSG signals records including ECG leads I and II, and airflow, were recorded by a digital polygraph (BITMED EGP800), according to the standard procedure defined by the American Thoracic Society [107]. PPG and SpO_2 were measured using a pulse oximeter (COSMO ETCO2/SpO2 Monitor Novametrix, Medical Systems). Signals were stored with a sampling rate of 100 Hz, except ECG signals, which were sampled at 500 Hz. OSAS evaluation from PSG data were scored by clinical experts using the standard procedures [108]. 10 out of the 21 children were diagnosed with OSAS. Ethical approval for this study was obtained from the Aragon clinical research local ethics committee (CEICA).

4.3 Methods

4.3.1 Preprocessing

The sampling rate of SCPPG signals is variable due to internal processing load [109], and it depends on the measuring device. The SCPPG signals were interpolated to a constant sampling rate of $f_s^{\mathrm{SP}} = 100$ Hz by using cubic splines. Furthermore, SCPPG signals are obtained as inverted PPG signals [37]. Thus, the signals were inverted by multiplying by -1 to be used for further processing.

Next, the data were divided into 60s-length data segments that were shifted every 10 s. A length of 60 s ensure at least 9 breaths of the lowest frequency eligible as respiratory rate in this work, which is 0.15 Hz. The baseline contamination was removed with a high-pass filter with a cutoff frequency of 0.3 Hz, and high frequency noise was considerably attenuated by a low-pass filter with a cutoff frequency of 35 Hz. Subsequently, the artifacts were automatically detected and removed by an algorithm based on Hjorth parameters presented in [54] which was described in Section 3.2.1

at page 45. Segments with 30% or more of the time containing artifactual signal were discarded.

Note that aliasing problems may affect methods since respiratory information is obtained only at pulse occurrence. For this reason, fragments associated to a respiratory rate higher than the half mean pulse rate were excluded from the study.

4.3.2 Pulse-to-pulse methods

Significant points detection

In contrast to Chapter 3 where the PPG pulses detection was based on maximum of R waves previously detected in the ECG signal. The ECG signal is not available in the databases studied in this chapter. Furthermore, an ECG-independent pulse detector is desirable. In order to detect SCPPG pulses, an automatic PPG pulses detector was developed. Conventional PPG signals were used for developing the pulse detector in order to obtain an algorithm generally applicable. Concretely, the PSG recordings described in Section 4.2.3 were used. These recordings were chosen because they present very abrupt changes in pulse rate and also in pulse amplitude fluctuations as they present DAP events, which are analyzed in Chapter 5. Because of these characteristics of PSG recordings, a pulse detector which work for them results easy to extend to other kind of recordings.

The developed algorithm consists of two phases: a linear filtering transformation, and an adaptive thresholding operation. The filtering transformation is designed to accentuate the abrupt upslopes of the PPG pulses over the smoother one of the dichrotic pulses. It consists of a low-pass-differentiator filter designed by applying a least square linear-phase FIR technique [110] using transition band from 7.7 Hz to 8 Hz, considering PPG pulses to be below those frequencies (see Fig. 4.1). The impulse response and the transfer function of this filter are shown in Fig. 4.2.

For peak, $n_{\mathrm{A}_i}^*$, detection in filtered signal $y(n)$, a time varying threshold $\gamma(n)$ gradually decreasing between detected peaks was used. This threshold keeps the value of the previous detected peak $\gamma(n) = y(n_{\mathrm{A}_{i-1}}^*)$ during a refractory period which corresponds to 150 ms ($N_r = 0.15 f_s^{\mathrm{SP}}$) and after this it begins to decrease linearly. If there is no new detection after a time period $\hat{m}_{\mathrm{AA}_i}$, the threshold will have decreased to a percentage $\alpha < 1$ of $y(n_{\mathrm{A}_{i-1}}^*)$ and from that instant it maintains its value:
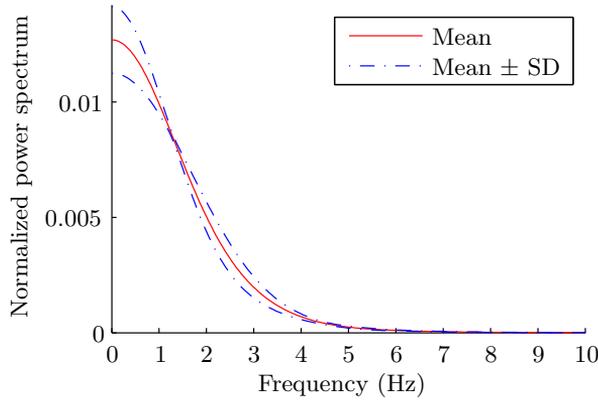
Figure 4.1: Inter-subject mean and SD of PPG pulses power spectrum, taking one pulse of each one of the 21 studied subjects and estimating its PSD by classic periodogram.

$$
\gamma(n) = \begin{cases}
y(n^*_{A_{i-1}}), & T_{r_i} \\
\dfrac{(\alpha-1)y(n^*_{A_{i-1}})}{\hat{m}_{AA_i} - N_r}\left(n - n^*_{A_{i-1}} - N_r\right) + y(n^*_{A_{i-1}}), & T_{d_i} \\
\alpha y(n^*_{A_{i-1}}), & T_{l_i}
\end{cases}, \quad (4.1)
$$

being T_{r_i} the time interval during refractory period, T_{d_i} the time interval during threshold decrease, and T_{l_i} the time interval during which the threshold maintains its lowest value as defines:

$$
\begin{cases}
T_{r_i} : (n - n^*_{A_{i-1}}) < N_r \\
T_{d_i} : N_r \le (n - n^*_{A_{i-1}}) < \hat{m}_{AA_i} \\
T_{l_i} : (n - n^*_{A_{i-1}}) \ge \hat{m}_{AA_i}
\end{cases}, \qquad \forall n \in \left[n^*_{A_{i-1}}, n^*_{A_i} \right], \qquad (4.2)
$$

where α was set to 0.2, and the $\hat{m}_{AA_i}$ period is an estimation of the inter-peak interval calculated as the median of three peak-to-peak intervals previously detected:

$$
\hat{m}_{AA_i} = \text{median}\left\{ \left(n^*_{A_{i-4}} - n^*_{A_{i-3}}\right), \left(n^*_{A_{i-3}} - n^*_{A_{i-2}}\right), \left(n^*_{A_{i-2}} - n^*_{A_{i-1}}\right) \right\}. \quad (4.3)
$$

Finally, the maximum of each PPG pulse n_{A_i} is set at the maximum point of PPG signal within a 300 ms-length interval beginning at each peak $n^*_{A_i}$ detected in transformed signal. Figure 4.3 shows an example of PPG pulses detection during a DAP event.
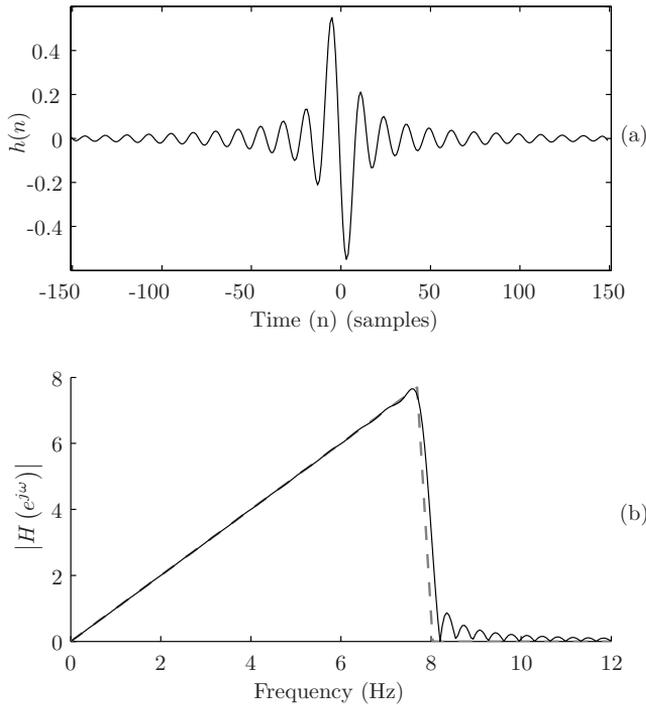
Figure 4.2: Implemented low-pass-differentiator filter: (a) shows the impulse response, and (b) the the transfer function (solid black line) over the ideal one (slashed grey line).

Then, baseline point of the ith SCPPG pulse was defined as the minimum previous to:

$$n_{\mathrm{B}_i} = \underset{n \in \left[n_{\mathrm{A}_i} - 0.4 f_s^{\mathrm{SP}}, n_{\mathrm{A}_i}\right]}{\arg \min} \left\{ x_{\mathrm{PPG}}(n) \right\}, \tag{4.4}$$

and subsequently, the fiducial point of each pulse in SCPPG used for PRV analysis was the medium-amplitude point n_{M_i}, defined as that point in which the amplitude has reached the 50% of its maximum:

$$n_{\mathrm{M}_i} = \underset{n \in \left[n_{\mathrm{B}_i}, n_{\mathrm{A}_i}\right]}{\arg \min} \left\{ \left| x_{\mathrm{PPG}}(n) - \frac{x_{\mathrm{PPG}}\left(n_{\mathrm{A}_i}\right) + x_{\mathrm{PPG}}\left(n_{\mathrm{B}_i}\right)}{2} \right| \right\}. \tag{4.5}$$

The reason for using n_{M_i} as fiducial point instead of using n_{A_i} is the robustness. The maximum of PPG and SCPPG pulses are typically located at smooth zones, so n_{A_i} can be considerably changed by a low level of noise. However, n_{M_i} is located at the upslope of the pulse which represents a very abrupt zone of the signal [51].
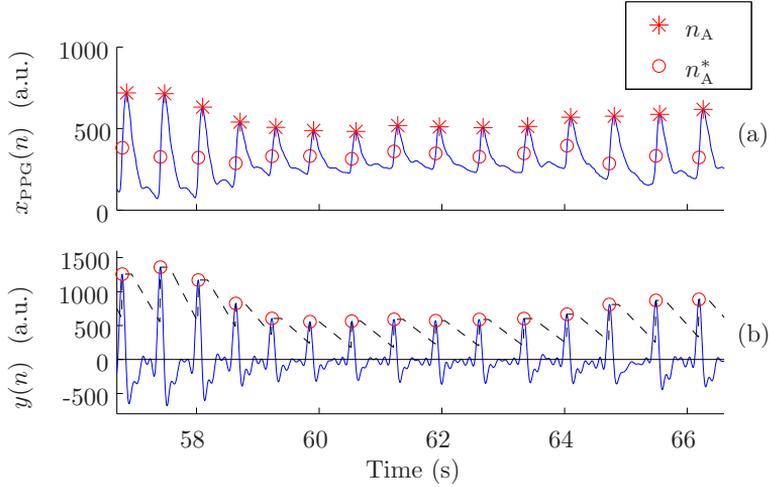
Figure 4.3: Example of detector behavior during a DAP event: (a) shows the PPG signal, and (b) shows its filtered signal (solid blue line) and the resulting time varying threshold (slashed black line).

The pulse onset n_{O_i} and end n_{E_i} points were detected by adapting the methodologies described in Chapter 3 to SCPPG signals. The light-reflection basis of SCPPG signals makes their pulses smoother and larger than those in transmitted-light-based PPG signals. Because of this, the intervals in which the maximum up-/down-slope points n_{U_i} and n_{D_i} are searched were enlarged from 300 ms to 400 ms:

$$n_{\mathrm{U}_i} = \arg\max_n \left\{ x'_{\mathrm{SCPPG}}(n) \right\}, \quad n \in [n_{\mathrm{A}_i} - 0.4 f_s^{\mathrm{SP}}, n_{\mathrm{A}_i}] \qquad (4.6)$$

$$n_{\mathrm{D}_i} = \arg\min_n \left\{ x'_{\mathrm{SCPPG}}(n) \right\}, \quad n \in [n_{\mathrm{A}_i}, n_{\mathrm{A}_i} + 0.4 f_s^{\mathrm{SP}}], \qquad (4.7)$$

and consequently, the intervals in which pulse onset n_{O_i} and end n_{E_i} points were also enlarged:

$$\Omega_{\mathrm{O}_i} = [n_{\mathrm{A}_i} - 0.4 f_s^{\mathrm{SP}}, \quad n_{\mathrm{U}_i}] \qquad (4.8)$$

$$\Omega_{\mathrm{E}_i} = [n_{\mathrm{U}_i}, \quad n_{\mathrm{A}_i} + 0.4 f_s^{\mathrm{SP}}]. \qquad (4.9)$$

Parameters f_c (cutoff frequency of the low-pass filter before obtaining the derivative signal $x'_{\mathrm{PPG}}(n)$) was set to 2 Hz, and η (percentage of maximum/minimum amplitude of $x'_{\mathrm{SCPPG}}(n)$ at $n_{\mathrm{O}_i}/n_{\mathrm{E}_i}$) was set to 0.5 as described in Section 4.4.1.
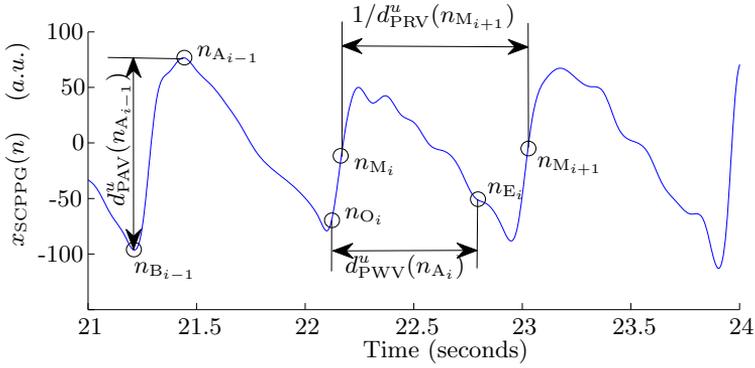
Figure 4.4: Pulse-to-pulse-methods-based DR signals over a SCPPG signal.

Derived respiration signals

The 3 PPG-based DR signals used in Chapter 3 (PRV, PAV, and PWV) were also used in this study:

$$d^u_{\mathrm{PRV}}(n) = \sum_i f^{\mathrm{SP}}_s \frac{1}{n_{\mathrm{N}_i} - n_{\mathrm{N}_{i-1}}} \delta\left(n - n_{\mathrm{N}_i}\right) \tag{4.10}$$

$$d^u_{\mathrm{PAV}}(n) = \sum_i \left[x_{\mathrm{SCPPG}}\left(n_{\mathrm{A}_i}\right) - x_{\mathrm{SCPPG}}\left(n_{\mathrm{B}_i}\right)\right] \delta\left(n - n_{\mathrm{A}_i}\right) \tag{4.11}$$

$$d^u_{\mathrm{PWV}}(n) = \sum_i \frac{1}{f^{\mathrm{SP}}_s}\left(n_{\mathrm{E}_i} - n_{\mathrm{O}_i}\right) \delta\left(n - n_{\mathrm{A}_i}\right). \tag{4.12}$$

Figure 4.4 illustrates the pulse-to-pulse-methods-based DR signals over a SCPPG signal. The same processing applied in Chapter 3 was applied here in order to obtain the final 4 Hz outlier–rejected evenly sampled band–pass filtered version of DR signals, denoted without the "u" superscript: a MAD-based outlier rejection, a cubic splines interpolation, and a band-pass filtering (0.075-1 Hz).

4.3.3 Non-pulse-to-pulse methods

Amplitude and frequency modulation sequences were extracted from SCPPG signal as described in [104]. The amplitude and frequency modulation sequences are extracted from a time-frequency spectrum obtained by the variable frequency complex demodulation (VFCDM) method [111].

The VFCDM-based time-frequency spectrum obtainment procedure can be divided in 2 steps: estimations of a time-frequency spectrum by com-

plex demodulation (CDM) denoted fixed frequency CDM (FFCDM) in this thesis, and subsequently applying VFCDM selecting only the dominant frequencies of interest for improving the time-frequency resolution.

Fixed frequency complex demodulation

Let $x(t)$ be a narrow-band oscillation:

$$x(t) = x_{\text{DC}}(t) + A(t)\cos\left(2\pi f_0 t + \Phi(t)\right), \tag{4.13}$$

where f_0 is the center frequency, $A(t)$ is the instantaneous amplitude, $\Phi(t)$ is the phase, and $x_{\text{DC}}(t)$ is the DC component.

$A(t)$ and $\Phi(t)$ can be extracted for a given f_0 from $x(t)$ by multiplying it by $e^{-j2\pi f_0 t}$, shifting f_0 to zero frequency:

$$z(t) = x(t)e^{-j2\pi f_0 t} = x_{\text{DC}}(t)e^{-j2\pi f_0 t} + \frac{A(t)}{2}e^{j\Phi(t)} + \frac{A(t)}{2}e^{-j(4\pi f_0 t + \Phi(t))}. \tag{4.14}$$

Then, a low-pass filter can be applied to $z(t)$, with a cutoff-frequency less than f_0, obtaining the middle term of (4.14):

$$z_{\text{LP}}(t) = \frac{A(t)}{2}e^{j\Phi(t)}, \tag{4.15}$$

from which $A(t)$ and $\Phi(t)$ can be obtained as:

$$A(t) = 2\left|z_{\text{LP}}(t)\right| \tag{4.16}$$

$$\Phi(t) = \tan^{-1}\left(\frac{\text{Im}(z_{\text{LP}}(t))}{\text{Re}(z_{\text{LP}}(t))}\right). \tag{4.17}$$

Variable frequency complex demodulation

Consider a case when modulating frequency varies as a function of time, $f_0(t)$. Equation 4.13 can be rewritten as:

$$x(t) = x_{\text{DC}}(t) + A(t)\cos\left(\int_0^t 2\pi f_0(\tau)d\tau + \Phi(t)\right). \tag{4.18}$$

The frequency shift in (4.14) can be performed this time by multiplying by $e^{-j\int_0^t 2\pi f_0(\tau)d\tau}$ obtaining:

$$z(t) = x(t)e^{-j\int_0^t 2\pi f_0(\tau)d\tau} = x_{\text{DC}}(t)e^{-j\int_0^t 2\pi f_0(\tau)d\tau} + \frac{A(t)}{2}e^{j\Phi(t)} +$$

$$+ \frac{A(t)}{2}e^{-j\left(\int_0^t 4\pi f_0(\tau)d\tau + \Phi(t)\right)}, \tag{4.19}$$

from which the middle term can be obtained similarly to the FFCDM case, i.e., by using a low-pass filter with a cut-off frequency lower than $f_0(t)$. The expression of this term is the same of $z_{\mathrm{LP}}(t)$ in (4.15), and instantaneous amplitude $A(t)$ and phase $\Phi(t)$ can be obtained similarly to the FFCDM case (see (4.16) and (4.17), respectively). The instantaneous frequency $f(t)$ can be obtained from $\Phi(t)$ [112]:

$$f(t) = f_0(t) + \frac{1}{2\pi}\frac{d\Phi(t)}{dt}. \tag{4.20}$$

In this way, a time-frequency spectrum can be obtained by first applying FFCDM using a set of central frequencies:

$$f_{0_k} = (k-1)(2f_\omega), \qquad k = 1, 2, \mathrm{int}\left(\frac{f_{\max}}{2f_\omega}\right), \tag{4.21}$$

where the bandwidth between successive center frequencies is $2f_\omega$, and $f_{\max}$ denotes the highest signal frequency. A FIR low-pass filter with a cut-off frequency f_ω was applied for obtaining each $z_{\mathrm{LP}_k}(n)$.

The dominating frequencies $f_k(t)$ can be obtained by (4.20) based on instantaneous phase (4.17), and $A_k(t)$ can be obtained from (4.16). Subsequently, $f_k(t)$ were used as central frequencies for applying VFCDM using a cut-off frequency for the low-pass filter of $f_\omega/2$, refining time-frequency resolution [111].

Parameter f_ω was set to 0.6 Hz. Further details are given in [104].

Derived respiration signals

Once the VFCDM-based time-frequency spectrum $S_{\mathrm{VFCDM}}(n, f)$ is computed, $d_{\mathrm{FM}}(n)$ is determined by extracting the frequency component that has the largest amplitude for each time point at the heart rate frequency band, since heart rate is considered the carrier wave:

$$d_{\mathrm{FM}}(n) = \underset{f \in \Omega_{\mathrm{HR}}}{\arg\max}\left\{S_{\mathrm{VFCDM}}(n, f)\right\}, \tag{4.22}$$

where Ω_{HR} denotes the frequency band in which heart rate is expected. This band is defined by using the spectrum of the SCPPG signal $S_{\mathrm{SCPPG}}(f)$:

$$f_{\mathrm{HR}} = \underset{f}{\arg\max}\left\{S_{\mathrm{SCPPG}}(f)\right\}, \qquad f \in [0.5\mathrm{Hz}, 2\mathrm{Hz}] \tag{4.23}$$

$$\Omega_{\mathrm{HR}} = [f_{\mathrm{HR}} - 0.2\mathrm{Hz}, f_{\mathrm{HR}} + 0.3\mathrm{Hz}]. \tag{4.24}$$
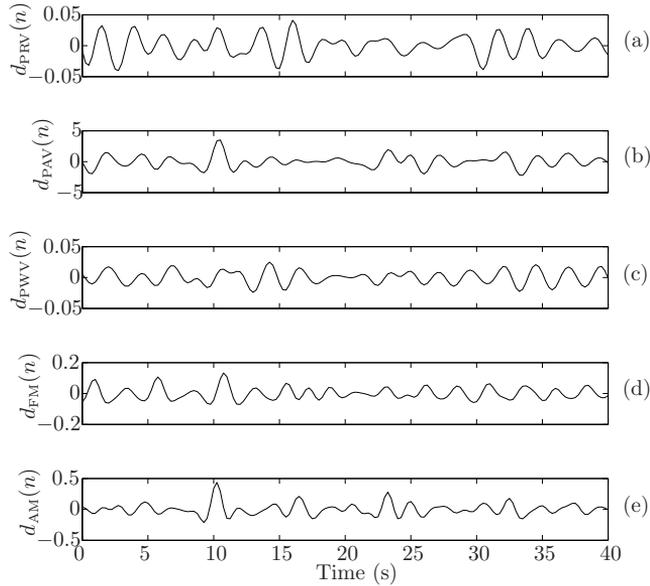
Figure 4.5: Example of DR signals studied in this paper: $d_{\mathrm{PRV}}(n)$ (a), $d_{\mathrm{PAV}}(n)$ (b), $d_{\mathrm{PWV}}(n)$ (c), $d_{\mathrm{FM}}(n)$ (d), and $d_{\mathrm{AM}}(n)$ (e). In this expample, the subject was asked to breathe at 0.4 Hz.

A similar procedure is used for extracting the amplitude modulation:

$$d_{\mathrm{AM}}(n) = \max_{f} \left\{ S_{\mathrm{VFCDM}}(n, f) \right\}, f \in \Omega_{\mathrm{HR}}. \tag{4.25}$$

The same processing applied to pulse-to-pulse-methods-based DR signals (Section 4.3.2) was applied also to $d_{\mathrm{FM}}(n)$ and $d_{\mathrm{AM}}(n)$, i.e., a 4-Hz cubic spline interpolation followed by a band-pass filter (0.15-0.7 Hz). Fig. 4.5 shows an example of studied DR signals.

4.3.4 Respiratory rate estimation algorithm

Respiratory rate was estimated from the jth DR signal by using its PSD $S_j(f)$, which was estimated by applying a modified periodogram using a Hamming window. Figure 4.6 shows an example of $S_j(f)$ for each one of the studied DR signals. The respiratory rate $\hat{f}$ is estimated within the band [0.15 Hz, 0.7 Hz], as the frequency at which the absolute maximum of $S_j(f)$ is located.

In addition, respiratory rate was also estimated by combining information from several DR signals by using an algorithm based on a "peakness"-conditioned average of PSDs as those used in Chapter 2 and Chapter 3.
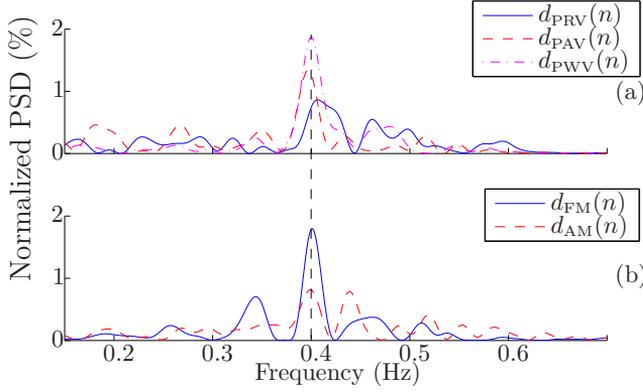
Figure 4.6: Example of normalized PSD of DR signals studied in this paper: $d_{\text{PRV}}(n)$ (a), $d_{\text{PAV}}(n)$ (b), $d_{\text{PWV}}(n)$ (c), $d_{\text{FM}}(n)$ (d), and $d_{\text{AM}}(n)$ (e). In this example, the subject was asked to breathe at 0.4 Hz.

This time, the "peakness" of the jth PSD is redefined as:

$$P_j = \frac{\int_{f_p(j)-0.05}^{f_p(j)+0.05} S_j(f)df}{\int_{0.15\text{Hz}}^{0.7\text{Hz}} S_j(f)df}, \tag{4.26}$$

where $f_p(j)$ denotes the highest peak within the studied band [0.15, 0.7 Hz] in the PSD of the jth DR signal.

The "peakness"-conditioned average is computed as:

$$\bar{S}(f) = \sum_j \chi_j^{\text{A}} \chi_j^{\text{B}} S_j(f), \tag{4.27}$$

where the two criteria χ^{A} and χ^{B} used in Chapter 2 and Chapter 3 are also used, allowing to take part in the average only to those spectra whose "peakness" is higher than a fixed value (χ^{A}) and which are the most peaked for each subject at each segment (χ^{B}):

$$\chi_j^{\text{A}} = \begin{cases} 1, & P_j \geq \xi \\ 0, & otherwise \end{cases} \tag{4.28}$$

$$\chi_j^{\text{B}} = \begin{cases} 1, & P_j \geq \max_j \{P_j\} - \lambda \\ 0, & otherwise \end{cases}. \tag{4.29}$$

Finally, $\hat{f}$ is estimated as the frequency at which the absolute maximum of $\bar{S}(f)$ is located within the studied band [0.15 Hz, 0.7 Hz]:

$$\hat{f} = \underset{f \in [0.15, 0.7]}{\arg\max} \left\{ \bar{S}(f) \right\}. \tag{4.30}$$

Respiratory rate was estimated from each one of the five DR signals separately, and from two combinations:

- $C_{\mathrm{PRV,PAV,PWV}}$: $d_{\mathrm{PRV}}(n)$, $d_{\mathrm{PAV}}(n)$, and $d_{\mathrm{PWV}}(n)$

- C_{ALL}: $d_{\mathrm{PRV}}(n)$, $d_{\mathrm{PAV}}(n)$, $d_{\mathrm{PWV}}(n)$, $d_{\mathrm{FM}}(n)$, and $d_{\mathrm{AM}}(n)$

Furthermore, the Kruskal-Wallis statistical test and the Bonferroni correction were used for analysis of differences of e_{R} for the different methods. The non-parametric Kruskal-Wallis statistical test was chosen because it was observed that is not normal distributed, and the Bonferroni correction was applied in order to control the familywise error rate because multiple comparisons were performed.

4.3.5 Estimation of power of oscillations

In order to study the respiratory rate influence in the resulting magnitude of PPG-based DR signals, the power of oscillations in DR signals at the respiratory band was estimated by an algorithm based on PSD. This time, one PSD was obtained from each one of the 2-minutes-length recordings corresponding to each subject and each respiratory rate. These PSDs are denoted $S_j^*(f)$ and they were computed by using the Welch periodogram using a 96-samples-length (24 seconds) Hamming window with an overlap of 50%.

Subsequently, the principal frequency of the oscillations at the respiratory band was estimated as:

$$\hat{f}_j^* = \arg\max\left\{S_j^*(f)\right\}, \quad f \in [f_{\mathrm{R}} - 0.05\mathrm{Hz}, \quad f_{\mathrm{R}} + 0.05\mathrm{Hz}], \qquad (4.31)$$

where f_{R} denotes the respiratory rate at which subject is requested to breath.

Then, the power of the oscillations at the respiratory band was estimated as:

$$\mathcal{P}_j = \frac{f_s^{\mathrm{SP}}}{N_{\mathrm{FFT}}} \sum_{f=\hat{f}_j^* - 0.025\mathrm{Hz}}^{\hat{f}_j^* + 0.025\mathrm{Hz}} S_j^*(f), \qquad (4.32)$$

where N_{FFT} denotes the number of points of $S_j^*(f)$.

The Friedman statistical test was used in order to study whether there are significant differences (p-value < 0.05) for different respiratory rates for each device.

4.4 Results

4.4.1 Pulse width parameters optimization

Optimal values for f_c and η were obtained by a similar procedure to that described in Section 3.3.1. They were computed all the 323 possible combinations corresponding to $\eta \in [0, 0.8]$ with a step of 0.05, and $f_C \in [1, 10]$ Hz with a step of 0.5 Hz, and the relative error of estimated respiratory rate was obtained as:

$$e_R = \frac{\hat{f} - f_R}{f_R} \times 100. \tag{4.33}$$

The values which minimized the mean of absolute value of e_R were obtained and chosen as optimal. These values coincided for the 3 studied devices and they were $\eta = 0.5$ and $f_c = 2$ Hz.

4.4.2 Respiratory rate estimation

The percentages of 60-s-length fragments excluded by the artifact and aliasing criteria described in Section are shown in Table 4.1.

Table 4.1: Percentage of fragments excluded from the study due to the artifact and aliasing criteria.

f_R (Hz)	iPhone 4S		iPod 5		HTC One M8	
	Artifact	Aliasing	Artifact	Aliasing	Artifact	Aliasing
0.2	15.38%	0.00%	8.47%	0.00%	20.98%	0.00%
0.3	17.51%	0.00%	9.63%	0.00%	19.52%	0.00%
0.4	16.36%	0.00%	6.95%	0.00%	18.10%	0.00%
0.5	14.03%	1.36%	4.79%	6.38%	22.13%	0.00%
0.6	14.09%	24.55%	7.53%	35.48%	8.57%	15.71%

Relative error e_R was obtained for each studied DR signal and combination. Medians and IQRs obtained for e_R from different DR signals and combinations, for each f_R and device, are shown in Table 4.2, and Fig. 4.7 illustrates them in boxplots.

Table 4.3 shows those pairs of methods for which obtained e_R showed significant differences (p-value< 0.05) between each other, according to the Kruskall-Wallis statistical test and the Bonferroni correction.

Table 4.2: Obtained medians and IQRs for e_R from different DR signals and combinations, for each f_R and device.

f_R (Hz)	DR Signal / Combination	iPhone 4S Median/IQR	iPod 5 Median/IQR	HTC One M8 Median/IQR
0.2	$d_\mathrm{FM}(n)$	0.10%/2.44%	0.10%/0.00%	0.10%/2.44%
	$d_\mathrm{AM}(n)$	0.10%/2.44%	0.10%/4.88%	0.10%/4.88%
	$d_\mathrm{PRV}(n)$	0.10%/1.95%	0.10%/1.46%	0.10%/0.98%
	$d_\mathrm{PAV}(n)$	0.10%/2.93%	0.10%/3.05%	1.07%/15.87%
	$d_\mathrm{PWV}(n)$	0.10%/1.46%	0.10%/1.46%	0.10%/1.46%
	$C_\mathrm{PRV.PAV.PWV}$	-0.39%/1.46%	-0.39%/0.98%	-0.39%/0.98%
	C_ALL	-0.39%/1.10%	-0.39%/0.98%	-0.39%/0.98%
0.3	$d_\mathrm{FM}(n)$	0.91%/1.63%	-0.72%/1.63%	0.91%/18.31%
	$d_\mathrm{AM}(n)$	-0.72%/3.66%	-0.72%/2.03%	-0.72%/3.26%
	$d_\mathrm{PRV}(n)$	-0.07%/0.98%	-0.07%/1.06%	-0.07%/1.38%
	$d_\mathrm{PAV}(n)$	-0.07%/1.95%	-0.39%/1.38%	-0.39%/2.36%
	$d_\mathrm{PWV}(n)$	0.10%/0.98%	-0.07%/0.65%	-0.39%/1.63%
	$C_\mathrm{PRV.PAV.PWV}$	0.91%/0.65%	-0.07%/0.98%	-0.07%/0.73%
	C_ALL	-0.07%/0.65%	-0.07%/0.98%	-0.07%/0.98%
0.4	$d_\mathrm{FM}(n)$	0.10%/4.88%	0.10%/1.22%	0.10%/10.99%
	$d_\mathrm{AM}(n)$	-2.34%/41.50%	-1.12%/36.62%	-1.12%/34.18%
	$d_\mathrm{PRV}(n)$	-0.15%/1.22%	-0.15%/1.22%	0.10%/2.20%
	$d_\mathrm{PAV}(n)$	-0.15%/3.17%	-0.39%/24.66%	-0.63%/15.38%
	$d_\mathrm{PWV}(n)$	-0.15%/1.46%	-0.15%/1.22%	-0.15%/2.69%
	$C_\mathrm{PRV.PAV.PWV}$	-0.15%/0.49%	-0.15%/0.73%	-0.15%/1.22%
	C_ALL	-0.15%/0.73%	-0.15%/0.73%	-0.15%/0.98%
0.5	$d_\mathrm{FM}(n)$	-0.39%/3.17%	-0.39%/1.95%	-0.39%/11.72%
	$d_\mathrm{AM}(n)$	-39.94%/55.91%	-39.45%/59.57%	-25.78%/56.64%
	$d_\mathrm{PRV}(n)$	-0.20%/4.64%	-0.20%/1.17%	-0.20%/11.91%
	$d_\mathrm{PAV}(n)$	-0.59%/44.14%	-0.39%/45.90%	-0.20%/26.56%
	$d_\mathrm{PWV}(n)$	-0.20%/2.29%	0.00%/1.95%	-1.37%/39.06%
	$C_\mathrm{PRV.PAV.PWV}$	-0.20%/0.78%	0.00%/0.78%	-0.20%/1.17%
	C_ALL	0.00%/0.98%	0.00%/0.78%	-0.20%/4.69%
0.6	$d_\mathrm{FM}(n)$	-0.72%/50.05%	0.10%/46.39%	-3.97%/44.76%
	$d_\mathrm{AM}(n)$	-49.95%/65.10%	-57.28%/66.73%	-37.74%/59.41%
	$d_\mathrm{PRV}(n)$	-0.47%/36.42%	-0.23%/4.11%	-13.90%/56.32%
	$d_\mathrm{PAV}(n)$	-2.99%/59.57%	-51.66%/69.42%	-31.64%/54.32%
	$d_\mathrm{PWV}(n)$	-0.39%/32.63%	-0.07%/8.63%	-14.71%/48.50%
	$C_\mathrm{PRV.PAV.PWV}$	-0.23%/2.40%	-0.07%/3.01%	-13.49%/54.57%
	C_ALL	-0.23%/2.12%	-0.07%/1.99%	-2.51%/37.64%
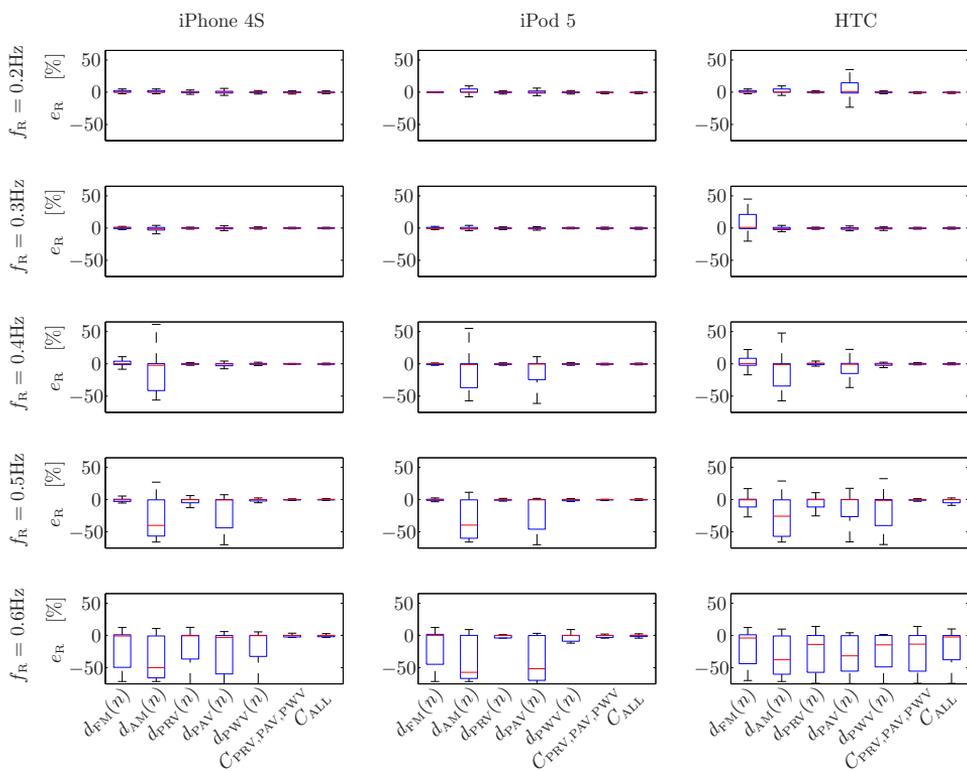
Figure 4.7: Boxplots of relative error e_{R} for the different methods, devices, and respiratory rates f_{R}.

Table 4.3: Pairs of methods for which obtained e_{R} showed significant differences (p-value< 0.05) between each other, according to the Kruskall-Wallis statistical test and the Bonferroni correction. Note in the text that observed differences are due to outliers.

	$f_{\mathrm{R}} \in \{0.2, 0.3, 0.4\}$ Hz	$f_{\mathrm{R}} \in \{0.5, 0.6\}$ Hz
iPhone 4S	{ FM, AM }, { FM, PRV } , { FM, PAV } , { FM, PWV } , { FM,$C_{\mathrm{PRV,PAV,PWV}}$} , { FM,C_{ALL}} , { AM, PWV }	{ FM, AM } , { FM, PRV } , { AM, PRV } , { AM, PAV } , { AM, PWV } , { AM,$C_{\mathrm{PRV,PAV,PWV}}$} , { AM,C_{ALL}} , { PRV, PAV } , { PAV, PWV } , {PAV,$C_{\mathrm{PRV,PAV,PWV}}$} , { PAV,C_{ALL}}
iPod 5	{ FM-AM }, { FM-PAV } , { AM,PRV } , { AM,PAV } , { AM,PWV } , { AM,$C_{\mathrm{PRV,PAV,PWV}}$} , { AM, C_{ALL}} , { PRV,PAV } , { PAV,PWV } , { PAV, $C_{\mathrm{PRV,PAV,PWV}}$} , { PAV,C_{ALL}}	{ FM,AM } , { FM,PAV } , { AM,PRV } , { AM,PAV } , { AM,PWV } , { AM, $C_{\mathrm{PRV,PAV,PWV}}$} , { AM, C_{ALL}} , { PRV,PAV } , { PAV,PWV } , { PAV, $C_{\mathrm{PRV,PAV,PWV}}$} , { PAV, C_{ALL}}
HTC	{ FM,AM } , { FM,PRV } , { FM,PAV } , { FM,PWV } , { FM, $C_{\mathrm{PRV,PAV,PWV}}$} , { FM, C_{ALL}}	{ FM,AM } , { FM,PAV } , { FM,PWV } , { AM,PRV } , { AM, $C_{\mathrm{PRV,PAV,PWV}}$} , { AM,C_{ALL}}

4.4.3 Respiratory rate influence in the resulting magnitude of DR signals

Table 4.4 shows inter-subject medians and IQRs of obtained $\mathcal{P}_{\mathrm{PRV}}$, $\mathcal{P}_{\mathrm{PAV}}$ and $\mathcal{P}_{\mathrm{PWV}}$, for each device and each respiratory rate. Figure 4.8 shows boxplots for these powers.

Significant differences according to the Friedman statistical test were found for the following groups (p-value < 0.05):

- PRV:

    - Conventional PPG: 0.2-0.5Hz, 0.2-0.6Hz, and 0.3-0.6Hz
    - iPhone 4S: 0.2-0.4Hz, 0.2-0.5Hz, and 0.2-0.6Hz
    - iPod 5: 0.2-0.4Hz, 0.2-0.5Hz, 0.2-0.6Hz, and 0.3-0.6Hz
    - HTC One M8: 0.2-0.4Hz, 0.2-0.5Hz, 0.2-0.6Hz, 0.3-0.5Hz, 0.3-0.6Hz, and 0-4-0.6Hz

- PAV:

    - Conventional PPG: None
    - iPhone 4S: None
    - iPod 5: 0.3-0.6Hz, and 0.4-0.6Hz
    - HTC One M8: 0.2-0.5Hz, 0.2-0.6Hz, 0.3-0.6Hz, and 0.4-0.6Hz

- PWV:

    - Conventional PPG: 0.2-0.6Hz
    - iPhone 4S: 0.2-0.3Hz, 0.2-0.4Hz, 0.2-0.5Hz, and 0.2-0.6Hz
    - iPod 5: 0.2-0.4Hz, 0.2-0.5Hz, 0.2-0.6Hz, 0.3-0.6Hz, and 0.5-0.6Hz
    - HTC One M8: 0.2-0.4Hz, 0.2-0.5Hz, 0.2-0.6Hz, 0.3-0.6Hz, and 0.4-0.6Hz

4.5 Discussion

In this chapter, the methods for deriving respiratory rate from PPG signal which were presented in Chapter 3 are adapted to SCPPG signals. Two combinations are studied. One of them combines information from pulse-to-pulse methods PRV, PAV, and PWV presented in Chapter 3 ($C_{\mathrm{PRV.PAV.PWV}}$).

Table 4.4: Inter-subject medians and IQR of obtained $\mathcal{P}_{PRV}$, $\mathcal{P}_{PAV}$ and $\mathcal{P}_{PWV}$, for each device and each respiratory rate.

	f_R	$\mathcal{P}_{PRV}$ (s^{-2})	$\mathcal{P}_{PAV}$ $(a.u.^2)$	$\mathcal{P}_{PWV}$ (s^2)
	(Hz)	Median/IQR	Median/IQR	Median/IQR
Conventional PPG	0.2	4.19E-05/2.22E-05	3.80E-04/6.49E-04	6.12E-06/1.40E-05
	0.3	9.70E-06/1.19E-05	3.13E-04/1.43E-03	2.84E-06/4.80E-06
	0.4	5.40E-06/5.43E-06	3.30E-04/1.83E-03	1.84E-06/4.02E-06
	0.5	3.88E-06/3.73E-06	2.20E-04/7.83E-04	1.17E-06/2.67E-06
	0.6	2.93E-06/2.35E-06	1.78E-04/1.21E-03	4.63E-07/3.41E-07
iPhone 4S	0.2	1.39E-05/1.74E-05	5.95E-04/1.05E-03	3.14E-06/5.02E-06
	0.3	5.47E-06/8.29E-06	3.20E-04/9.38E-04	1.02E-06/2.08E-06
	0.4	2.01E-06/4.79E-06	3.15E-04/7.62E-04	6.64E-07/1.08E-06
	0.5	2.31E-06/5.02E-06	1.84E-04/6.66E-04	5.98E-07/1.04E-06
	0.6	2.26E-06/8.85E-06	1.56E-04/4.53E-04	6.30E-07/1.28E-06
iPod 5	0.2	1.49E-05/1.81E-05	1.65E-04/3.81E-04	4.53E-06/5.48E-06
	0.3	4.72E-06/6.76E-06	1.12E-04/9.49E-04	1.33E-06/1.88E-06
	0.4	2.23E-06/4.83E-06	1.95E-04/7.24E-04	7.01E-07/1.09E-06
	0.5	2.27E-06/4.83E-06	1.71E-04/3.47E-04	6.42E-07/1.37E-06
	0.6	1.81E-06/2.97E-06	5.81E-05/1.41E-04	2.32E-07/8.60E-07
HTC One M8	0.2	2.03E-05/2.65E-05	2.31E-04/2.88E-04	4.54E-06/8.94E-06
	0.3	4.26E-06/6.33E-06	1.21E-04/4.65E-04	1.19E-06/1.46E-06
	0.4	2.88E-06/4.34E-06	1.35E-04/2.98E-04	1.27E-06/1.21E-06
	0.5	2.48E-06/3.72E-06	7.21E-05/2.01E-04	4.37E-07/7.88E-07
	0.6	1.35E-06/1.80E-06	5.32E-05/9.18E-05	2.68E-07/6.68E-07
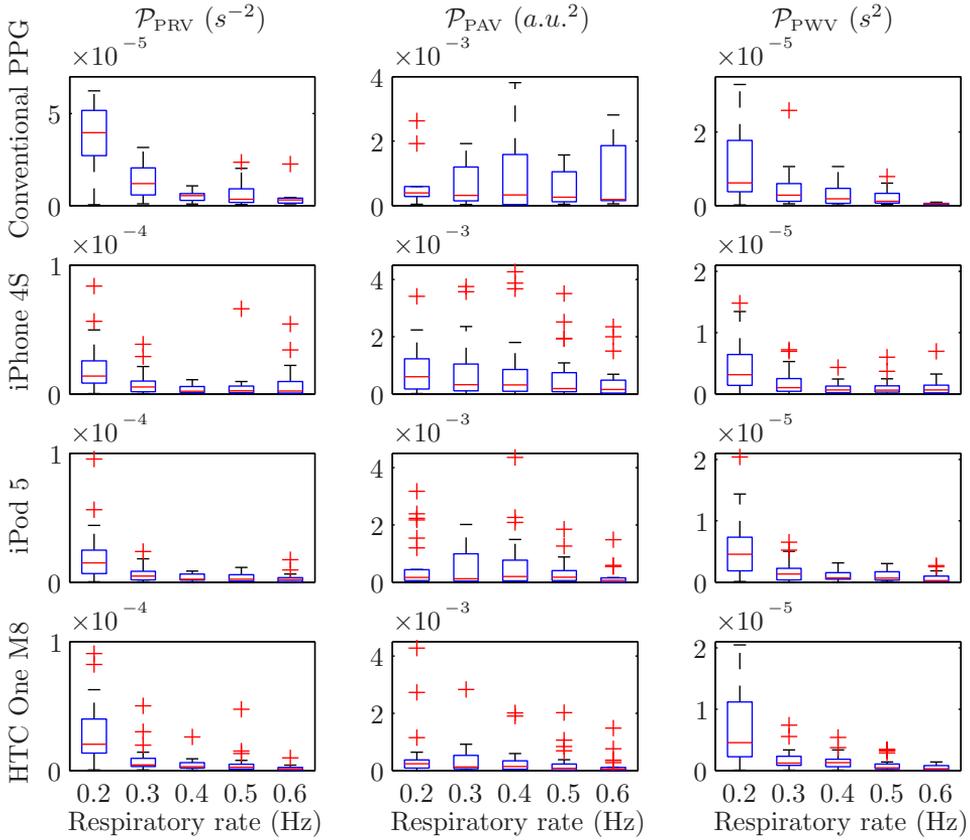
Figure 4.8: Boxplots of obtained $\mathcal{P}_{\mathrm{PRV}}$, $\mathcal{P}_{\mathrm{PAV}}$, and $\mathcal{P}_{\mathrm{PWV}}$, for each device and each respiratory rate.

The other methodology uses these pulse-to-pulse methods in combination with non-pulse-to-pulse methods presented in [104] (C_{ALL}).

The low sampling rate and the ambient-light noise considerably affect the quality of SCPPG signals. In order to deal with this issue, the artifact detector presented in [54] and was described in Section 3.2.1 at page 45 was used to automatically exclude the artifactual fragments, which represents up to a 22.13% of the total fragments (HTC One M8 at $f_{\mathrm{R}} = 0.5$ Hz).

PPG-amplitude- and rate-based DR signals (as those based on PAV, PRV, AM and FM) present LF modulations below 0.15 Hz due to the sympathetic activity, which can be considered as noise from the point of view of deriving respiratory information. As stated in Chapter 3, the power of these modulations is usually comparable or even higher than the respiration-related modulations, and this may confound respiratory rate estimation. For this reason, the studied frequency band starts at 0.15 Hz in this chapter (being 0.2 Hz the lower expected respiratory rate) in order to study if respiration-related modulations already studied in PPG signals are still present in SCPPG signals, with independence of this kind of noise. However, the frequency band should be extended in further studies nearer to the final application. A possible solution to deal with the LF-modulation problem could be the one used at initialization of algorithms described in Chapter 2 and Chapter 3, based on a 2-steps search (first in [0.15, 0.4] Hz band and subsequently extending it to wider band if no "peaked" peak is found).

The metronome frequency was used as reference for respiratory rate because a respiratory signal was not available when data were collected for the iPod 5 and HTC One M8 experiments. However, a respiratory signal from a respiration belt was available for 10 of the subjects in the iPhone 4S experiments and according to it, subjects breathed at the metronome respiratory rate with an error of 0.12/1.01 mHz (median/IQR). Furthermore, the analyzed PPG data for studying the respiratory rate influence in the resulting magnitude of DR signals, includes also a respiratory signal from a respiration belt and according to it, subjects breathed at the metronome respiratory rate with an error of 0.22/1.05 mHz. These results suggest that subjects breathe according to the metronome frequency accurate enough to consider it as a reference.

Those fragments associated with a respiratory rate higher than half mean pulse rate were also excluded, because the pulse-to-pulse methods would track an alias in such situations. This problem affects high f_{R} (0.5 and 0.6 Hz), e.g., for tracking a $f_{\mathrm{R}} = 0.6$ Hz using pulse-to-pulse methods, it

would be necessary to have a mean pulse rate of 1.2 Hz, i.e., 72 beats per minute. However, a high f_R with a low pulse rate does not represent a realistic physiological situation. In such situations when the ANS requires a high respiratory rate, it also requires a high heart rate (which leads to a high pulse rate), e.g., during exercise.

An analysis of the influence of respiratory rate in the power of respiration-related oscillations in PRV, PAV, and PWV has been also performed in this chapter. Significant differences according to the Friedman statistical test were found in the powers $\mathcal{P}_{PRV}$, $\mathcal{P}_{PAV}$ and $\mathcal{P}_{PWV}$ for some groups. When analyzing PRV and PWV, clear tendencies of power decrease as f_R increases were observed, while less evident tendencies were observed when analyzing PAV. Estimated PSD of PAV signals showed other non-respiration-related oscillations, which act as noise from the point of view of the study of respiration-related oscillations and make longer the IQR of $\mathcal{P}_{PAV}$. However, a median decrease tendency when respiratory rate increases can be still observed. These results suggest that the power of respiration-related oscillations in PRV, PAV and in PWV decreases when respiratory rate increases. A possible reason for this observation is that the ANS response which generates the respiration-related modulations in PRV, PAV and PWV may act as a physiological low-pass filter, and other mechanical effects may also interfere in PAV and PWV. A limitation of this study is the absence of a measure of the tidal volume. Tidal volume may also have effect on the power of the respiration-related oscillations in PRV, PAV and PWV as it does in RSA [106]. Furthermore, it is natural to decrease the tidal volume when forcing to increase the respiratory rate during rest conditions. In this way, when a decrease of $\mathcal{P}_{PRV}$, $\mathcal{P}_{PAV}$ or $\mathcal{P}_{PWV}$ is observed, it cannot be determined how much of this decrease is due to a decrease of tidal volume, and how much is due to an increase of respiratory rate.

The observed decrease in the power of respiration-related modulations as the respiratory rate increases may be the reason why, in general, all studied methods obtained low median (around 0.5%) and low IQR (around 2.5%) of e_R until reaching a given f_R, which depends on the method and on the device, e.g., $d_{PWV}(n)$ maintain good performance in e_R terms up to 0.5 Hz when using the iPhone 4S, and up to 0.4 Hz when using the HTC One M8.

Results obtained for $d_{PWV}(n)$ were comparable to those obtained for $d_{PRV}(n)$ and better than for the other DR signals in general, obtaining low medians and IQR for e_R with f_R up to 0.4 Hz and even 0.5 Hz when using the iPhone 4S and iPod 5 devices. Occasionally, $d_{PWV}(n)$ and $d_{PRV}(n)$ obtained worse results (higher median/IQR for e_R) than another DR signal, such as

$d_{FM}(n)$ when using the iPod 5 device with $f_R = 0.2$ Hz (0.10/0.00% vs. -0.10/1.46%), or when using the HTC One M8 device with $f_R = 0.4$ Hz (-0.39/11.72% vs.-0.20/11.91% and -1.37/39.06%).

Both combinations $C_{PRV.PAV.PWV}$ and C_{ALL} obtained low median (less than 0.5%) and IQRs (less than 2.5%) for e_R, in every case where at least one of the DR signals included in the combinations obtained low median and IQR for e_R, and even in some cases where none of the DR signals obtained low median and IQR for e_R. For instance, in the case of the iPhone 4S at $f_R = 0.6$ Hz, combinations obtained low median and IQR for e_R although DR signals obtained very high IQRs for e_R (up to 65.10%). Similarly, at $f_R = 0.5$ Hz, both combinations still obtained low median and IQR for e_R, even though in this case d_{AM} and d_{PAV} obtained high IQR (55.91% and 44.14%, respectively). These observations demonstrate the advantages of combining information.

C_{ALL} obtained similar results to $C_{PRV.PAV.PWV}$ in e_R terms, and significant statistical differences were not found between their associated e_R, for all devices either at normal ranges of spontaneous respiratory rate (0.2-0.4 Hz) or higher ones (0.5-0.6 Hz). These results suggest that C_{ALL} offers no advantages over $C_{PRV.PAV.PWV}$. A possible reason for this observation may be that respiratory information in $d_{FM}(n)$ and $d_{AM}(n)$ is mainly redundant with respiratory information in $d_{PRV}(n)$, $d_{PAV}(n)$ and/or $d_{PWV}(n)$. It is reasonable to believe that respiratory information in $d_{AM}(n)$ and $d_{PAV}(n)$ is redundant to a large extent, because they are based on similar effects: respiration-induced amplitude modulations, of the SCPPG signal in one case, and of pulses of SCPPG in the other one. A similar case occurs with $d_{FM}(n)$ and $d_{PRV}(n)$. Note that statistical differences were found in some cases between $d_{AM}(n)$ and $d_{PAV}(n)$ (iPhone 4S at 0.5-0.6 Hz and iPod 5 at both 0.2-0.4 Hz and 0.5-0.6 Hz) and between $d_{FM}(n)$ and $d_{PRV}(n)$ (iPhone 4S at both 0.2-0.4 Hz and 0.5-0.6 Hz, and HTC One M8 at 0.2-0.4 Hz). However before interpreting this observation it must be kept in mind that when a method fails in tracking respiration, the obtained e_R, especially when errors are big, has clear tendencies (see Fig. 4.7) so statistical differences in e_R should not be considered as an indicator of differences in the physiological origin of those respiratory-related modulations. When the statistical tests is repeated taking only those e_R between -15% and 15% (excluding outliers), no statistical differences are found between these methods in any device/respiratory rate condition, so corroborating results independence with the used methodology in respiratory frequency derivation when the methods are able to catch

the respiration. The differences are then in the different ability to provide meaningful estimation.

One limitation of this study is that the inter-device variability for the same model of smartphones cannot be assessed because only one device per model has been tested. Slight differences in flashlight or camera lens may affect results. However, the form factor and so the distance between flashlight and camera lens, which is the most important signal-acquisition difference between different smartphone models, remains the same for devices of the same model. Nevertheless, if different models of smartphone would be wanted to be compared in the task of deriving respiratory rate, further studies using several devices for each model should be elaborated.

4.6   Conclusions

This chapter addresses respiratory information extraction from SCPPG signals by adapting the methods for deriving respiratory rate from PPG signal described in Chapter 3, and combining them with other methods [104] which have been previously applied to SCPPG signals [41,105], but they were neither combined with each other nor with other methods. Results suggest that normal ranges of spontaneous respiratory rates (0.2-0.4 Hz) can be accurately estimated from SCPPG signals based on PWV or PRV with low e_{R} (median of around 0.5% and IQR of around 2.5%). The accuracy can be further improved by combining them with other methods such as PRV, PAV, AM and/or FM methods. Indeed, the combination of these methods resulted in lower e_{R} values within normal ranges of spontaneous respiratory rate, but with small degradation in its performance at higher rates (up to 0.5 Hz when using HTC One M8, and up to 0.6 Hz when using the iPhone 4S or iPod 5 devices).

These promising results suggest that accurate normal ranges of respiratory rates can be obtained from general people using only smartphones without using any external sensors. The methods could be extended to other models of smartphones or tablet devices, the only requirement is that these smartphones and tablets contain a video camera to image a fingertip pressed to it. As smartphones and tablets have become common, they meet the criteria of ready access and acceptance. Hence, our mobile phone/tablet approach has the potential to be widely-accepted by the general population and can facilitate the capability to measure some of the vital signs using only fingertip of the subject.

Chapter 5

PPG for obstructive sleep apnea syndrome diagnosis in children

5.1 Introduction

In the last decade, application of different techniques for home sleep apnea monitoring has been extensively developed. Some of them are based on the ECG signal. These ECG-based methods usually use HRV in combination with beat morphology features which are known to be modulated by respiration [113–115].

Other methods are based on the PPG signal, which is particularly interesting in sleep studies context because monitoring sleep apnea from only a pulse oximeter would allow us to consider an ambulatory diagnosis with its both social and economic advantages. Several works propose pulse-oximeter-based methods for OSAS detection in adults. These pulse-oximeter-based methods usually use SpO_2 either alone [116, 117] or in combination with PPG signal [118]. OSAS in children is quite different than in adults, e.g., the apnea-hypoapnea index does not give an accurate picture of the nature of the breathing disturbance in children, while it is the most often used parameter to characterize disordered breathing in adults [119].

However, some pulse-oximeter-based methods have been proposed also for children. It is known that vasoconstriction causes considerable DAP [52, 53]. Based on this, in [54], obstructive sleep apnea is tried to be indirectly detected by DAP events under the hypothesis that the sympathetic activation associated to the arousal caused as response to the apnea, in-

duces also vasoconstriction. The relation between apnea and DAP events was demonstrated, but the obtained results showed low specificity, i.e., there are many DAP events which are not related to apnea. Later, a HRV analysis during the DAP events was proposed in [55] to discriminate those DAP events which are related to an apnea from those which are not, improving the accuracy of subject classification and showing that combination of DAP events and HRV could be an alternative for sleep apnea screening.

The use of HRV requires ECG as an additional recording. This is a disadvantage that takes more relevance in sleep studies context where a high number of sensors over the patient can affect the physiological sleep. In this chapter, the study presented in [55] is extended evaluating the use of PRV obtained from the PPG signal instead of the HRV. The correlation between HRV and PRV [49,50] decreases during obstructive apnea episodes [56], but PRV still carries useful information which can be exploited.

5.2   Materials

5.2.1   Polysomnographic recordings

The database used in this study is described in Section 4.2.3. It includes, among others, overnight PPG signals sampled at $F_s = 100$ Hz from 21 children who were referred to hospital for suspected sleep-disordered breathing. 10 out of the 21 children were diagnosed with OSAS.

5.2.2   Rat-model recordings

This dataset is composed of recordings from seven male Sprague-Dawley rats (390-465 g). The rats were intraperitoneally anesthetized with uretane (see Table 5.1). One of them was excluded due to technical problems. They were connected to an electronically controlled nasal mask system that consists of two tubes, one open to atmosphere and the other connected to a positive pressure pump avoiding re-breathing on the animal. Airway obstructions on the tubes by electrical-operated valves, simulate obstructive-sleep-apnea episodes.

The protocol consisted of 2 steps. In a first step, recurrent 15s-apnea episodes for 15 minutes intervals, with a subsequent resting period of 15 minutes were used. Apnea index of 20, 40 and 60 apnea/hour were applied. In a second step, apnea index of 60 apnea/hour was applied with different durations of the apnea episodes (5, 10 and 15 s). In both cases the order

Table 5.1: Rat population and anesthesia dose.

Rat number	Weight (g)	Uretane 10% (ml)	Onset time	End time
1.1	433	8.5	10:50h	15:45h
1.2	450	7.5	9:10h	13:45h
1.3	391	7.2	15:15h	20:55h
1.4	457	7	9:20h	14:40h
1.6	428	7	16:00h	20:30h
1.7	465	7.2	11:30h	17:20h

of the 15-minutes apnea intervals were randomly selected. The different phases of the protocol are illustrated in Fig. 5.1.
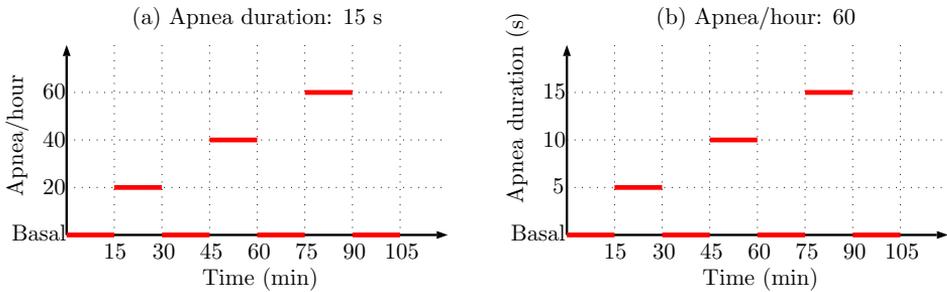
Figure 5.1: Different phases of the protocol for the rat-model OSAS recordings.

PPG and SpO_2 signals were recorded by using the pulse oximeter for rat StarrLife Mouse Ox Plus with a sampling rate of 1250 Hz and 15 Hz, respectively. ECG leads I and III were recorded by using Biopac ECG100C module and E-08-21BEP electrodes with a sampling rate of 1250 Hz. Respiratory pressure and flow were recorded by using a UIM100C module with a sampling rate of 156.25 Hz, and the apnea generator signal, which is a two level signal that controls the electrical-operated valves, was recorded also with a UIM100C module with a sampling rate of 10000 Hz. Figure 5.2 shows an example of ECG, PPG, SpO_2, and respiratory flow signals recorded from a rat.
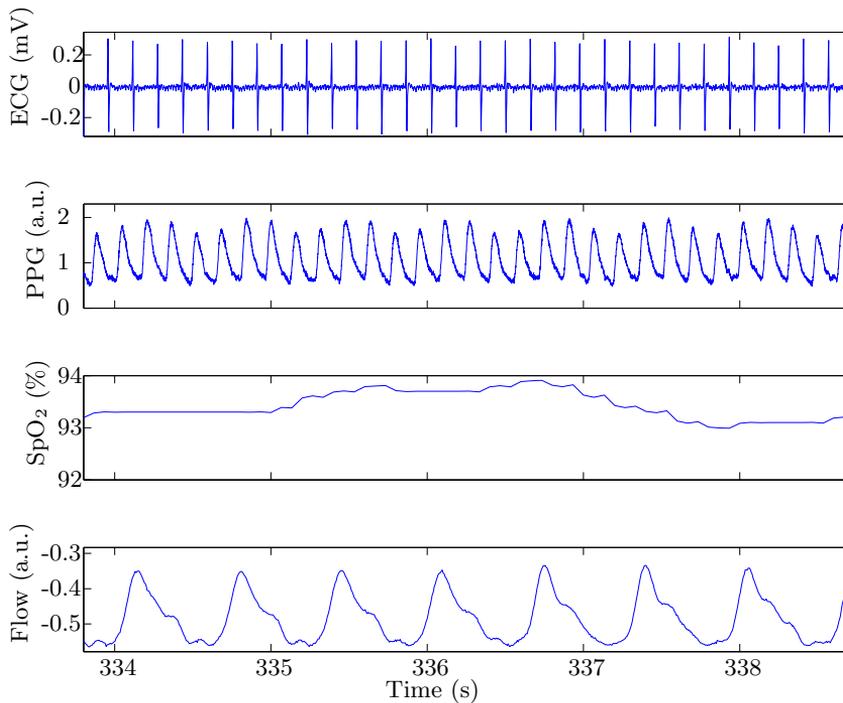
Figure 5.2: Example of ECG, PPG, SpO$_2$, and respiratory flow signals recorded from a rat.

5.3 Methods

5.3.1 Preprocessing

The same preprocessing applied to PPG signals in Chapter 3 was applied to PPG signals from children database, i.e., a low-pass filtering with a cut-off frequency of 35 Hz, and the artifact detector based on Horth parameters described in [54]. Apex (n_{A_i}), basal (n_{B_i}) and medium (n_{M_i}) points were detected as described in Section 4.3.2, being the medium points used as fiducial points as in Chapter 4 because of robustness reasons. Normal sinus pulses n_{N_i} were determined after removal/replacing ectopic and miss-detected pulses using the method proposed in [88].

5.3.2 DAP events detection

The DAP events were automatically detected by applying the algorithm described in [54], which consists of an RMS-based envelope estimation and an adaptive-threshold-based decision rule.

The envelope estimation stage is based on RMS series. First, a mean subtraction is performed by using a moving average filter. $x_{\mathrm{PPG_{DC}}}(n)$ is the mean-suppressed version of $x_{\mathrm{PPG}}(n)$. Then, each sample of the envelope $x_{\mathrm{PPG_E}}(n)$ is estimated from a N_{E}-samples-length running window of $x_{\mathrm{PPG_{DC}}}(n)$:

$$x_{\mathrm{PPG_E}}(n) = \sqrt{\frac{1}{N_{\mathrm{E}}} \sum_{k=n-(N_{\mathrm{E}}-1)}^{n} x^2_{\mathrm{PPG_{DC}}}(k)}. \qquad (5.1)$$

N_{E} was set to be equivalent to 2 cardiac cycles (T denotes the cardiac cycle estimated by using a zero-crossing detector applied to $x_{\mathrm{PPG_{DC}}}(n)$) which allows the tracking of attenuation changes greater than 3 beats. This decision rises the risk of an increase in short-length false positives, caused by high signal variability, and several DAP events, rather than a single event, can be interpreted as being different when the signal amplitude is near the threshold of the decision rule. To account for this, a minimum duration of events and a minimum distance between events is imposed. In that way, short-length false positives are suppressed and detection close in time are grouped together [54].

The decision rule is based on an adaptive threshold. A DAP event is considered when $x_{\mathrm{PPG_E}}(n)$ is lower than the established adaptive threshold for at least a minimum duration. In mathematical terms, the threshold is defined as:

$$\xi(n) = \begin{cases} \dfrac{U_P}{100 L_p} \displaystyle\sum_{k=n-(L_P-1)-T_{L_P,n}}^{n} x_{\mathrm{PPG_E}}(k), & n \in \{n_{\mathrm{adapt}}\}_{\xi} \\ \xi(n-1), & \text{otherwise} \end{cases} \quad , \qquad (5.2)$$

where $\{n_{\mathrm{adapt}}\}_{\xi}$ is the sample set that fulfills the criterion of eligibility for threshold adapting, $T_{L_P,n}$ is the number of samples not in $\{n_{\mathrm{adapt}}\}_{\xi}$ inside the interval $[n - (L_P - 1) - T_{L_P,n}, n]$, so that L_P is always the number of samples in $\{n_{\mathrm{adapt}}\}_{\xi}$ from the interval.

Thus, the threshold $\xi(n)$ is computed as the U_P percent of the mean of $x_{\mathrm{PPG_E}}(n)$ using the last L_P samples in $\{n_{\mathrm{adapt}}\}_{\xi}$.

The sample set that fulfills the criterion of eligibility for threshold adapting, $\{n_{\mathrm{adapt}}\}_{\xi}$, is composed of all samples except those accomplishing any of the following conditions:

- A DAP event is detected, i.e., when $x_{\mathrm{PPGE}}(n) < \xi(n-1)$.

- An artifact is detected in PPG signal (see Section 3.2.1 at page 45).

- When an abrupt change is detected in $x_{\mathrm{PPGE}(n)}$, considering abrupt changes those samples accomplishing:

$$\left| x_{\mathrm{PPGE}(n)} - x_{\mathrm{PPGE}(n-1)} \right| > \frac{5}{f_s^{\mathrm{P}}} A_{\mathrm{PPGE}}, \qquad (5.3)$$

where A_{PPGE} is half of the oscillation amplitude range of $x_{\mathrm{PPGDC}}(n)$ at the beginning of the recording.

The following values for the parameters were used: $U_P = 45\%$, $L_P = 30 f_s^{\mathrm{P}} T$. Further details are given in [54].

5.3.3   PRV analysis

The inverse interval function was generated by using the normal sinus occurrences n_{N_i}:

$$d_{\mathrm{PRV}}^u(n) = \sum_i \frac{1}{n_{\mathrm{N}_i} - n_{\mathrm{N}_{i-1}}} \delta\left(n - n_{\mathrm{N}_i}\right). \qquad (5.4)$$

Subsequently, a 2-Hz evenly sampled version was generated by cubic splines interpolation. The evenly sampled version of this signal is denoted $d_{\mathrm{PRV}}(n)$ in this thesis.

The smoothed pseudo Wigner-Ville distribution (SPWVD) [120] was used to analyse the spectral parameters of the PRV in a time-frequency map, using a 5 minutes-length time window centred at the onset of the studied DAP event. The SPWVD was chosen because of its high time and frequency resolution and its independent smoothing in time and frequency. The discrete SPWVD can be seen as the discrete Fourier transform of the autocorrelation function $r_x(n, k)$, filtered and windowed:

$$S_x(n, k) = |h(k)|^2 \left[\sum_{n'=-N+1}^{N-1} g(n') r_x(n + n', k) \right], \qquad (5.5)$$

where $|h(k)|^2$ defines the windowing and $g(n')$ defines the filtering. Both $h(k)$ and $g(n)$ were defined as Hamming windows. The length of the analyzed segment was set to 5 minutes to ensure that is long enough to contain at least one period of the lowest frequency in the studied band, which is 0.0033 Hz.

Power in the very low frequency (VLF) (0.0033-0.04 Hz) ($\mathcal{P}_{\mathrm{VLF}}(n)$), LF (0.04-0.15 Hz) ($\mathcal{P}_{\mathrm{LF}}(n)$), HF (0.15-0.5 Hz) ($\mathcal{P}_{\mathrm{HF}}(n)$) bands, and low to high frequency ratio ($\mathcal{R}_{\mathrm{LF/HF}}(n)$) were computed. Their normalized versions with respect to the total power ($\mathcal{P}_{\mathrm{VLF}}(n) + \mathcal{P}_{\mathrm{LF}}(n) + \mathcal{P}_{\mathrm{HF}}(n)$) were also computed, and they follow the same nomenclature with an additional n as subscript, e.g., $\mathcal{P}_{\mathrm{HF}_n}(n)$ is the normalized version of $\mathcal{P}_{\mathrm{HF}}(n)$.

Classifier

A linear discriminant analysis (LDA) [121] was used to discriminate between DAP events related and not related to apnea episodes. LDA is a classificatory statistical technique that estimates the probability of each case belongs to each of the groups previously defined (qualitative dependent variable) by studying a set of features (quantitative independent variables) of this case. Finally, the classification is performed by assigning each case to the group with highest probability of belonging.

For DAP event classification, the features are based on the PRV around them, and there are two classes (or groups): apnea related DAP events (Ga) and non apnea related DAP events (Gn). Let $\boldsymbol{y}_j = [y_{1j}, y_{2j}, ..., y_{dj}]$ be a row vector with d values where each element represents a feature value from j^{th} DAP. To assign $\boldsymbol{y}_j$ to class k of the c possible classes, the discriminant value f_k for each class is evaluated from the following equation:

$$f_k = \boldsymbol{\mu}_k \boldsymbol{\Sigma}^{-1} \boldsymbol{y}_j^T - \frac{1}{2} \boldsymbol{\mu}_k \boldsymbol{\Sigma}^{-1} \boldsymbol{\mu}_k^T + log(\pi_k), \qquad (5.6)$$

where T represents the transpose and $\boldsymbol{\mu}_k$ is the row mean vector obtained from the whole N_k training vectors belonging to class k as defines (5.7), and $\boldsymbol{\Sigma}$ represents the pooled covariance defined in (5.8).

$$\boldsymbol{\mu}_k = \frac{1}{N_k} \sum_{j=1}^{N_k} \boldsymbol{y}_{jk} \qquad (5.7)$$

$$\boldsymbol{\Sigma} = \frac{1}{N - c} \sum_{k=1}^{c} \sum_{j=1}^{N_k} (\boldsymbol{y}_{jk} - \boldsymbol{\mu}_k)^T (\boldsymbol{y}_{jk} - \boldsymbol{\mu}_k), \qquad (5.8)$$

where N is the total number of cases $\boldsymbol{y}_j$ in the training set.

The term π_k represent the prior probability that $\boldsymbol{y}_j$ belongs to a class k. A practical way to evaluate π_k is:

$$\pi_k = \frac{N_k}{N}. \qquad (5.9)$$

Finally $\boldsymbol{y}_j$ is assigned to the class, k with higher f_k so the π_k term can be removed from (5.6) if $\boldsymbol{y}_j$ has the same probability for all classes.

Features set

In order to quantify the evolution of autonomic variations when a DAP event is associated or not associated to apnea, four time windows were defined in specific time intervals related to the onset of DAP events. Three of the four windows have a length of 5 s.: The reference window (w_{r_j}) which begins 15 s. before n_{DO_j}, the DAP window (w_{d_j}) which begins 2 s. before the DAP, and the post-DAP window (w_{p_j}) which begins 15 s. after n_{DO_j}. The fourth window is called global window. It begins 20 s. before n_{DO_j} and its length is 40 s. Fig 5.3 illustrates w_{r_j}, w_{d_j}, and w_{p_j} over the mean of $d_{\mathrm{PRV}}(n)$ during related and non related to apnea DAP events.
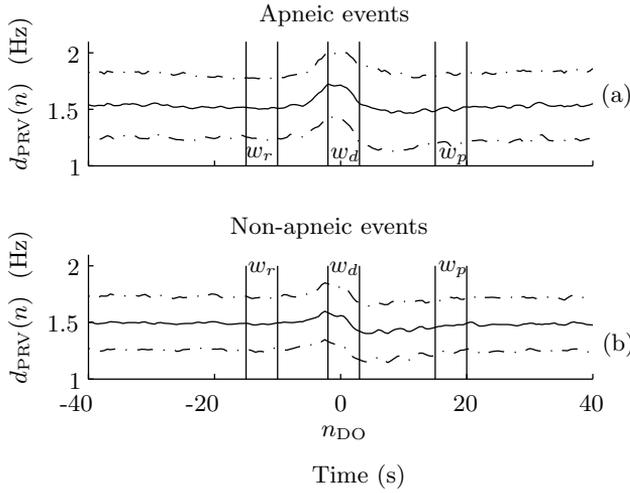
Figure 5.3: $d_{\mathrm{PRV}}(n)$ mean $\pm$ SD for apneic (a) and non-apneic (b) DAP events. Reference (w_r), DAP episode (w_d), and post-DAP episode (w_p) windows, with DAP onset at time 0 s.

The feature set contains the means of $\mathcal{P}_{\mathrm{VLF}_n}(n)$, $\mathcal{P}_{\mathrm{LF}_n}(n)$, $\mathcal{P}_{\mathrm{HF}_n}(n)$, and $\mathcal{R}_{\mathrm{LF/HF}}(n)$ signals, computed within the four defined windows. The mean and the variance of $d_{\mathrm{PRV}}(n)$ within the same four windows are also considered. These last two indexes are computed after a normalization by subtracting the mean value and dividing by the variance of the 5 min-length segment centred at n_{DO_j}. This is done since it was hypothesized that the relative variation in the analysed window with respect to baseline differs between apneic or non-apneic episodes. In addition, for each index the dif-

ference between w_{r_j} and w_{p_j} was computed making a total of 34 features extracted from the pulse rate.

Feature selection

Features must be selected and weighted in order to select the feature set that provides the best discrimination of DAP events. This training stage was performed by studding the features in a subset of manually labeled DAP events.

For training the classifier, 268 DAP events were extracted. These DAP events were clustered in two classes: apneic DAPs (Ga) and non apneic DAPs (Gn) based on physiological characteristics. DAP events were classified into Ga when SpO_2 falls at least 3% or airflow decreases at least 50% respect to the baseline for a minimum duration of 5 seconds and into Gn otherwise. A summary is presented in Table 5.2.

Table 5.2: Clustering of DAP events

Clinical diagnosis	DAP group		Total
	Ga	Gn	
Normal	41	107	148
Pathological	98	22	120
Total	139	129	268

Feature selection was addressed using the wrapper method forward approach, i.e., by adding gradually one more feature and selecting the one which provides the highest accuracy. For evaluating the accuracy of every feature set, leave-one-out validation method was performed.

5.3.4 Clinical study

In order to evaluate the proposed techniques, PSG registers were splitted into 1-hour length fragments, and they were labeled as control, doubt or pathological based on SpO_2 desaturation. To establish this separation, it was considered a baseline level β corresponding to the SpO_2 signal mode of the entire night recording, and $t_{\beta-3}$ is the total time with SpO_2 signal below $\beta - 3\%$. The fragment is clustered as pathological if $t_{\beta-3}$ is more than 3 min. This implies a minimum of 5% of the time with evident oxygen desaturation which corresponds to a severe OSAS criteria in children [119] of 18 apneas/hour having a mean duration of 10 seconds. If $t_{\beta-3}$ is less than

0.9 min., which corresponds to 5 apneas/hour, the fragment is clustered as normal. Fragments which are not clustered as normal or pathological are clustered as doubt. Table 5.3 shows this classification.

Table 5.3: PSG fragments classification.

Clinical diagnosis	subjects	fragments	PSG fragments classification		
			normal	doubt	pathological
Normal	10	46	42	4	0
Pathological	11	59	28	20	11
Total	21	105	70	24	11

These one hour fragments were automatically classified in normal or pathological based on the DAP per hour ratio using the DAP coming from the DAP detector in [54], r_{DAP}, or alternatively considering only those DAP classified as apneic events with the methodology presented in Section 5.3.3, $r_{\mathrm{DAP}}^{\mathrm{PRV}}$. Receiver operating characteristic (ROC) curves were calculated for both indexes and the optimum thresholds in terms of maximizing accuracy were established. In addition, Wilcoxon non parametric statistical analysis was carried out for both indexes in order to evaluate their discriminant power between groups. Then, the percentage of time under pathological fragments based on r_{DAP} and $r_{\mathrm{DAP}}^{\mathrm{PRV}}$ was analysed as a rule to consider a subject as pathological or not. The threshold for this percentage was selected for maximizing accuracy. Only 15 subjects (8 OSAS) were included in this study since subjects with less than 4 hours of acceptable quality signal were excluded.

Those DAP events in which PRV could not be obtained over its global window w_g were excluded for calculation of r_{DAP} and $r_{\mathrm{DAP}}^{\mathrm{PRV}}$ indexes. However, in [55] the excluded DAP events were those in which HRV could not be obtained from ECG. This represents two different exclusion criteria, based on quality of PPG and ECG signals, respectively. For comparison purposes, it also were studied the subgroup of DAPs which results after discarding those DAPs in which PRV or HRV could not be obtained, denoting their indexes with an additional subscript 2, for example, $r_{\mathrm{DAP}_2}^{\mathrm{PRV}}$.

5.3.5   OSAS in rat model

Rat model of OSAS is a realistic approach for understanding and studying physiological mechanisms involved in sleep apnea [122,123]. Rats are usually anesthetized for in vivo experiments. Anesthetics can affect cardiovascular

functions and even the ANS could be blocked. The type, dose and method of administrating anesthetics can disturb in different manner the sympathetic activity of instrumented rats [124].

Observing the recorded signals during the protocol, all simulated obstructive apnea events showed changes in respiratory flow and falls in SpO_2 to at least 90%, but DAP events were not observed during apnea events (see Fig. 5.4). A possible reason for this observation could be a sympathetic blockade. In order to study the effect of anesthesia on ANS activity during obstructive apnea episodes in this rat model, mean of $\mathcal{P}_{LF_n}(n)$ and $\mathcal{R}_{LF/HF}(n)$ within 3 15-s-length windows defined around the kth apnea event were computed: $w_{b_k}^{RAT}$ (the 15 s before the kth apnea), $w_{d_k}^{RAT}$ (the 15 s during the kth apnea), and w_a^{RAT} (the 15 s after the kth apnea). Figure 5.4 illustrates the location of these windows. Only the longer apneas (length of 15 s) were considered in this study since, individually, they are the most aggressive and so they should lead to the strongest ANS response.
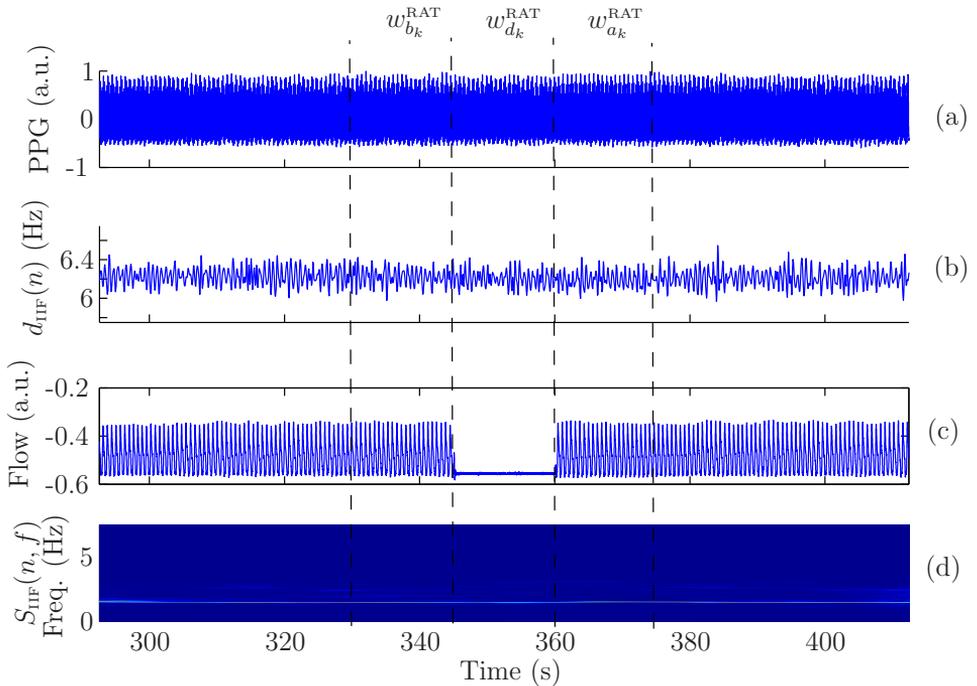
Figure 5.4: PPG (a), $d_{PRV}(n)$ (b), respiratory flow (c), and SPWVD of $d_{PRV}(n)$ (d) from a rat during a simulated apnea episode, with the location of the 3 studied windows $w_{b_k}^{RAT}$, $w_{d_k}^{RAT}$, and $w_{a_k}^{RAT}$.

The LF and HF bands were re-defined to be appropriate for a rat model: [0.04-1] Hz, [1-3] Hz, respectively [125]. The inverse interval function was this time interpolated to 15 Hz (instead of 2 Hz), and a time-frequency PRV spectrum was obtained from a 3-min-length interval centered at each apnea event, by using the SPWVD. $\mathcal{P}_{\mathrm{LF}_n}$ was computed as the power in the LF band normalized to the power in the whole studied band (LF and HF, [0.04-3] Hz).

Means of $\mathcal{P}_{\mathrm{LF}_n}$ and $\mathcal{R}_{\mathrm{LF/HF}}$ within each one of the 3 windows were computed. In addition, the differences between $w_{d_k}^{\mathrm{RAT}}$ and $w_{b_k}^{\mathrm{RAT}}$, and between $w_{a_k}^{\mathrm{RAT}}$ and $w_{d_k}^{\mathrm{RAT}}$ were also computed for each one of these means. The Friedman statistical test, which is a paired-non-parametric statistical test, was applied in order to study whether these indexes (means of $\mathcal{P}_{\mathrm{LF}_n}(n)$ and $\mathcal{R}_{\mathrm{LF/HF}}(n)$) show significant statistical differences between the 3 windows $w_{b_k}^{\mathrm{RAT}}$, $w_{d_k}^{\mathrm{RAT}}$, and $w_{a_k}^{\mathrm{RAT}}$. This same test was also applied in order to study if significant statistical differences are shown in the differences between $w_{d_k}^{\mathrm{RAT}}$ and $w_{b_k}^{\mathrm{RAT}}$, and between $w_{a_k}^{\mathrm{RAT}}$ and $w_{d_k}^{\mathrm{RAT}}$.

5.4   Results

5.4.1   OSAS in children

Table 5.4: PSG fragments and subjects classification results obtained by using the two different DAP event discarding criteria: related to PPG signal quality (r_{DAP} and $r_{\mathrm{DAP}}^{\mathrm{PRV}}$), and related to ECG and PPG signal quality (r_{DAP_2}, $r_{\mathrm{DAP}_2}^{\mathrm{PRV}}$ and $r_{\mathrm{DAP}_2}^{\mathrm{HRV}}$). Results include accuracy (Acc), sensitivity (Se), specificity (Sp), and area under curve (AUC).

	PSG fragments classification				Subjects classification		
	Acc	Se	Sp	AUC	Acc	Se	Sp
	(%)	(%)	(%)	(%)	(%)	(%)	(%)
r_{DAP}	67.90	90.91	64.29	76.30	80.00	87.50	71.43
$r_{\mathrm{DAP}}^{\mathrm{PRV}}$	70.37	81.82	68.57	78.38	86.67	100.00	71.43
r_{DAP_2}	60.49	72.73	58.57	69.55	73.33	75.00	71.43
$r_{\mathrm{DAP}_2}^{\mathrm{PRV}}$	59.26	81.82	55.71	71.36	80.00	87.50	71.43
$r_{\mathrm{DAP}_2}^{\mathrm{HRV}}$	76.54	63.64	78.57	71.10	73.33	62.50	85.71

The best features for classification obtained by the wrap method were the mean of $d_{\mathrm{PRV}}(n)$ signal within the DAP event window, the mean of

$\mathcal{P}_{\mathrm{VLF}_n}(n)$ within the post-DAP window, the mean of $\mathcal{R}_{\mathrm{LF/HF}}(n)$ during the reference window, and the mean of $d_{\mathrm{PRV}}(n)$ signal within the global window. Table 5.4 shows results of PSG fragment and subject classification by using the two described DAP event discarding criteria. The Wilcoxon test shows better discriminant power between normal and pathological fragments for $r_{\mathrm{DAP}}^{\mathrm{PRV}}$ ($p = 0.0034$) than for r_{DAP} ($p = 0.0067$).

5.4.2 OSAS in rat model

Table 5.5 shows the median and IQR for means of $\mathcal{P}_{\mathrm{LF}_n}(n)$ and $\mathcal{R}_{\mathrm{LF/HF}}(n)$ within the windows $w_{b_k}^{\mathrm{RAT}}$, $w_{d_k}^{\mathrm{RAT}}$, and $w_{a_k}^{\mathrm{RAT}}$, and Table 5.6 shows the same for their differences between w_d^{RAT} and $w_{b_k}^{\mathrm{RAT}}$, and $w_{a_k}^{\mathrm{RAT}}$ and $w_{d_k}^{\mathrm{RAT}}$.

Table 5.5: Median and IQR for means of $\mathcal{P}_{\mathrm{LF}_n}(n)$ and $\mathcal{R}_{\mathrm{LF/HF}}(n)$ within the windows $w_{b_k}^{\mathrm{RAT}}$, $w_{d_k}^{\mathrm{RAT}}$, and $w_{a_k}^{\mathrm{RAT}}$.

	$w_{b_k}^{\mathrm{RAT}}$	$w_{d_k}^{\mathrm{RAT}}$	$w_{a_k}^{\mathrm{RAT}}$
	Median / IQR	Median / IQR	Median / IQR
$\mathcal{P}_{\mathrm{LF}_n}(n)$	7.67% / 28.71%	8.01% / 31.11%	8.45% / 26.63%
$\mathcal{R}_{\mathrm{LF/HF}}(n)$	0.08 / 0.46	0.09 / 0.52	0.09 / 0.42

Table 5.6: Median and IQR for means of the differences of $\mathcal{P}_{\mathrm{LF}_n}(n)$ and $\mathcal{R}_{\mathrm{LF/HF}}(n)$ within the windows $w_{d_k}^{\mathrm{RAT}}$ and $w_{b_k}^{\mathrm{RAT}}$, and $w_{a_k}^{\mathrm{RAT}}$ and $w_{d_k}^{\mathrm{RAT}}$.

	$w_{d_k}^{\mathrm{RAT}} - w_{b_k}^{\mathrm{RAT}}$	$w_{a_k}^{\mathrm{RAT}} - w_{d_k}^{\mathrm{RAT}}$
	Median / IQR	Median / IQR
$\mathcal{P}_{\mathrm{LF}_n}(n)$	0.21% / 4.50%	0.25% / 4.44%
$\mathcal{R}_{\mathrm{LF/HF}}(n)$	0.00 / 0.07	0.00 / 0.06

According to the Friedman statistical test, there were no significant differences in mean of $\mathcal{P}_{\mathrm{LF}_n}(n)$ and $\mathcal{R}_{\mathrm{LF/HF}}(n)$ during the 3 windows $w_{b_k}^{\mathrm{RAT}}$, $w_{d_k}^{\mathrm{RAT}}$, and $w_{a_k}^{\mathrm{RAT}}$ (p-value=0.2107). The differences between $w_{d_k}^{\mathrm{RAT}}$ adn $w_{b_k}^{\mathrm{RAT}}$, and $w_{a_k}^{\mathrm{RAT}}$ and $w_{d_k}^{\mathrm{RAT}}$ also showed no statistical differences (p-value=0.5809).

5.5 Discussion

The PPG signal presents interesting characteristics that can be used to detect apneic episodes. In [55], a diagnostic method based on DAP events which satisfies some HRV related conditions was proposed, requiring ECG in addition to PPG signal. The minimization of signal recordings takes special relevance in sleep studies because the use of many sensors could disturb the physiological sleep. The use of PRV obtained from PPG signal instead of HRV obtained from ECG signal is proposed in this chapter avoiding the need of ECG recording and simplifying ambulatory monitoring.

Selected features addressed by the wrap method were different to those selected features of HRV in [55]. The reason of this difference could be that although HRV and PRV are highly correlated in normal breathing [50], this correlation decreases considerably during obstructive apnea episodes [56].

Before introducing the PRV information, the fragment and subject classification obtained an Acc of 67.90% and 80.00%, respectively. The introduction of PRV information increased the classifier performance obtaining an Acc of 70.37% for fragment classification and 86.67% for subject classification. In terms of Acc, both r_{DAP} and $r_{\mathrm{DAP}}^{\mathrm{PRV}}$ have obtained better subject classification results than the ones obtained with HRV in [55] (73.33% for r_{DAP} and 80.00% for $r_{\mathrm{DAP}}^{\mathrm{HRV}}$). This improvement could be explained by the DAP exclusion criteria, which in [55] is related to the quality of ECG but in this work it is related to the quality of PPG signal where also DAP events are detected, and this could improve the DAP event detection by excluding DAP events which are related to an artifact and not related to an apnea.

By excluding those DAP events in which HRV or PRV could not be obtained (bad quality of ECG or PPG signal), obtained Acc decreased for all $r_{\mathrm{DAP}_2}^{*}$ indexes in both fragment and subject classification. This decrease could be explained by the loss of information implied by the DAP events exclusion, which is higher than in r_{DAP}^{*} indexes because more DAP events are excluded. In fragment classification, $r_{\mathrm{DAP}_2}^{\mathrm{HRV}}$ obtained better Acc (76.54%) than $r_{\mathrm{DAP}_2}^{\mathrm{PRV}}$ (59.26%), while in subject classification, the index which obtained the highest Acc was $r_{\mathrm{DAP}_2}^{\mathrm{PRV}}$ with 80.00%, over $r_{\mathrm{DAP}_2}^{\mathrm{HRV}}$ and r_{DAP_2}, both with 73.33%.

HRV and PRV give additional information to the classifier, but using them implies a loss of information due to the DAP exclusion. However, results obtained for $r_{\mathrm{DAP}}^{\mathrm{HRV}}$ (ECG quality exclusion criteria) or $r_{\mathrm{DAP}}^{\mathrm{PRV}}$ (PPG quality exclusion criteria) outperform those obtained without introducing infor-

mation from PRV/HRV, so the additional information given by PRV/HRV compensates the loss of information associated to the DAP event exclusion.

A limitation of this study is that the procedure for labeling the 1-h PSG fragments is based only on SpO_2. According to American Sleep Disorders Association criteria [126], SpO_2 is not sufficiently accurate or validated to recommend for use in OSAS diagnosis. Nevertheless, all pathological fragments defined according to this procedure correspond to children suffering from OSAS, see Table 5.3 and subjects classification use clinical diagnosis as the reference.

Another limitation of this study is that the optimal thresholds for both r_{DAP} and r_{DAP}^{PRV} were obtained from all the fragments. In other words, for the subject classification, training and test sets are the same. The fragment classification accuracy was also computed using the leave-one-out validation method, obtaining sightly smaller accuracies (64.20% for r_{DAP} and 67.90% for r_{DAP}^{PRV}).

Moreover, Table 5.3 shows an unbalanced sample with 70 normal and 11 pathological fragments. The fragment classification was also performed after balancing the groups. Optimal thresholds for both r_{DAP} and r_{DAP}^{PRV} were computed. Obtained results were exactly the same.

The small number of subjects in the database (21, 10 of them suffering of OSAS) is another limitation. This study should be validated over a longer database.

5.5.1 OSAS in rat model

Although all simulated apnea episodes showed falls in SpO_2 bellow 90%, none of them showed an associated DAP event. Furthermore, mean of $\mathcal{P}_{LF_n}(n)$ presented extremely low values before (median of 7.67%), during (median of 8.01%), and after apnea (8.45%). Slight increases were observed during and after apnea. However, no statistical differences according to the Friedman test were found in means of $\mathcal{P}_{LF_n}(n)$ or $\mathcal{R}_{LF/HF_n}(n)$ during the three studied windows.

These results suggest that sympathetic system may be blocked by the anesthetics, making this rat model unsuitable for the analysis of methods based on ANS response, such as those presented in this chapter which are based on DAP and PRV.

5.6 Conclusions

This chapter addresses the OSAS diagnosis in children based on PPG signal. A method based on DAP event detection and their classification as apnea- or non-apnea-related using ANS information obtained by the PRV is presented. Results obtained with PRV (Acc=86.67%) are comparable to those extracted from HRV in [55] (Acc=80.00%), suggesting that PRV can be used to discriminate apneic and non-apneic DAP events. As PRV is obtained from PPG signal (as DAP events are), no additional (ECG) signal is required which takes special relevance in sleep studies.

The rat model is suitable to study the consequences of OSAS, but anesthetic effects can limit the ANS response, preventing the use of the model in studies based on this response. Thus, DAP events, HRV or PRV cannot be studied with this rat model. In this way HRV, PRV, and or DAP events analysis during apnea could be an indirect tool to assess the effect and deep of anesthesia.

Chapter 6

Conclusions

This chapter summarizes the original contributions and main conclusions of the thesis, and proposes possible extensions of the work.

6.1 Summary and conclusions

As stated in Chapter 1, the objective of this thesis was to develop non-invasive methods for respiration information extraction from biomedical signals which are widely adopted in clinical routine. Novel methods for deriving respiratory rate from ECG and from PPG signal were developed and compared with other methods in the literature.

6.1.1 Electrocardiogram-based methods

Chapter 2 presented a novel ECG-based method for deriving respiratory rate. It exploits respiration-related variations in QRS slopes and R-wave angle. A method for combining information from several respiratory signals was also developed and used to combine several respiratory signals derived from different lead sets. The proposed method does not depend on a specific lead set, and so, do not lead to a significantly lower performance when any problem appears at any lead.

The method demonstrated its robustness in high non-stationary noisy environments such as stress test obtaining an error of $0.76 \pm 7.30\%$ (measuring the 85.07% of the time, with NLDL), measuring up to the 99.81% of the time (with an error of $1.95 \pm 9.26\%$, with 12ECG lead set). Accuracy and measuring time represent a trade-off situation for which the VCG lead set displayed the best results obtaining an error of $0.52 \pm 8.99\%$ measuring the 96.09% of the time, outperforming existing methods in literature.

6.1.2   Pulse-photoplethysmogram-based methods

Chapter 3 presented a novel PPG-based method for deriving respiratory rate. It exploits respiration-related variations in pulses width. The proposed method is much less affected by the sympathetic tone than other methods in literature which are usually based on pulses amplitude and/or rate. It obtained better performance than other single PPG-based methods in respiratory rate estimation error terms ($1.27 \pm 7.81\%$). Furthermore, a method for combining information from several respiratory signals was developed and used to obtain a respiratory rate estimation from the proposed PWV-based in combination with other known PPG-based methods (PAV and PRV), improving the accuracy of the estimation (obtained relative error was $0.17 \pm 6.67\%$) and outperforming other methods in literature which involve ECG or BP recording.

Chapter 4 presented an adaptation of the PPG-based methods to derive respiratory rate from smartphone devices using SCPPG signals. Results suggest that normal ranges of spontaneous respiratory rates (0.2-0.4 Hz) can be accurately estimated from SCPPG signals based on PWV or PRV with low relative error (median on the order of 0.5% and IQR on the order of 2.5%). The performance of the methods considerable decreases when reaching a respiratory rate depending on the method and the device. However, the results showed a smaller degradation at higher respiratory rates when combining PWV- and PRV-based methods with other SCPPG-based methods in the literature such as PAV-, AM-, and/or FM-based methods, obtaining relative errors of the same order up to 0.5 Hz when using the HTC One M8, and up to 0.6 Hz when using the iPhone 4S or the iPod 5 devices.

Chapter 5 presented an automatic algorithm to diagnose OSAS in children based on the PPG signal. The method is based on DAP event detection and their classification as apnea- or non-apnea-related using ANS information obtained by the PRV. Obtained results are comparable (Acc = 86.67%) to those obtained with other methods in the literature which require the ECG signal as an additional recording. Reducing the number of sensors over the patient takes special relevance in sleep studies where it is desirable to minimize the physiological sleep disturbance. The proposed method have the advantage of not requiring any additional signal and so could be used for diagnosing OSAS in children from only a pulse oximeter, allowing to consider an ambulatory diagnosis with its both social and economic advantages. However, the number of subjects in the database is

low (21 subjects, 10 of them suffering of OSAS) and this study should be validated over a longer database.

Furthermore, a rat model for OSAS was studied, but no DAP events or PRV alteration in the LF band were observed during induced apnea events, suggesting a sympathetic system blockade by the anesthetics. Thus, proposed methods in this thesis could not be studied using this model, since they are based on ANS response. In this way HRV, PRV, and or DAP events analysis during apnea could be an indirect tool to assess the effect and deep of anesthesia.

6.2 Future work

Possible research lines to expand the work in this thesis are presented bellow.

- Study of the potential of the methods presented in this thesis to obtain respiratory volumes from the ECG and from PPG signal. Potential applications may include motorization of athletes, and screening of asthma and OSAS. This study would require ECG, PPG, and respiratory volume (recorded by spirometry) signals simultaneously recorded.

- Characterization of PWV during sleep apnea events. This thesis has shown PWV to be an accurate method to obtain respiratory rate. However, the morphological variations of PPG pulses in PSG recordings due to the DAP events may reduce its potential for apnea detection. This study would require PSG (including PPG signals) recordings whose apnea events are manually annotated by experts.

- Extension of the PPG-based methods to exercise environments. Many commercial wearable health/fitness tracker devices use PPG signals for mean pulse rate measurement. PPG is a very interesting signal for this kind of devices due to the simplicity and the low price of its recording. However, PPG signals are very sensible to motion artifacts. To deal with motion artifacts, wearable devices usually use accelerometers. Obtaining PRV is more challenging than obtaining mean pulse rate because PRV require the accurate detection of each one of the PPG pulses, and the extraction of signals based on pulse morphological features such as PWV and PAV results even more challenging. However, some noise-cancellation systems for PPG signals based on accelerometers (e.g., an adaptive Wigner filtering) could be studied with the purpose of deriving respiratory rate from PPG signal

in presence of motion artifacts and so, allowing wearable health/fitness tracker devices to estimate respiratory rate and ANS information through PRV. Some potential applications could be the estimation of anaerobic threshold [7–9] or the assessment of stress level. This study would require PPG, accelerometer, respiration and ECG simultaneous recordings in presence of motion artifacts.

References

[1] B Krieger, D Feinerman, A Zaron, and F Bizousky. Continuous noninvasive monitoring of respiratory rate in critically ill patients. *CHEST*, 90(5):632–634, 1986.

[2] T R Gravelyn and J G Weg. Respiratory rate as an indicator of acute respiratory dysfunction. *Journal of the American Medical Association*, 244(10):1123–1125, 1980.

[3] B I Browning, G D'Alonzo, and M J Tobin. Respiratory rate as an indicator of respiratory dysfunction in patients with cystic fibrosis. *CHEST*, 97(6):1317–1321, 1990.

[4] A. Garde, B. F. Giraldo, R. Jané, T. D. Latshang, A. J. Turk, T. Hess, M. M. Bosch, D. Barthelmes, T. M. Merz, J. Pichler Hefti, O. D. Schoch, and K. E. Bloch. Time-varying signal analysis to detect high-altitude periodic breathing in climbers ascending to extreme altitude. *Medical and Biological Engineering and Computing*, pages 1–14, 2015.

[5] D. P. Francis, K. Willson, L. C. Davies, A. J. S. Coats, and M. Piepoli. Quantitative general theory for periodic breathing in chronic heart failure and its clinical implications. *Circulation*, 102:2214–2221, 2000.

[6] N. W. James, G. M. Adams, and A. F. Wilson. Determination of anaerobic threshold by ventilatory frequency. *International Journal of Sports Medicine*, 10(3):192–196, 1989.

[7] J Neary, Y Bhambhani, and H Quinney. Validity of breathing frequency to monitor exercise intensity in trained cyclists. *International Journal of Sports Medicine*, 16(4):255–259, 1995.

[8] D Carey, J Hughes, R Raymond, and G Pliego. The respiratory rate as a marker for the ventilatory threshold: comparison to other ventilatory parameters. *Journal of Exercise Physiology*, 8(2):30–38, 2005.

[9] D Carey, L A Schwarz, G J Pliego, and R L Raymond. Respiratory rate is a valid and reliable marker for the anaerobic threshold: implications for measuring change in fitness. *Journal of Sports Science and Medicine*, 4(4):482–488, 2005.

[10] R. Bailón, L. Sörnmo, and P. Laguna. ECG-derived respiratory frequency estimation. In G. Clifford, F. Azuaje, and P. E. McSharry, editors, *Advanced methods and tools for ECG data analysis*, chapter 8. Artech House, 2006.

[11] A. C. Guyton and J. E. Hall. *Text book of medical physiology*. W. B. Saunders Co., 2006.

[12] R. Hainsworth. The control and phisiological importance of heart rate. In M. Malik and J. A. Camm, editors, *Heart rate variability*, chapter 1. Futura Publishing Company, Inc., 1995.

[13] G G Berntson, J T Cacioppo, and K S Quigley. Respiratory sinus arrhythmia: Autonomic origins, physiological mechanism, and psychological implications. *Psychophysiology*, 30:183–196, 1993.

[14] L. Sörnmo and P. Laguna. *Bioelectrical Signal Processing in Cardiac and Neurological Applications*. ELSEVIER, 2005.

[15] E. Goldberger. Simple, indifferent, electrocardiographic electrode of zero potential and technique of obtaining augmented, unipolar, extremity leads. *American Heart Journal*, 23(4):483–492, 1942.

[16] E. Goldberger. *Unipolar lead electrocardiography*. Lea & Febiger, 2005.

[17] F. N. Wilson, F. D. Johnston, A. G. Macleod, and P. S. Barker. Electrocardiograms that represent the potential variations of a single electrode. *American Heart Journal*, 9(4):447–458, 1934.

[18] E. Simonson and A. Keys. A quantitative comparison of unipolar and augmented unipolar limb leads. *Circulation*, 1:954–963, 1950.

[19] Task Force of the European Society of Cardiology and the North American Society of Pacing and Electrophysiology. Heart rate variability: standards of measurement, physiological interpretation and clinical use. *Circulation*, 93(5):1043–1065, 1996.

[20] S. Akselrod, D. Gordon, T. A. Ubel, D. C. Shannon, A. C. Barger, and R. J. Cohen. Power spectrum analysis of heart rate fluctuation:

a quantitative probe of beat to beat cardiovascular control. *Science*, 213:220–222, 1981.

[21] R. Bailón, L. Sörnmo, and P. Laguna. A robust method for ECG-based estimation of the respiratory frequency during stress testing. *IEEE Transactions on Biomedical Engineering*, 53(7):1273–1285, 2006.

[22] R. Bailón, P. Laguna, L. Mainardi, and L. Sörnmo. Analysis of heart rate variability using time-varying frequency bands based on respiratory frequency. In *Engineering in Medicine and Biology Society, 2007. Proceedings of the 29th Annual International Conference of the IEEE*, pages 6674–6677, 2007.

[23] Y. Goren, L. R. Davrath, I. Pinhas, E. Toledo, and S. Akselrod. Individual time-dependent spectral boundaries for improved accuracy in time-frequency analysis of heart rate variability. *IEEE Transactions on Biomedical Engineering*, 53(1):35–42, 2006.

[24] R Bailón, L Mainardi, M Orini, L Sörnmo, and P Laguna. Analysis of heart rate variability during exercise stress testing using respiratory information. *Biomedical Signal Processing and Control*, 5:299–310, 2010.

[25] A Bauer, M Malik, G Schmidt, P Barthel, H Bonnemeier, I Cygankiewicz, P Guzik, F Lombardi, A Müller, A Oto, R Schneider, M Watanabe, D Wichterle, and W Zareba. Heart rate turbulence: Standards of measurement, physiological interpretation, and clinical use. *Journal of the American College of Cardiology*, 52(17):1353–1365, 2008.

[26] D Wichterle, V Melenovsky, J Simek, J Malik, and M Malik. Hemodynamics and autonomic control of heart rate turbulence. *Journal of Cardiovascular Electrophysiology*, 17(3):286–291, 2006.

[27] G Schmidt, M Malik, P Barthel, R Schneider, K Ulm, L Rolnizky, A J Camm, J T Bigger, and A Schömig. Heart-rate turbulence after ventricular premature beats as a predictor of mortability after acute myocardial infarction. *The Lancet*, 353:1390–1396, 1999.

[28] J T Flaherty, S D Blumenschein, A W Alexander, R D Gentzier, T M Dallie, J P Boineau, and M S Spach. Influence of respiration on recording cardiac potentials. *American Journal of Cardiology*, 20(1):21–28, 1967.

[29] H Riekkinen and P Rautaharju. Body position, electrode level, and respiration effects on the frank lead electrocardiogram. *Circulation*, 53(1):40–45, 1976.

[30] S. W. Porges. Respiratory sinus arrhythmia: Physiological basis, quantitative methods, and clinical implications. In P. Grossman, K. H. L. Janssen, and D. Vaitl, editors, *Cardiorespiratory and Cardiosomatic Psychophysiology*, volume 114 of *NATO ASI Series*, pages 101–116. Springer US, 1986.

[31] P. Grossman and K. Wientjes. Respiratory sinus arrhythmia and parasympathetic cardiac control: Some basic issues concerning quantification, applications and implications. In P. Grossman, K. H. L. Janssen, and D. Vaitl, editors, *Cardiorespiratory and Cardiosomatic Psychophysiology*, volume 114 of *NATO ASI Series*, pages 117–138. Springer US, 1986.

[32] A. B. Hertzman. The blood supply of various skin areas as estimated by the photo-electric plethysmograph. *American Journal of Physiology*, 124:328–340, 1938.

[33] E. Gil. *Análisis multimodal de las señales fotopletismográfica de pulso y electrocardiográfica para el diagnóstico del síndrome de apnea obstructiva durante el sueño en niños*. PhD thesis, Universidad de Zaragoza, 2009.

[34] J. Allen and A. Murray. Age-related changes in the characteristics of the photoplethysmographic pulse shape at various body sites. *Physiological Measurement*, 24:297–307, 2003.

[35] J. Allen. Photoplethysmography and its application in clinical physiological measurement. *Physiological Measurement*, 28(3):R1–R39, 2007.

[36] P. A. Kyriacou. Pulse oximetry in the oesophagus. *Physiological Measurement*, 27(1):R1–R35, 2006.

[37] D Grimaldi, Y Kurylyak, F Lamonaca, and A Nastro. Adaptive filtering of ECG signal for deriving respiratory activity. In *The 6th IEEE International Conference on Intelligent Data Acquisition and Adcanced Computing Systems: Technology and Applications*, pages 488–491, 2011.

[38] E Jonathan and M Leahy. Investigating a smartphone imaging unit for photoplethysmography. *Physiological Measurement*, 31(11):N79–N83, 2010.

[39] Y Maeda, M Sekine, and T Tamura. The advantages of wearable green reflected photoplethysmography. *Journal of Medical Systems*, 35(5):829–834, 2011.

[40] K Matsuruma K, P Rolfe, J Lee, and T Yamakoshi. iphone 4s photoplethysmography: Which light color yields the most accurate heart rate and normalized pulse volume using the iphysiometer application in the presence of motion artifact? *Plos One*, 9(3):e91205, 2014.

[41] C G Scully, J Lee, J Meyer, A M Gorbach, D Granquist-Fraser, Y Mendelson, and K H Chon. Physiological parameter monitoring from optical recordings with a mobile phone. *IEEE Transactions on Biomedical Engineering*, 59(2):303–306, 2012.

[42] W Verkruysse, L O Svaasand, and J S Nelson. Remote plethysmographic imaging using ambient light. *Optics Express*, 16(26):2143421445, 2008.

[43] T. Pickering, J. Hall, L. Appel, B. Falkner, J. Graves, M. Hill, D. Jones, T. Kurtz, S. Sheps, and E. Roccella. Blood pressure measurement in humans. *Hypertension*, 45:142–161, 2005.

[44] M. Yelderman and A. Ream. Indirect measurement of mean blood pressure in the anesthetized patient. *Anesthesiology*, 50(3):253–256, 1979.

[45] J. Penáz. Photoelectric measurements of blood pressure, volume and flow in the finger. In *Digest of the 10th International Conference on Medical and Biological Engineering*, page 104, 1973.

[46] G. J. Langewouters, P. T. Rutgers, J. Leideman, and W. B. J. Hakvoort. Device for controlling the pressure in an inflatable pressure pad, US Patent App. 13/501,185, 09 2012.

[47] J. Van Egmond, M. Hasenbos, and J. Crul. Invasive v. noninvasive measurement of arterial pressure. comparison of two automatic methods and simultaneously measured direct intra-arterial pressure. *British Journal of Anaesthesia*, 57(4):434–444, 1985.

[48] I. Constant, D. Laude, I. Murat, and J. L. Elghozi. Pulse rate variability is not a surrogate for heart rate variability. *Clinical Science*, 97(4):391–397, 1999.

[49] S. Lu, H. Zhao, K. Ju, K. Shin, M. Lee, K. Shelley, and K. Chon. Can photoplethysmography variability serve as an alternative approach to obtain heart rate variability information? *Journal of Clinical Monitoring and Computing*, 22(1):23–29, 2008.

[50] E. Gil, M. Orini, R. Bailón, J.M. Vergara, L. Mainardi, and P. Laguna. Photoplethysmography pulse rate as a surrogate measurement of heart rate variability during non-stationary conditions. *Physiological Measurement*, 31:1271–1290, 2010.

[51] E. Gil, P. Laguna, J. P. Martínez, O. Barquero-Pérez, A. García-Alberola, and L. Sörnmo. Heart rate turbulence analysis based on photoplethysmography. *IEEE Transactions on Biomedical Engineering*, 60(11):3149–3155, 2013.

[52] Y. Mendelson. Pulse oximetry: theory and applications for noninvasive monitoring. *Clinical Chemistry*, 38(9):1601–1607, 1992.

[53] M. Nitzan, A. Babchenko, B. Khanokh, and D. Landau. The variability of the photoplethysmographic signal–a potential method for the evaluation of the autonomic nervous system. *Physiological Measurement*, 19(1):93–102, 1998.

[54] E. Gil, J. M. Vergara, and P. Laguna. Detection of decreases in the amplitude fluctuation of pulse photoplethysmography signal as indication of obstructive sleep apnea syndrome in children. *Biomedical Signal Porcessing and Control*, 3:267–277, 2008.

[55] E. Gil, M. Mendez, J. M. Vergara, S. Cerutti, A. M. bianchi, and P. Laguna. Discrimination of sleep apnea related decreases in the amplitude fluctuations of PPG signal in children by HRV. *IEEE Transactions on Biomedical Engineering*, 56(4):1005–1014, 2009.

[56] A. H. Khandoker, C. K. Karmakar, and M. Palaniswami. Comparison of pulse rate variability with heart rate variability during obstructive sleep apnea. *Medical Engineering and Physics*, 33:204–209, 2011.

[57] B. Yang and K. Chon. A novel approach to monitor nonstationary dynamics in physiological signals: Application to blood pressure, pulse

oximeter, and respiratory data. *Annals of Biomedical Engineering*, 38(11):3478–3488, 2010.

[58] D. J. Meredith, D. Clifton, P. Charlton, J. Brooks, C. W. Pugh, and L. Tarassenko. Photoplethysmographic derivation of respiratory rate: a review of relevant physiology. *Journal of Medical Engineering & Technology*, 36(1):1–7, 2012.

[59] A. Guilleminaut, A. Tilkian, and W. C. Dement. The sleep apnea syndromes. *Annu. Rev. Med.*, 27:465–484, 1976.

[60] P E Peppard, T Young, M Palta, and J Skatrud. Prospective study of the association between sleep-disordered breathing and hypertension. *The New England Journal of Medicine*, 342(19):1378–1384, 2000.

[61] H K Yaggi, J Concato, W N Kernan, J H Lichtman, L M Brass, and V Mohsenin. Obstructive sleep apnea as a risk factor for stroke and death. *The New England Journal of Medicine*, 353(19):2034–2041, 2005.

[62] C F George. Reduction in motor vehicle collisions following treatment of sleep apnoea with nasal cpap. *Thorax*, 56(7):508–512, 2001.

[63] A Roebuck, V Monasterio, E Gederi, M Osipov, J Behar, A Malhotra, T Penzel, and G D Clifford. A review of signals used in sleep analysis. *Physiological Measurement*, 35:R1–R57, 2014.

[64] E. F. Williams III, P. Woo, R. Miller, and R. M. Kellman. The effects of adenotonsillectomy on growth in young children. *Otolaryngology – Head and Neck Surgery*, 104:509–516, 1991.

[65] C. L. Marcus, J. L. Carroll, C. B. Koerner, A. Hamer, J. Lutz, and G. M. Loughlin. Determinants of growth in children with the obstructive sleep apnea syndrome. *The Journal of Pediatrics*, 125(4):556–562, 1994.

[66] A. Bar, A. Tarasiuk, Y. Segev, M. Philip, and A. Tal. The effect of adenotonsillectomy on serum insulin-like growth factor-i and growth in children with obstructive sleep apnea syndrome. *The Journal of Pediatrics*, 135(1):76–80, 1999.

[67] R. D. Chervin, K. H. Archbold, J. E. Dillon, P. Panahi, K. J. Pituch, R. E. Dahl, and C. Guilleminault. Inattention, hyperactivity, and

symptoms of sleep-disordered breathing. *Pediatrics*, 109:449–456, 2002.

[68] M. Weissbluth, A. T. Davis, J. Poncher, and J. Reiff. Signs of airway obstruction during sleep and behavioral, developmental, and academic problems. *Jourbnal of Developmental and Behavioral Pediatrics*, 4(2):119–121, 1983.

[69] N. J. Ali, D. Pitson, and J. R. Stradling. Sleep disordered breathing: effects of adenotonsillectomy on behaviour and psychological functioning. *European Journal of Pediatrics*, 155(1):56–62, 1996.

[70] C. E. Hunt and R. T. Brouillette. Abnormalities of breathing control and airway maintenance in infants and children as a cause of cor pulmonale. *Pediatric cardiology*, 3(3):249–256, 1982.

[71] M. Steier and S. C. Shapiro. Cor pulmonale from airway obstruction in children. *Journal of the American Medical Association*, 225, 1973.

[72] O. E. Brown, S. C. Manning, and B. Ridenour. Cor pulmonale secondary to tonsillar and adenoidal hypertrophy: management considerations. *International Journal of Pediatric Otorhinolaryngology*, 16(2):131–139, 1988.

[73] M. S. Schechter and Section on Pediatric Pulmonology, Subcommittee on Obstructive Sleep Apnea Syndrome. Technical report: Diagnosis and management of childhood obstructive sleep apnea syndrome. *Pediatrics*, 109(4):e69, 2002.

[74] C. L. Mason and L. Tarassenko. Quantitative assessment of respiratory derivation algorithms. In *Engineering in Medicine and Biology Society, 2001. Proceedings of the 23rd Annual International Conference of the IEEE*, volume 2, pages 1998–2001, 2001.

[75] G. B. Moody, R. G. Mark, A. Zoccola, and S. Mantero. Derivation of respiratory signals from multi-lead ECGs. In *Computers in Cardiology, 1985*, pages 383–386, 1985.

[76] F. Pinciroli, R. Rossi, and L. Vergani. Detection of electrical axis variation for the extraction of respiratory information. In *Computers in Cardiology, 1986*, pages 499–502, 1986.

[77] M. Varanini, M. Emdin, F. Allegri, M. Raciti, F. Conforti, A. Macerata, A. Taddei, R. Francesconi, G. Kraft, A. L. Abbate, and C. Marchesi. Adaptive filtering of ECG signal for deriving respiratory activity. In *Computers in Cardiology 1990, Proceedings.*, pages 621–624, 1990.

[78] S. Leanderson, P. Laguna, and L. Sörnmo. Estimation of the respiratory frequency using spatial information in the VCG. *Medical Engineering & Physics*, 25(6):501–507, 2003.

[79] E. Pueyo, L. Sörnmo, and P. Laguna. QRS slopes for detection and characterization of myocardial ischemia. *IEEE Transactions on Biomedical Engineering*, 55(2):468–477, 2008.

[80] D. Romero, M. Ringborn, P. Laguna, and E. Pueyo. Depolarization changes during acute myocardial ischemia by evaluation of QRS slopes: standard lead and vectorial approach. *IEEE Transactions on Biomedical Engineering*, 58(1):110–120, 2011.

[81] D. Romero, M. Ringborn, P. Laguna, and E. Pueyo. Detection and quantification of acute myocardial ischemia by morphologic evaluation of QRS changes by an angle-based method. *Journal of Electrocardiology*, 46:204–214, 2013.

[82] R. Freeman. Assessment of cardiovascular autonomic function. *Clinical Neurophysiology*, 117(4):716–730, 2006.

[83] A. Mincholé, E. Pueyo, J. F. Rodríguez, E. Zacur, M. Doblaré, and P. Laguna. Quantification of restitution dispersion from the dynamic changes of the T-wave peak to end, measured at the surface ECG. *IEEE Transactions on Biomedical Engineering*, 58(5):1172–1182, 2011.

[84] G. Borg. *Borg's perceived exertion and pain scales.* Human Kinetics, 1998.

[85] L. Edenbrandt and O. Pahlm. Vectorcardiogram synthesized from a 12-lead ECG: superiority of the inverse Dower matrix. *Journal of Electrocardiology*, 21(4):361–367, 1988.

[86] M. Guillem, A.V. Sahakian, and S. Swiryn. Adaptive filtering of ECG signal for deriving respiratory activity. In *Computers in Cardiology*, volume 33, pages 249–252, 2006.

[87] J. P. Martínez, R. Almeida, S. Olmos, A. P. Rocha, and P. Laguna. A wavelet-based ECG delineator: Evaluation on standard databases. *IEEE Transactions on Biomedical Engineering*, 51(4):570–581, 2004.

[88] J. Mateo and P. Laguna. Analysis of heart rate variability in presence of ectopic beats using the heart timing signal. *IEEE Transactions on Biomedical Engineering*, 50(3):334–343, 2003.

[89] L. Sörnmo. Vectorcardiographic loop alignment and morphologic beat-to-beat variability. *IEEE Transactions on Biomedical Engineering*, 45(12):1401–1413, 1998.

[90] M. Åmströn, J. García, P. Laguna, O. Pahlm, and L. Sörnmo. Detection of body position changes using the surface ECG. *Medical and Biological Engineering and Computing*, 41(2):164–171, 2003.

[91] G. Blain, O. Meste, A. Blain, and S. Bermon. Time-frequency analysis of heart rate variability reveals cardiolocomotor coupling during dynamic cycling exercise in humans. *Am. J. Physiol. Heart Circ. Physiol.*, 296:H1651–H1659, 2009.

[92] A. Johansson and P. A. Oberg. Estimation of respiratory volumes from the photoplethysmographic signal. Part I: experimental results. *Medical and Biological Engineering and Computing*, 37:42–47, 1999.

[93] A Garde, W Karlen, P Dehkordi, J M Ansermino, and G A Dumont. Empirical mode decomposition for respiratory and heart rate estimation from the photoplethysmogram. In *Computing in Cardiology 2013*, pages 799–802. IEEE Computer Society Press, 2013.

[94] A Garde, W Karlen, J M Ansermino, and G A Dumont. Estimating respiratory and heart rates from the correntropy spectral density of the photoplethysmogram. *Plos One*, 9(1):e86427, 2014.

[95] S. Dash, K. H. Shelley, D. G. Silverman, and K. H. Chon. Estimation of respiratory rate from ECG, photoplethysmogram, and piezoelectric pulse transducer signals: A comparative study of time–frequency methods. *IEEE Transactions on Biomedical Engineering*, 57(5):1099–1107, 2010.

[96] C Julien. The enigma of Mayer waves: Facts and models. *Cardiovascular Research*, 70:12–21, 2006.

[97] J Y Foo, C L Parsley, S J Wilson, G R Williams, M Harris, and D M Cooper. Relations between physiologic parameters and pulse transit time during loaded breathing. In *Engineering in Medicine and Biology Society, 2005. Proceedings of the 27th Annual International Conference of the IEEE*, volume 7, pages 7521–7524, 2005.

[98] C. P. chua and C. Heneghan. Pulse transit time-derived respiratory parameters and their variability across sleep stages. In *Engineering in Medicine and Biology Society, 2005. Proceedings of the 27th Annual International Conference of the IEEE*, volume 6, pages 6153–6156, 2005.

[99] P. S. Hamilton. A comparison of adaptative and nonadaptative filters for the reduction of powerline interference in the ECG. *IEEE Transactions on Biomedical Engineering*, 43:105–109, 1996.

[100] E. Gil, R. Bailón, J. M. Vergara, and P. Laguna. PTT variability for discrimination of sleep apnea related decreases in the amplitude fluctuations of PPG signal in children. *IEEE Transactions on Biomedical Engineering*, 57(5):1079–1088, 2010.

[101] P. Laguna, R. Jané, and Pere Caminal. Automatic detection of wave boundaries in multilead ECG signals: validation with the CSE database. *Computers and Biomedical Research*, 27:45–60, 1994.

[102] M A F Pinmentel, M D Santos, C Arteta, J Domingos, MA Maraci, and G Clifford. Respiratory rate estimation from the oscillometric waveform obtained from a non-invasive cuff-based blood pressure device. In *Engineering in Medicine and Biology Society, 2014. Proceedings of the 36th Annual International Conference of the IEEE*, pages 3821–3824, 2014.

[103] P A Shaltis, A Reisner, and H H Asada. Wearable, cuff-less ppg-based blood pressure monitor with novel height sensor. In *Engineering in Medicine and Biology Society, 2006. Proceedings of the 28th Annual International Conference of the IEEE*, pages 908–911, 2006.

[104] K H Chon, S Dash, and K Ju. Estimation of respiratory rate from photoplethysmogram data using time-frequency spectral estimation. *IEEE Transactions on Biomedical Engineering*, 56(8):2054–2063, 2009.

[105] Y Nam, J Lee, and K H Chon. Respiratory rate estimation from the built-in cameras of smartphones and tablets. *Annals of Biomedical Engineering*, 42(4):885–898, 2013.

[106] J A Hirsch and B Bishop B. Respiratory sinus arrhythmia in humans: how breathing pattern modulates heart rate. *American Journal of Physiology*, 241(4):H620–H629, 1981.

[107] American Thoracic Society. Standards and indications for cardiopulmonary sleep studies in children. *American Journal of Respiratory and Critical Care Medicine*, 153(2):866–878, 1996.

[108] American Thoracic Society. Cardiorespiratory sleep studies in children. *American Journal of Respiratory and Critical Care Medicine*, 160:1381–1387, 1999.

[109] J Lee, B A Reyes, D D McManus, O Mathias, and K H Chon. Atrial fibrillation detection using an iphone 4s. *IEEE Transactions on Biomedical Engineering*, 60(1):203–206, 2013.

[110] T. W. Parks and C. S. Burrus. *Digital filter design*. John Wiley & Sons, 1987.

[111] H Wang, K Siu, K Ju, and K H Chon. A high resolution approach to estimating timefrequency spectra and their amplitudes. *Annals of Biomedical Engineering*, 34(2):326–338, 2006.

[112] A. Monti, C. Medigue, and L. Margin. Instantaneous parameter estimation in cardiovascular time series by harmonic and time-frequency analysis. *IEEE Transactions on Biomedical Engineering*, 49(12):1547–1556, 2002.

[113] M. Bsoul, H. Minn, and L. Tamil. Apnea MedAssist: Real-time sleep apnea monitor using single-lead ECG. *IEEE Transactions on Information Technology in Biomedicine*, 15(3):416–427, 2011.

[114] A. H. Khandoker, J. Gubbi, and M. Palaniswami. Automated scoring of obstructive sleep apnea and hypoapnea events using short-term electrocardiogram recordings. *IEEE Transactions on Information Technology in Biomedicine*, 13(6):1057–1067, 2009.

[115] M. O. Mendez, A. M. Bianchi, M. Matteuci, S. Cerutti, and T. Penzel. Sleep apnea screening by autoregressive models from a single ECG

lead. *IEEE Transactions on Biomedical Engineering*, 56(12):2838–2850, 2009.

[116] J. V. Marcos, R. Hornero, D. Álvarez, M. Aboy, and F. del Campo. Automated prediction of the apnea-hypoapnea index from nocturnal oximetry recordings. *IEEE Transactions on Biomedical Engineering*, 59(1):141–149, 2012.

[117] R. Hornero, D. Álvarez, D. Abasolo, F. del Campo, and C. Zamarron. Utility of approximate entropy from overnight pulse oximetry data in the diagnosis of the obstructive sleep apnea syndrome. *IEEE Transactions on Biomedical Engineering*, 54(1):107–113, 2012.

[118] Deganit Barak-Shinar, Yariv Amos, and RichardK. Bogan. Sleep disordered breathing analysis in a general population using standard pulse oximeter signals. *Sleep and Breathing*, pages 1–7, 2013.

[119] C. L. Marcus. Sleep-disordered breathing in children. *American Journal of Respiratory and Critical Care Medicine*, 164:16–30, 2001.

[120] P. Flandrin. *Time-Frequency/Time-Scale Analysis*. Academic Press, 1999.

[121] W. Zhao, R. Chellappa, and N. Nandhakumar. Empirical performance analysis of linear discriminant classifiers. In *Computer Vision and Pattern Recognition, 1998. Proceedings. 1998 IEEE Computer Society Conference on*, pages 164–169, 1998.

[122] R Farré, M Nácher, A Serrano-Mollar, J B Gáldiz, F J Alvarez, D Navajas, and J M Montserrat. Rat model of chronic recurrent airway obstructions to study the sleep apnea syndrome. *Sleep*, 30(7):930–933, 2007.

[123] A Carreras, I Almendros, I Acerbi, J M Montserrat, D Navajas, and R Farr. Obstructive apneas induce early release of mesenchymal stem cells into circulating blood. *Sleep*, 32(1):117–119, 2009.

[124] A Shimokawa, T Kunitake, M Takasaki, and H Kannan. Differential effects of anesthetics on sympathetic nerve activity and arterial baroreceptor reflex in chronically instrumented rats. *Journal of the Autonomic Nervous System*, 72(1):46–54, 1998.

[125] M Kuwahara, K Yayou, K Ishii, S Hashimoto, H Tsubone, and S Sugano. Power spectral analysis of heart rate variability as a new method for assessing autonomic activity in the rat. *Journal of Electrocardiology*, 27(4):333–337, 1994.

[126] Standards of Practice Committee and American Sleep Disorders Association. Portable recording in the assessment of obstructive sleep apnea. *Sleep*, 17(4):378–392, 1994.

List of acronyms

AC Alternating Current. 11, 12

Acc Accuracy. 96, 98, 100

AM Amplitude Modulation. 81, 84, 102

ANS Autonomic Nervous System. 2, 3, 7–11, 15, 60, 82, 95, 99, 100, 102–104

AUC Area Under Curve. 96

BAV Blood pressure Amplitude Variability. 49, 57

BP Blood Pressure. vi, 10, 13, 14, 17, 22, 44, 45, 48–50, 55, 57, 58, 60, 61, 102

BRV Blood pressure Rate Variability. 49, 57

BWV Blood pressure Width Variability. 49, 57, 58

CDM Complex Demodulation. 69

CEICA Comité Ético de Investigación Clínica de Aragón (Aragon clinical research local ethics committee). 63

DAP Decreases in Amplitude fluctuations of the Pulse photoplethysmographic signal. 18, 19, 64, 65, 67, 85, 86, 89–100, 102, 103

DC Direct Current. 11, 12, 69

DR Derived Respiration. 44, 47–51, 55, 56, 58–60, 62, 68, 71–75, 78, 81–83

ECG Electrocardiogram. v–viii, 1–6, 8, 10, 15, 17, 19, 21–23, 25, 33, 36–41, 43, 44, 46, 48–50, 56–58, 60, 63, 64, 85–88, 94, 96, 98, 100–104

EDR Electrocardiogram Derived Respiration. v, vii, 10, 25–27, 29–31, 36, 38–41

FFCDM Fixed Frequency Complex Demodulation. 69, 70

FIR Finite Impulse Response. 64, 70

FM Frequency Modulation. 81, 84, 102

HF High Frequency. 9, 91, 96

HRT Heart Rate Turbulence. 10, 15

HRV Heart Rate Variability. 8–10, 14, 15, 18, 19, 48, 57, 85, 86, 94, 98–100, 103

IQR Interquartile Range. 56, 58, 59, 74, 75, 78, 81–84, 97

LDA Linear Discriminatn Analysis. 91

LDL Loop Derived Lead. 23, 24, 33–37, 39, 41, 56

LF Low Frequency. 9, 51, 59, 81, 91, 96, 103

MAD Median Absolute Deviation. 26, 29, 50, 68

NLDL N-Loops Derived Lead. 23, 24, 33–37, 39, 41, 56, 60, 101

OSAS Obstructive Sleep Apnea Syndrome. vi, viii, 2, 15, 16, 18, 63, 85–87, 93, 94, 99, 100, 102, 103

PAV Pulse Amplitude Variability. 17, 43, 44, 48, 50, 52–54, 56–58, 60, 68, 78, 81, 82, 84, 102, 103

PPG Pulse photoplethysmographic. v–viii, 2, 10–19, 22, 43–50, 55–58, 60–68, 73, 78, 81, 84–88, 90, 94–96, 98, 100–104, 107

PRT Pulse Rate Turbulence. 15

PRV Pulse Rate Variability. 14, 15, 17, 19, 43, 44, 48, 50, 52–54, 56–58, 60, 62, 66, 68, 78, 81, 82, 84, 86, 90, 91, 94, 96, 98–100, 102–104

PS Power Spectrum. 29, 50–52

PSD Power Spectrum Density. 9, 65, 71–73, 82

PSG Polysomnography. vi, 16, 63, 64, 93, 94, 96, 97, 99, 103

PTT Pulse Transit Time. 43, 49, 57, 58, 60

PWV Pulse Width Variability. vi, viii, 17, 43, 44, 47–49, 52–54, 56–60, 68, 78, 82, 84, 102, 103

RMS Root Mean Square. 9, 89

ROC Receiver Operating Characteristic. 94

RSA Respiratory Sinus Arrhythmia. 10, 82

SCPPG Smartphone-Camera-acquired PPG. vi, viii, 12, 13, 16, 18, 61–64, 66–68, 70, 78, 81, 83, 84, 102

SD Standard Deviation. 9, 35, 36, 56, 57, 59, 65, 92

Se Sensitivity. 96

SNR Signal to Noise Ratio. 44

Sp Specificity. 96

SpO$_2$ Peripheral Oxygen Saturation. 2, 11, 14–16, 56, 58, 63, 85, 87, 88, 93, 95, 99

SPWVD Smoothed Pseudo Wigner-Ville Distribution. 90, 95, 96

SVD Singular Value Decomposition. 29

VCG Vectorcardiogram. 6, 7, 21, 23, 24, 27, 28, 33–37, 39–41, 48, 56, 101

VFCDM Variable Frequency Complex Demodulation. 68–70

VLF Very Low Frequency. 91